Universidade de Aveiro
2021

Patrícia Inês Carvalho Godinho

C-Glicosil flavonóides como potenciais drogas anticoronavírus com dupla ação

C-Glycosyl flavonoids as potential anticoronavirus drugs with dual action

2021

Universidade de Aveiro
2021

Patrícia Inês Carvalho Godinho

C-Glicosil flavonóides como potenciais drogas anticoronavírus com dupla ação

C-Glycosyl flavonoids as potential anticoronavirus drugs with dual action

Dissertação apresentada à Universidade de Aveiro para cumprimento dos requisitos necessários à obtenção do grau de Mestre em Bioquímica, com especialização em Bioquímica Clínica, realizada sob a orientação científica da Doutora Vera Lúcia Marques da Silva, Professora Auxiliar do Departamento de Química da Universidade de Aveiro e coorientação científica da Doutora Raquel María González Soengas, Professora Associada do Departamento de Química Orgânica e Inorgânica da Universidade de Oviedo

o júri

presidente

Prof. Doutor Brian James Goodfellow
professor auxiliar do Departamento de Química da Universidade de Aveiro

Prof. Doutora Vera Lúcia Marques da Silva
professora auxiliar do Departamento de Química da Universidade de Aveiro

Prof. Doutora Clementina Maria Moreira dos Santos
professora adjunta da Escola Superior Agrária do Instituto Politécnico de Bragança

agradecimentos

À Doutora Vera L. M. Silva, a orientadora da dissertação, agradeço toda a atenção, apoio e dedicação prestados. Agradeço toda a disponibilidade, tranquilidade e confiança que depositou em mim e toda a compreensão demonstrada ao longo do percurso desta tese. Por fim, agradeço também todos os ensinamentos, quer práticos quer teóricos, que me transmitiu ao longo da tese.

À professora Raquel M. G. Soengas, coorientadora da dissertação, agradeço todo o apoio científico que me deu. Apesar de distante, a Doutora Raquel esteve sempre presente, tendo sido uma enorme ajuda a superar todos os obstáculos. Deste modo, foi uma constante e importante fonte de ajuda e de motivação para esta tese.

Ao Dr. Hilário Tavares e Dra. Cristina Barros, agradeço o seu contributo e disponibilidade prestados para a obtenção dos espetros de RMN e espetros de massa, respetivamente.

Agradeço aos meus colegas de laboratório por todo o apoio prestado, a entreajuda, a amizade e o bom ambiente que houve no laboratório. Um especial agradecimento ao Jorge González Rodriguez, que no pouco tempo que esteve cá em Portugal, conseguiu partilhar os seus conhecimentos e me ajudou a crescer. Além disso, agradeço toda a amizade, apoio e confiança que me deu. Agradeço a todos os elementos do grupo de Química Orgânica com quem privei, por todas as palavras de apoio e sugestões que me foram dadas durante a dissertação.

Por fim agradeço à minha família e amigos. À Tânia, João, Fábio, Maria Barbedo, Maria Rita e Hugo por todas as palavras amigas dadas e pelo apoio e ajuda que prestaram durante a dissertação. Agradeço aos meus pais, irmão e cunhada por toda a paciência, apoio, chamadas de atenção e acima de tudo pela motivação e inspiração que me dão, que permitiu concluir esta dissertação.

palavras-chave

SARS-CoV-2, glicosil flavonoides, antivirais, glicoproteína Spike, protease 3CL, α-glucosidase

resumo

A pandemia da COVID-19 que decorre atualmente, causada pela Síndrome Respiratória Aguda Grave Coronavírus 2 (SARS-CoV-2), espalhou-se por todo o mundo, causando milhões de mortes, e tornou-se uma preocupação global. Apesar de terem sido desenvolvidas e administradas vacinas, a doença continua ativa e ainda não estão disponíveis terapêuticas antivirais eficazes para a prevenção e o tratamento da SARS-CoV-2. Além disso, uma vez que novos e potencialmente mortais coronavírus (CoVs) podem surgir a qualquer momento com o potencial de se tornarem pandémicos, é crucial o desenvolvimento de agentes terapêuticos contra estes vírus. A pesquisa científica e os desafios médicos para salvar vidas revelaram a evolução genética e a bioquímica do ciclo de vida do SARS-CoV-2 em comparação com outros coronavírus. O SARS-CoV-2 ataca principalmente o trato respiratório, por meio da sua ligação da glicoproteína Spike à enzima conversora de angiotensina 2 (ACE2) da célula hospedeira, iniciando a replicação e transcrição do genoma viral pela $3CL^{pro}$. Deste modo, têm vindo a ser desenvolvidas algumas estratégias para a inibição da SARS-CoV-2, que têm como alvo a glicoproteína Spike e a $3CL^{pro}$.

Na busca por medicamentos anticoronavírus, alguns grupos de investigação têm-se focado no estudo de flavonoides glicosilados. Os glicosil flavonoides, distribuídos abundantemente pelo reino vegetal, têm recebido muita atenção devido às suas atividades antioxidantes, anti-inflamatórias, anti carcinogénicas e antidiabéticas amplamente reconhecidas, e pela sua capacidade de modular a função de enzimas celulares essenciais. Recentemente, os glicosil flavonoides também mostraram atividade antiviral promissora contra o SARS-CoV-2. Apesar de os *O*-glicosil flavonóides serem os mais comuns na natureza, os *C*-glicosil flavonoides têm atraído recentemente muito interesse, devido à sua estabilidade à hidrólise química e enzimática.

Assim, o primeiro objetivo deste trabalho foi a síntese de novos *C*-glicosil flavonóides para avaliar sua atividade antiviral contra o SARS-CoV-2. A síntese dos *C*-glicosil flavonóides foi efetuada através da reação acoplamento de Heck entre um 3-bromo flavonóide e um alceno de açúcar modificado. Embora a síntese de *C*-glicosil flavonas não tenha sido conseguida, foi possível sintetizar *C*-glicosil 2-estiril-4*H*-cromen-4-onas, embora a reação origine uma mistura de isómeros.

Os novos compostos obtidos foram caracterizados por técnicas de espectroscopia de ressonância magnética nuclear (RMN) mono- (^{1}H e ^{13}C) e bi-dimensionais (HSQC, HMBC, NOESY). Sempre que possível, foram também caracterizados por espectrometria de massa e espectrometria de massa de alta resolução.

Visto que os novos *C*-glicosil 2-estiril-4*H*-cromen-4-onas sintetizados possuem isómeros, a avaliação da atividade antiviral não pôde ser efetuada. Mais estudos para separar os isômeros formados são necessários, bem como a avaliação da atividade antiviral frente à $3CL^{pro}$ e α-glucosidases. Além disso, estudos de *docking* molecular serão conduzidos para entender as interações dos novos *C*-glicosil flavonóides sintetizados com a $3CL^{pro}$ da SARS-CoV-2 e as α-glucosidases.

keywords

SARS-CoV-2, glycosyl flavonoids, antivirals, Spike glycoprotein, Protease 3CL, α-glucosidase

abstract

The ongoing COVID-19 pandemic, caused by *Severe Acute Respiratory Syndrome Coronavirus 2* (SARS-CoV-2), has spread all over the world, causing millions of deaths, and became a major global concern. Although protective vaccines have been developed and administered, efficient antiviral agents for the prevention and treatment of SARS-CoV-2 are not yet available. Moreover, since new and deadly CoVs can emerge at any time with the potential of becoming pandemics, it is crucial the development of therapeutic agents against these potentially deadly CoVs. The scientific research and the medical challenges to save lives revealed the genetic evolution and the biochemistry of SARS-CoV-2 life cycle in comparison with other coronaviruses. The SARS-CoV-2 attacks primarily the respiratory tract, through its binding of Spike glycoprotein to angiotensin converting enzyme 2 (ACE2) of the host cell, initiating the replication and transcription of viral genome by $3CL^{pro}$. There have been developed some strategies towards SARS-CoV-2 inhibition, which target the Spike glycoprotein and $3CL^{pro}$.

In the search for anti-coronaviral drugs, researchers soon turned their heads towards glycosylated flavonoids. Glycosyl flavonoids, widespread in the plant kingdom, have received a lot of attention due to their widely recognized antioxidant, anti-inflammatory, anticarcinogenic, antidiabetic activities, and to their ability to modulate key cellular enzymes function. Recently, glycosyl flavonoids have also shown promising antiviral activity against SARS-CoV-2. Despite *O*-glycosyl flavonoids are by far the most common in nature, *C*-glycosyl flavonoids have attracted much recent interest, due to their enhanced stability to chemical and enzymatic hydrolysis.

Thus, the first aim of this work was the synthesis of new *C*-glycosyl flavonoids to evaluate their antiviral activity towards the SARS-CoV-2. The synthesis of *C*-glycosyl flavonoids was achieved through the cross-coupling Heck reaction between a 3-bromo flavonoid and a modified sugar alkene. Although the synthesis of *C*-glycosyl flavones was not well-succeeded, it was possible to synthesize *C*-glycosyl 2-styryl-4*H*-chromen-4-ones, although, the presence of isomers was observed.

The new synthesized compounds were unequivocally characterized by mono- (^{1}H and ^{13}C) and two-dimensional (HSQC, HMBC, NOESY) nuclear magnetic resonance (NMR) spectroscopy techniques. Whenever possible, they were also characterized by mass spectrometry and high-resolution mass spectrometry.

Since the new synthesized *C*-glycosyl 2-styryl-4*H*-chromen-4-ones were obtained as a mixture of isomers, the evaluation of the antiviral activity could not be performed. Further studies to separate the isomers are needed, as well as the evaluation of the antiviral activity towards the $3CL^{pro}$ and α-glucosidases. Furthermore, molecular docking studies will be conducted to understand the interactions of the new synthesize *C*-glycosyl flavonoids with SARS-CoV-2 $3CL^{pro}$ and the α-glucosidases.

Contents

List of Abbreviations

3CL^{pro}	Chymotrypsin-like protease 3
4-PPy	4-Pyrrolidinopyridine
Ac	Acetyl
ACE2	Angiotensin converting enzyme 2
AngII	Angiotensin II
atm	Atmosphere
BALF	Bronchoalveolar lavage fluid
Bn	Benzyl
Bz	Benzoyl
COSY	Correlated spectroscopy
COVID-19	Coronavirus disease 2019
CoVs	Coronaviruses
COX-2	Cyclooxygenase-2
CRP	C-reactive protein
CTL	Cytotoxic T lymphocytes
d	Doublet
DCC	Dicylclohexylcarbodiimide
dd	Doublet of doublets
ddd	Doublet of doublets of doublets
DDQ	2,3-dichloro-5,6-dicyano-1,4-benzoquinone
DMF	*N*,*N*-dimethylformamide
DMP	Dess-Martin periodinane
DMSO	Dimethyl sulfoxide
EGCG	Epigallocatechin gallate
equiv	Equivalents
FasL	Fas ligand
GCG	Gallocatechin gallate
h	Hours
HIV-1	*Human immunodeficiency virus type 1*
HMBC	Heteronuclear multiple bond correlation
HRMS	High-resolution mass spectrometry

HSQC	Heteronuclear single quantum correlation
IC_{50}	Inhibitory concentration of 50% of activity
ICTV	International Committee on Taxonomy of Viruses
INF-γ	Interferon-gamma
iNOS	Nitric oxide synthase
ISG15	Interferon-stimulated gene product 15
IUPAC	International Union of Pure and Applied Chemistry
J	Coupling constant (Hz)
JAK/STAT-1	Janus kinase/Signal transducer and activator of transcription
m	Multiplet
m.p.	Melting point
m/z	Mass/charge ratio (mass spectrometry)
MERS-CoV	*Middle East respiratory syndrome coronavirus*
min	Minutes
MOM	Methoxymethyl
mRNA	Messenger RNA
MS	Mass spectrometry
NAG	*N*-acetyl-β-glucosamine
NBS	*N*-bromo succinimide
NETs	Neutrophil extracellular traps
NF-κB	Nuclear factor kappa B
NK	Natural killer
NLRP3	NLR family pyrin domain containing 3
NMP	*N*-methylpyrrolidone
NMR	Nuclear magnetic resonance
NO	Nitric oxide
NOESY	Nuclear overhauser effect spectroscopy
nsp	Non-structural proteins
ORF	Open reading frames
Ph	Phenyl
Piv	Pivaloyl
PL^{pro}	Papain-like protease

ppm	Parts per million
PTT	Phenyltrimethylammonium tribromide
r.t.	Room temperature
RBD	Receptor binding domain
RdRp	RNA-dependent RNA polymerase
RTC	RNA replicase-transcriptase complex
s	Singlet
SARS-CoV	*Severe acute respiratory syndrome coronavirus*
SARS-CoV-2	*Severe acute respiratory syndrome coronavirus 2*
ssRNA	Single-stranded ribonucleic acid
STAT3	Signal transducer and activator of transcription 3
t	Triplet
TBAB	Tetrabutylammonium bromide
TBDPS	*tert*-Butyldiphenylsilyl
TBS	*tert*-butyldimethylsilyl
THF	Tetrahydrofuran
TLC	Thin-layer chromatography
TLRs	Toll-like receptors
***p*-TSA**	*p*-Toluenesulfonic acid
UV	Ultraviolet
WHO	World Health Organization

Chapter 1: Introduction

1.1. Severe acute respiratory syndrome coronavirus 2

In December 2019, an outbreak of a severe pneumonia of unknown origin started in Wuhan, China. Soon after, similar cases were found in other countries around the world, and the number of infected people increased rapidly. At the end of January 2020, the World Health Organization (WHO) officially announced this pneumonia, caused by a new coronavirus, to be a public health emergency of global concern due to its rapid spread. The disease caused by this virus was named Coronavirus disease 2019 (COVID-19). Later, on 11 March 2020, WHO declared it a global pandemic. Once the genetic analysis and information about the COVID-19 became available, the International Committee on Taxonomy of Viruses (ICTV) gave its official name - *severe acute respiratory syndrome coronavirus 2* (SARS-CoV-2).[1,2] At the time of writing, over 243 million confirmed cases and over 4.9 million deaths have been reported since the start of the pandemic (https://www.who.int/publications/m/item/weekly-epidemiological-update-on-covid-19---26-october-2021)

Coronaviruses (CoVs) can be found in humans and in different animal species, such as bats, camels, and civets. They belong to the subfamily *coronavirinae* from the family *coronaviridae*. This subfamily can be divided into four genera, *Alphacoronavirus*, *Betacoronavirus*, *Gammacoronavirus* and *Deltacoronavirus*. SARS-CoV-2 belongs to the *Betacoronavirus* family, which can only infect mammals.[3,4] CoVs are enveloped and spherical viruses that possess in their genome a single-stranded ribonucleic acid (ssRNA) of 27-32 kilobases in length, with a positive polarity, which means that the base sequence orientation of the RNA is 5'→3'.[4] The viral RNA contains open reading frames (ORF) that comprise two-thirds of the genome and consist of sixteen non-structural proteins (nsp), which includes the RNA-dependent RNA polymerase (RdRp) and other replicase proteins. These are primarily processed by the virally encoded chymotrypsin-like protease 3 ($3CL^{pro}$), with additional cleavage performed by the viral papain-like proteases (PL^{pro}). The remaining one-third of the viral RNA encodes four essential structural proteins, such as Spike glycoprotein, envelope protein, membrane and nucleocapsid (**Figure 1**).[5,6] The genome of CoVs is one of the largest RNA genomes, giving extra plasticity to this family of viruses in accommodating and modifying genes.[7] In fact, CoVs have a high-rate mutation due to RdRp, which is responsible for the replication of RNA viruses, thus being more error-prone.[4,8] Until SARS-CoV-2 appeared, there were at least six known

coronaviruses that could infect humans. The viruses that can cause severe acute respiratory syndromes are *severe acute respiratory syndrome coronavirus* (SARS-CoV), which caused an outbreak in 2002, and *Middle East respiratory syndrome coronavirus* (MERS-CoV), emerged in 2012, and SARS-CoV-2. The other four viruses, HCoV-NL63, HCoV-229E, HCoV-OC43 and HKU1, can cause mild upper respiratory diseases.[4] The genome of SARS-CoV-2 shows similarities to other *Betacoronavirus*, sharing ~80% sequence identity with SARS-CoV and ~50% sequence identity with MERS-CoV.[9]

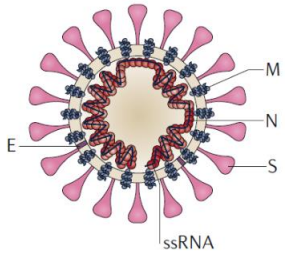

Figure 1. Schematic diagram of the coronavirus virion. Abbreviations: E, envelope; M, membrane; N, nucleocapsid; S, Spike glycoprotein and ssRNA, single stranded ribonucleic acid. (Adapted from reference 4)

The primary tropism of SARS-CoV-2 is the lungs since patients exhibit respiratory-like illness that progresses to severe pneumonia. This virus enters the host via respiratory tract, which makes the first targets the airway and alveolar epithelial cells, vascular endothelial cells, and alveolar macrophages (**Figure 2**). In fact, these cells express receptors for SARS-CoV-2 entry, which reinforces these cells are the spot/point in the early infection.[9]

The CoVs are transmitted through respiratory droplets and direct contact with contaminated surfaces. The incubation period of SARS-CoV-2 is short, usually taking approximately 5-6 days, whereas the other SARS-CoV and MERS-CoV usually take 2-11 days. The SARS-CoV-2 infection causes severe flu-like symptoms that can progress to acute respiratory distress, pneumonia, renal failure, and even death. The most common symptoms are fever, cough, dyspnea, fatigue, and muscle pain.[1,9] SARS-CoV-2 can lead to myocardial injury, arrhythmic complications, neurological complications, such as headache, myalgia, anosmia, ageusia and even stroke.[10–12]

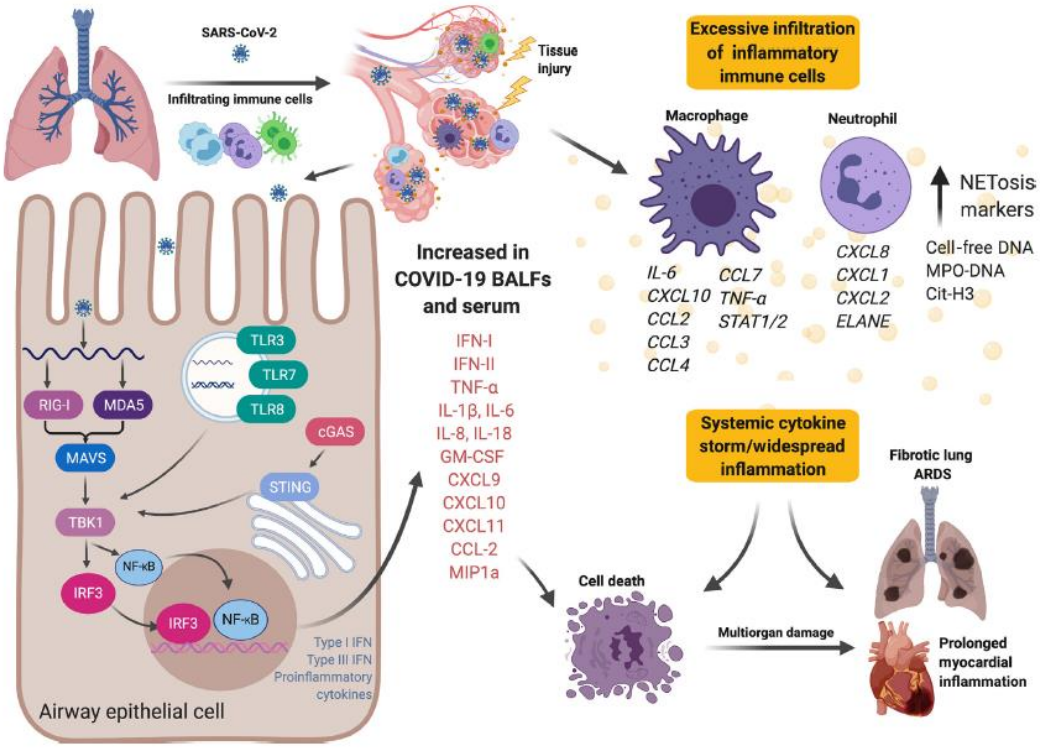

Figure 2. Overview of lung pathology in patients with severe acute respiratory syndrome coronavirus 2. (Withdrawn from reference 9)

The SARS-CoV-2 infection in patients with severe symptoms lead to proinflammatory macrophages and neutrophils in bronchoalveolar lavage fluid (BALF), with elevated proinflammatory cytokines (IL-6 and IL-8, e.g.) in the BALF, along with high expression of inflammatory chemokines (CCL2, e.g.) in macrophages. (**Figure 2**). A noticeable "cytokines storm" occur in patients critically ill with COVID-19. These proinflammatory mediators can elevate C-reactive protein (CRP) from the liver through signal transducer and activator of transcription 3 (STAT3)-IL-6 signaling, which can be correlated with the elevated production of serum IL-6. Additionally, patients with severe symptoms exhibit a pronounced formation of neutrophil extracellular traps (NETs) inside microvessels, that are possible potentiators of pathogenesis. Dysfunction of pulmonary endothelial cells through vascular leakage and compromised barrier function can promote tissue edema and endotheliitis, by the recruitment of activated neutrophiles and monocytes. Therefore, this limits gas exchange and facilitates a hypoxic environment, leading to respiratory and organ failure.[9]

This way, several strategies have been adopted to develop SARS-CoV-2 inhibitors since its outbreak. The main strategies developed aim to block the attachment and entry of the virus into host cells and interfere with viral replication and translation in order to prevent the release of viruses and the infection of other cells.

1.1.1. Spike glycoprotein

The Spike glycoprotein mediates the entry of SARS-CoV-2 into host cells. This glycoprotein assembles into stable homotrimers that protrude from the surface of mature virions and is critical for SARS-CoV-2 entry into the host cell.[5] The SARS-CoV-2 Spike glycoprotein is a trimeric class I fusion protein on the envelope, that consists of two functional subunits: a receptor binding subunit (S1) and a membrane fusion (S2).[13] The S1 subunit contains a N-terminal domain and a receptor binding domain (RBD), which is responsible for binding to a host cell receptor. The S2 subunit contains basic elements, whose functions include fusing the membrane of virus to the host cells.[5] The S1 subunit in CoVs has special domains that recognize different entry receptors. However, SARS-CoV-2 to bind and enter the host cell, it must recognize the host angiotensin converting enzyme 2 (ACE2) through RBD. The main mutations in the RBD of SARS-CoV-2 Spike glycoprotein result in additional contacts with ACE2, which explains its higher affinity when compared to other CoVs.[9,14] The SARS-CoV-2 RBD includes two structural domains: the core and the external subdomains. The core subdomain is composed of five β strands arranged in an antiparallel manner and a conserved disulfide bond between two β strands. The external subdomain is dominated by a flexible loop that connects two β strands by a stabilized disulfide bond.[15]

The Spike glycoprotein has two conformation states that are referred to as the "down" conformation and the "up" conformation. The "down" conformation is the closed state in which the receptor is inaccessible to the fusion, whereas the "up" conformation is the open state, where the receptor is accessible (**Figure 3**). Thus, the fusion of SARS-CoV-2 and the host cell happens when the conformation is "up".[2,5] The binding of SARS-CoV-2 and the host cell triggers a cascade of events that lead to the fusion of the host cell and the viral membranes, which is required for cell entry. The Spike glycoprotein exists in a metastable prefusion conformation, where the S1 and S2 subunits remain non-covalently bound. When the S1 subunit binds to the host cell receptor, it destabilizes the prefusion trimer, which leads to RBD of the S1 subunit to suffer conformational movements that

transiently hide or expose the determinants of receptor binding, and to transition to the S2 subunit for a stable post-fusion conformation.[2,5] Both the S1 and S2 subunits of the Spike glycoprotein are extensively decorated with N-linked glycans, possessing 22 N-linked glycan sites. Therefore, at the surface of the envelope Spike displays 66 N-linked glycosylation sites. These glycosylation sites mediate the protein folding, stability, and shaping viral tropism. The Spike glycoprotein is biosynthesized in the secretory pathway, where the nascent polypeptides are translocated into the endoplasmic reticulum lumen and are modified with the $Glc_3Man_9GlcNAc_2$ glycan structure. This glycan undergoes rapid hydrolytic trimming, with the first steps involving the trimming of glucose units by α-glucosidases I and II. The intermediates from the truncated glycan are necessary for the recognition of calnexin chaperones and calreticulin that facilitate the protein folding. The correctly folded proteins with a $Man_9GlcNAc_2$ structure form $Man_8GlcNAc_2$ glycoproteins trimmed in the B branch that are translocated to the Golgi apparatus.[13,16]

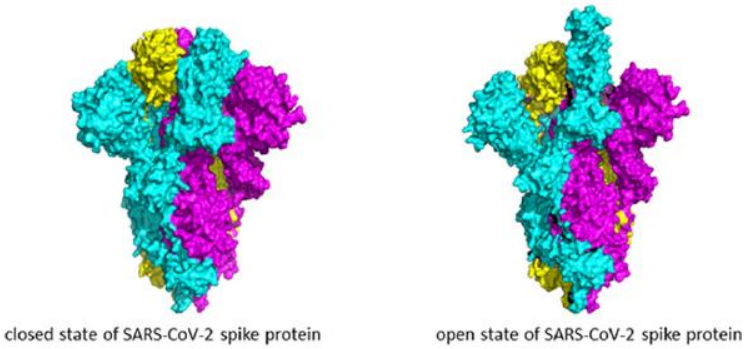

Figure 3. Cryo-EM structure of SARS-CoV-2 Spike glycoprotein. The closed state (left) and open state (right) of Spike glycoprotein. (Adapted from reference 5)

The receptor recognition mechanism of SARS-CoV-2 determines the infectivity, pathogenesis, and the host range of the virus.[17] In fact, several studies have shown that SARS-CoV-2 has higher affinity to ACE2 than other SARS-CoV, which has important implications on the potential animal-to-human transmission of SARS-CoV-2.[17,18] The surface of ACE2 has two major binding hotspots that are essential for SARS-CoV-2 binding. The SARS-CoV-2 RBD interacts with ACE2 through hydrophilic residues located along the interface, which form a solid network of hydrogen bonds and salt bridges interactions.[15] The ACE2 possesses glycans on the interface, however the glycosylation states differ on the tissue, cell type, and the age of the human host. Zhao *et al.* observed glycan-mediated interactions between the Spike glycans and one ACE2 receptor glycan.[19]

On the other hand, Lan *et al.* found that there are 13 hydrogens bonds and 2 salt bridges at the SARS-CoV-2 RBD-ACE2 interface. This hydrogen bonding interactions are made through tyrosine residues from SARS-CoV-2 RBD with polar hydroxyl group on the ACE2. Furthermore, ACE2 has a N-acetyl-β-glucosamine (NAG) glycan attached to an asparagine residue. Although, there was no evidence that SARS-CoV-2 RBD interacts with the NAG glycan, this does not exclude the fact that the glycans after the first NAG may interact with SARS-CoV-2 RBD. It has been proposed that the glycan-RBD interaction has an important role in the binding of SARS-CoV-2 to ACE2.[18]

1.1.2. 3C-Like Protease and Papain-Like Protease

Both 3C-like protease ($3CL^{pro}$) and papain-like protease (PL^{pro}) are non-structural protein encoded by the SARS-CoV-2 genome on the ORF. After the fusion of SARS-CoV-2 with the host cell, the viral RNA is released into the cytosol, which is translated into the replicase proteins.[9] Two replicase polyproteins (pp1a and pp1ab) are cleaved by these proteases, releasing 15-16 non-structural proteins (nsps) at consensus cleavage sites to form the RNA replicase-transcriptase complex (RTC), which is essential for the transcription and replication processes.[9,20–22] Some of these nsps encode proteins with essential functions for virus-mediated RNA replication, so targeting these proteins is an effective antiviral strategy for suppressing viral genome replication in order to cure CoV infection.

The main protease $3CL^{pro}$ of SARS-CoV-2 showed 96% sequence similarity to that of SARS-CoV, and the differences are only at twelve positions in the sequence alignment.[23] The number of amino acid residues in both proteases was identical (306), beginning from Ser1 to Gln306.[24] Recent kinetic characterizations revealed only 2- and 3-fold differences in the kcat/Km values of SARS-CoV and SARS-CoV-2, $3CL^{pro}$ and PL^{pro}, respectively.[25] However, recent studies also revealed marked differences in the kinetic values of SARS-CoV-2 PL^{pro} for ubiquitin (Ub) and interferon-stimulated gene product 15 (ISG15) as compared to its SARS-CoV counterpart.[26] The $3CL^{pro}$ is a dimeric cysteine protease, where each monomer contains one independent active site, rendering the monomers less active than the dimer. The active site is composed of a cysteine and a histidine, where the cysteine acts as a nucleophile and the histidine residue acts as a base.[20–22] The two replicase polyproteins (pp1a e pp1ab), also known as promoters, are packed at almost a right angle.[22] These polyproteins contain three distinct subdomains,

which are named domain I, domain II, and domain III. The domains I and II are antiparallel β-barrels with six strands and are responsible for the interaction with the substrate. Furthermore, these two domains are responsible for the autocatalytic ability of cysteine and histidine residues since the active site is situated between these domains. The domain III consists of five α-helices and is attached to domain II through a long loop. This domain preserves the accurate conformation of the dimer and is therefore critical for the enzymatic activity. The removal of the domain III results in the inactivation of the protease.[20,22,27]

The substrate binds to the cleft that is located between the domains I and II. The amino acids from the N terminus to the C terminus, that belong to the substrate, are numbered as -P4-P3-P2-P1↓P1'-P2'-P3'-P4'-, with the cleavage site between P1 and P1'.[22,28] The $3CL^{pro}$ recognizes the residues from P4 to P1', where P1, P2 and P1' determine the specificity due to their high conservation. The amino acid glutamine in the P1 position is a fundamental requirement. The P2 position prefers leucine but can tolerate hydrophobic amino acids, whereas the P1' position tolerates small residues like serine or alanine. The recognition beyond P1' is not conserved.[29] Therefore, the active sites of $3CL^{pro}$ are composed of four subsites, such as S4, S2, S1 and S1'. These subsites are highly conserved among the CoVs $3CL^{pro}$ and since they are crucial for substrate recognition, they have been the subject of numerous drug design studies.[30] The S1' subsite holds a cysteine residue with a thiol which anchors inhibitors through a covalent linkage, that is crucial to maintain the antiviral activity.[30]

Great efforts have been made to target the SARS-CoV-2 $3CL^{pro}$, while PL^{pro}, which is also responsible for the processing of replicase proteins, has received much less attention. SARS-CoV PL^{pro} is also a cysteine protease, divided into four sub-domains: the N-terminal ubiquitin-like domain (Ubl, β1–3), the α-helical thumb domain (α2–7), the β-stranded finger domain (β4–7), and the palm domain (β8–1). In the finger sub-domain, four conserved cysteine (C189 and C192 on the loop between β4–5, C224 and C226 on the loop between β6–7) form a zinc finger belonging to the "zinc ribbon" fold group. The active site contains a classic catalytic triad, composed of Cys111, His272, and Asp286. Residue Cys111 is located 3.6 Å away from the catalytic histidine Hys272. Residue Hys272 donates a hydrogen bond to Asp286 with the length of 3.0 Å. The hydrogen bond

between Asp108 and Trp93 (2.8 Å) strengthens the conformation of the oxygen anion hole.[31]

Although the primary function of PL^{pro} is to process the viral polyprotein in a coordinated action with $3CL^{pro}$, this protease has the additional function of cleaving ubiquitin and ISG15 from host-cell proteins, thus allowing coronaviruses to escape the host innate immune responses.[32] SARS-CoV-2 PL^{pro} and SARS-CoV PL^{pro} are closely related and diverge from MERS-PL^{pro}. In fact, SARS-CoV-2 and SARS-CoV PL^{pro} proteases share ~82% amino acid sequence identity, so most of the structural features of the orthologs are conserved.[33] However, both proteases exhibit differences in their substrate preferences. Thus, SARS-CoV PL^{pro} strongly reduced the appearance of ubiquitinated substrates, with a lesser effect on ISGylated substrates, whereas SARS-CoV-2-PL^{pro} preferentially reduced the appearance of ISGylated protein substrates.[34] Considering the important roles of PL^{pro} in virus life cycle targeting, this protease is an attractive target for the development of antiviral drugs.[35]

1.1.3. RNA-dependent RNA polymerase

RNA-dependent RNA polymerase (RdRp) is a core component of the virus RTC, involved in the replication and transcription of the SARS-CoV-2 genome through the synthesis of a nascent RNA strand.[36] The RdRp possesses an active site with two magnesium ions that catalyze the phosphodiester bond formation – the RNA template and the ribonucleotide 5′-triphosphatases. Furthermore, there are two channels that meet in the active site, where the main channel contains the RNA template, and the secondary channel allows the ribonucleotide units to build the RNA molecule in the 5′→3′ direction.[37]

The RdRp of SARS-CoV-2 is composed of a core protein known as nsp12[38] as well as two additional subunits, nsp8 and nsp7, required for proper activity.[39] The overall conformation of this RdRp has recently been reported[40] and is highly similar to the RdRp of SARS-CoV, sharing an amino acid identity of 96%. On the other hand, the homology between SARS-CoV-2 RdRp and MERS-CoV RdRp is only 70%.[36] The core protein is a single chain of approximately 900 amino acids and resembles a right hand, subdivided into a finger domain, palm domain, and thumb domain.[36,40] Subunits nsp7 and nsp8 bind to the thumb, and an additional copy of nsp8 binds to the finger domain.[36,40] Two additional Zn ions are also required for the structural stability of the RdRp that are located outside the catalytic site. One of the Zn ion is attached to four amino acid residues (His295, Cys301,

Cys306, and Cys310) in the N-terminal domain, while the second Zn ion is attached to four amino acid residues (Cys487, His642, Cys645, Cys646) located in the finger domain.[36]

As RdRp is a crucial enzyme in the life cycle of coronaviruses, a huge number of attempts have been made to develop anti-RdRp compounds which are under clinical testing.[41]

1.2. Flavonoids and glycosyl flavonoids

Flavonoids are a large group of polyphenolic compounds, consisting of different sub-classes, such as flavonols, flavones, flavanonols, flavanones, flavanols (or catechins), isoflavones, chalcones and anthocyanidins.[42] In plants, flavonoids are formed as secondary metabolites that provide color to seeds, flowers, and fruits. Furthermore, they also give protection by blocking the entry of solar ultraviolet (UV) radiation, and against pathogenic microorganisms; they also regulate plant growth and enzyme activity.[43,44] These compounds are widely distributed in the plant kingdom and are therefore the most common polyphenols in human diet.[45] In fact, flavonoids have received a lot of attention due to their benefits on preventing and managing chronic diseases, such as diabetes, cancer, cardiovascular diseases, influenza, obesity and much more.[46,47] These health benefits are mainly due to their highly recognized antioxidant[48,49], anti-inflammatory[50,51], neuroprotective[52,53], anticarcinogenic[54,55], antidiabetic[56], antimicrobial[57], and antiviral[58,59] properties, together with their capacity to modulate key cellular enzyme functions.[60] In view of the wide range of biological activities displayed by flavonoids, researchers soon turned their heads towards these natural products in the search for weapons against the new coronavirus.

In nature, flavonoids are extensively distributed in their glycosylated form, as glycosyl flavonoids. The glycosyl part of these hybrid derivatives is not only related to improved solubility and the absorption profile, but also has a great influence on recognition processes, and consequently, on the biological profile. Glycosyl flavonoids are structurally composed of a flavonoid aglycone linked to a sugar moiety. Different sugar moieties, can be found in its structure such as glucose, galactose, rhamnose, arabinose, and rutinose.[47] When compared to the flavonoid aglycone, the sugar moiety usually demonstrates improved properties, or may even have different properties, since sugars are involved in most of life processes.[61] Flavonoids are poorly soluble in aqueous solutions, in which they also have the tendency to form insoluble polymers. Upon glycosylation, the solubility of

flavonoids in water is greatly enhanced, leading to an improvement of their pharmacological properties. Thus, glycosylation not only increases flavonoids bioavailability, but also decreases their acute toxicity or harmful effects.[62] The stability of flavonoids towards oxidative degradation is also affected upon glycosylation; thus, the addition of the sugar moiety that can block the phenolic group, results in enhanced stability.[63,64] In general terms, most biological activities are usually less pronounced in glycosides, but some specific bioactivities, including the anti-*human immunodeficiency virus* (HIV) and the anti-*rotavirus*, are enhanced.[47]

Glycosyl flavonoids are divided into two groups: *O*-glycosyl flavonoids and *C*-glycosyl flavonoids. In nature, they exist primarily as *O*-glycosyl flavonoids, where the sugar moiety is linked by an *O*-glycosidic bond to the flavonoid aglycone. In the *C*-glycosyl flavonoids, the flavonoid and sugar group are linked by a *C*-glycosidic bond. The types of glycosidic bonds, and the regioselectivity and stereoselectivity of the glycosylation are related with the glycosyl transferase used in their biosynthesis.[61] Despite *O*-glycosyl flavonoids are the most common and structurally diverse metabolites in plants, *C*-glycosyl flavonoids exhibit different activities and properties in comparison to the *O*-glycosyl flavonoids. Since *C*-glycosidic bonds are less prone to hydrolysis than *O*-glycosidic bonds, *C*-glycosyl flavonoids present enhanced stability towards enzymatic and chemical hydrolysis and improved activity of the aglycones after their *C*-glycosylation.[45] In fact, the deglycosylation of *C*-glycosyl flavonoids is not imperative for their absorption, and this is corroborated by the presence of intact *C*-glycosyl flavonoids in the human urine after the oral consumption.[45]

1.2.1. Biological activity of flavonoids and glycosyl flavonoids

Flavonoids have received a lot of attention over the years due to their biological benefits. In fact, flavonoids have long been associated with their powerful antioxidant activities. Since oxidative stress has recently been proposed as an essential factor that increases the severity of COVID-19, interest in natural flavonoids has grown exponentially over the past year.[65] Since flavonoids can be found in nature in their glycosidic form, the sugar molecules attached to the flavonoid aglycone may play a crucial role in biological activity. The *C*-glycosyl flavonoids have been scarcely studied, however, there are some studies evaluating their antioxidant, anti-inflammatory, antidiabetic, anticancer and antiviral activities.[45,66]

In some studies, the antioxidant activity of flavonoids and glycosyl flavonoids was evaluated, however, glycosylation seems to generally reduce antioxidant activity. For example, the radical scavenging activities of quercetin and its glycosides, isolated from *Halimodendron halodendron*, were determined in DPPH assay, and quercetin (**1**) and 3-*O*-methylquercetin (**2**) presented the highest antioxidant activities. The 3,3'-di-*O*-methylquercetin-7-*O*-β-D-glucopyranoside (**3**) and narcissoside (**4**) presented weak radical scavenging activity (**Figure 4**). This study indicated that the *O*-glycosylation decreases the DPPH radical scavenging activity.[67] Choi *et al.* tested the *in vitro* and cellular antioxidant capacities of quercetin and its glycosides. Although isoquercitrin (**5**) and quercitrin (**6**) show moderate antioxidant activity, quercetin (**1**) and hyperin (**7**) displayed strong cellular antioxidant capacity (**Figure 4**). These results suggested that the high cell-permeability of quercetin (**1**) and hyperin (**7**) was due to the hydrophobicity and the specific membrane receptor for galactose in the Hepatoma HepG2 cells.[68] Hesperidin (**8**) showed high antioxidant activity; however, it has been shown that this property is not limited to radical scavenging. In fact, hesperidin has the capability to attenuate tissue damage through antioxidant cellular defenses via the ERK/Nrf2 signaling pathway, which leads to the decrease in intracellular pro-oxidants and an increase in bilirubin as an internal antioxidant.[69]

Besides their antioxidant activity, flavonoids are also well-known anti-inflammatory agents due to their cytokine-modulatory effects. The severity of SARS-CoV-2 infection is related to hypercytokinemia, an exaggerated immune response associated with an excessive and uncontrolled release of proinflammatory cytokine mediators – the so-called cytokine storm.[70] Choi *et al.* also tested the anti-inflammatory activity of quercetin (**1**) and its glycosides.[68] Although every compound presented anti-inflammatory activity, quercetin showed the highest efficacy in suppressing the nitric oxide (NO) production, decreasing the inducible nitric oxide synthase (iNOS) and cyclooxygenase-2 (COX-2) expression, and suppressing the nuclear factor kappa B (NF-κB) activation. Quercetin (**1**) and quercitrin (**6**) showed a dose-dependent decrease of iNOS levels, while treatment with hyperin (**7**) and isoquercitrin (**5**) presented a non-dose-dependent suppressive effect. Consequently, the other mediator of the pro-inflammatory process, COX-2, was also attenuated in a dose-dependent manner. These results indicated that quercetin (**1**) and its glycosides inhibit NO production in LPS-stimulated RWAS 264.7

cells through attenuation of iNOS and COX-2 expression. The decrease of these levels is induced through suppression NF-κB activation via phosphorylation, since NF-κB upregulates the iNOS and COX-2 expression. Hesperidin (**8**) also showed anti-inflammatory activity through down-regulation of iNOS and COX-2 in various *in vitro* and *in vivo* studies.[68] More recently, hesperidin was found to attenuate high levels of angiotensin II (AngII) in hypertensive rat models.[71] The anti-inflammatory effect mediated through anti-angiotensin action has previously been described for other flavonoid derivatives, such as glycosyl flavonoid nepitrin (**9**).[72]

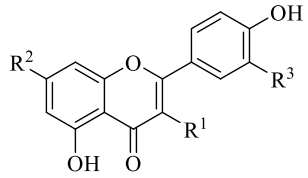

(**1**) Quercetin; $R^1 = R^2 = R^3 = OH$
(**2**) 3-O-Methylquercetin; $R^1 = OCH_3$, $R^2 = R^3 = OH$
(**3**) 3,3'-Di-*O*-Methylquercetin-7-*O*-glucoside; $R^1 = R^3 = OCH_3$, R^2 = 7-*O*-β-D-glucopyranoside
(**5**) Isoquercitrin (Quercetin 3-*O*-glucoside); R^1 = 3-*O*-β-D-glucopyranoside, $R^2 = R^3 = OH$
(**6**) Quercitrin (Quercetin 3-*O*-rhamnoside); R^1 = 3-*O*-α-L-rhamnopyranoside, $R^2 = R^3 = OH$
(**7**) Hyperin (Quercetin 3-*O*-galactoside); R^1 =3-*O*-β-D-galactopyranoside, $R^2 = R^3 = OH$

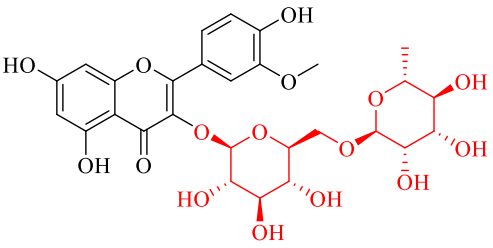

(**4**) Narcissoside
(Isorhamnetol 3-*O*-rutinoside)

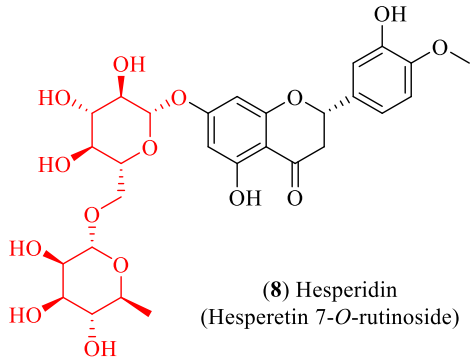

(**8**) Hesperidin
(Hesperetin 7-*O*-rutinoside)

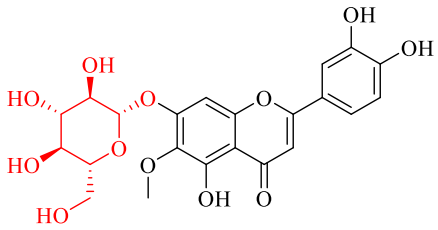

(**9**) Nepitrin
(Nepetin 7-*O*-glucoside)

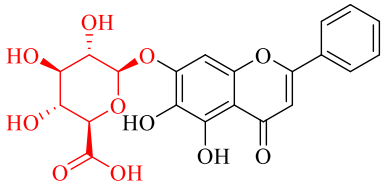

(**10**) Baicalin
(Baicalein 7-*O*-glucuronide)

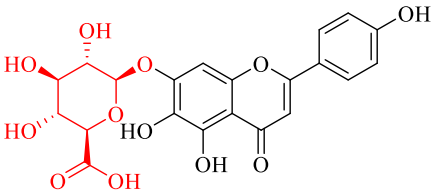

(**11**) Scutellarin
(Scutellarein 7-*O*-glucuronide)

Figure 4. Antioxidant and anti-inflammatory flavonoids and glycosyl flavonoids.

Several other glycosyl flavonoids have been reported to modulate inflammatory mediators or signaling cascades, including toll-like receptors (TLRs) and NLR family

pyrin domain containing 3 (NLRP3) inflammasomes. For example, baicalin (**10**) showed an effective protection of neurons from microglia-mediated neuroinflammation via the suppression of NLRP3 inflammasomes and the TLR4/NF-κB signaling pathway[73], while scutellarin (**11**) displayed the suppression of NLRP3 inflammasome activation in macrophages.[74] Considering that the deregulation of TLRs and NLRP3 is closely related to the severity of SARS-CoV-2 pathology, it can be assumed that glycosyl flavonoids could exert significant antiviral and immunomodulatory effects mediated through TLRs or NLRP3 inflammasomes in COVID-19 patients. However, these potential effects need to be evaluated further in well-defined pre-clinical and clinical studies.

As most viral envelope glycoproteins contain N-linked glycans, α-glucosidase inhibitors have been proposed as potentially useful broad-spectrum antiviral agents based on their activity on a variety of enveloped viruses.[75] In this regard, some flavonoids and glycosyl flavonoids have been evaluated for their inhibitory activity of glucosidases. Hyperin (**7**), quercitrin (**6**), baicalin (**10**), astragalin (**12**), rutin (**13**) and pectolinarin (**14**) (**Figures 4 and 5**) exhibited low α-glucosidase inhibitory activity. On the other hand, luteolin (**15**) and cynaroside (**16**) showed strong inhibitory activity against α-glucosidase (IC_{50} 1.7 – 3.5 μM), while lonicerin (**17**) and rhoifolin (**18**) inhibited α-amylase significantly (IC_{50} 8.4 – 84.0 μM).[76] Shibano *et al.* studied the antioxidant and antidiabetic activity of several glycosyl flavonoids. The DPPH radical scavenging activities of the glycosyl flavonoids isolated from *Commelina communis* L., showed that isoquercitrin (**5**), cynaroside (**16**), orientin (**19**) and isoorientin (**20**) (**Figures 4 and 5**) were potent antioxidants. In addition to their antioxidant activity, narcissoside (**4**), isoquercitrin (**5**), vitexin (**21**), and swertisin (**22**) (**Figures 4 and 5**) inhibited α-glucosidase (IC_{50} 0.51, 0.24, 0.42 and 0.37 μM, respectively).[77] Choo *et al.* reported the α-glucosidase inhibitory potential of vitexin (**21**) and isovitexin (**23**) (**Figure 5**) isolated from the leaves *Ficus deltoidea*. In this *in vivo* study, vitexin (**21**) and isovitexin (**23**) showed a high percentage of postprandial blood glucose reduction on the sucrose-loaded normoglycemic mice and induced diabetic rats. Therefore, the report supports the use of vitexin and isovitexin for managing diabetes mellitus and its complications.[78]

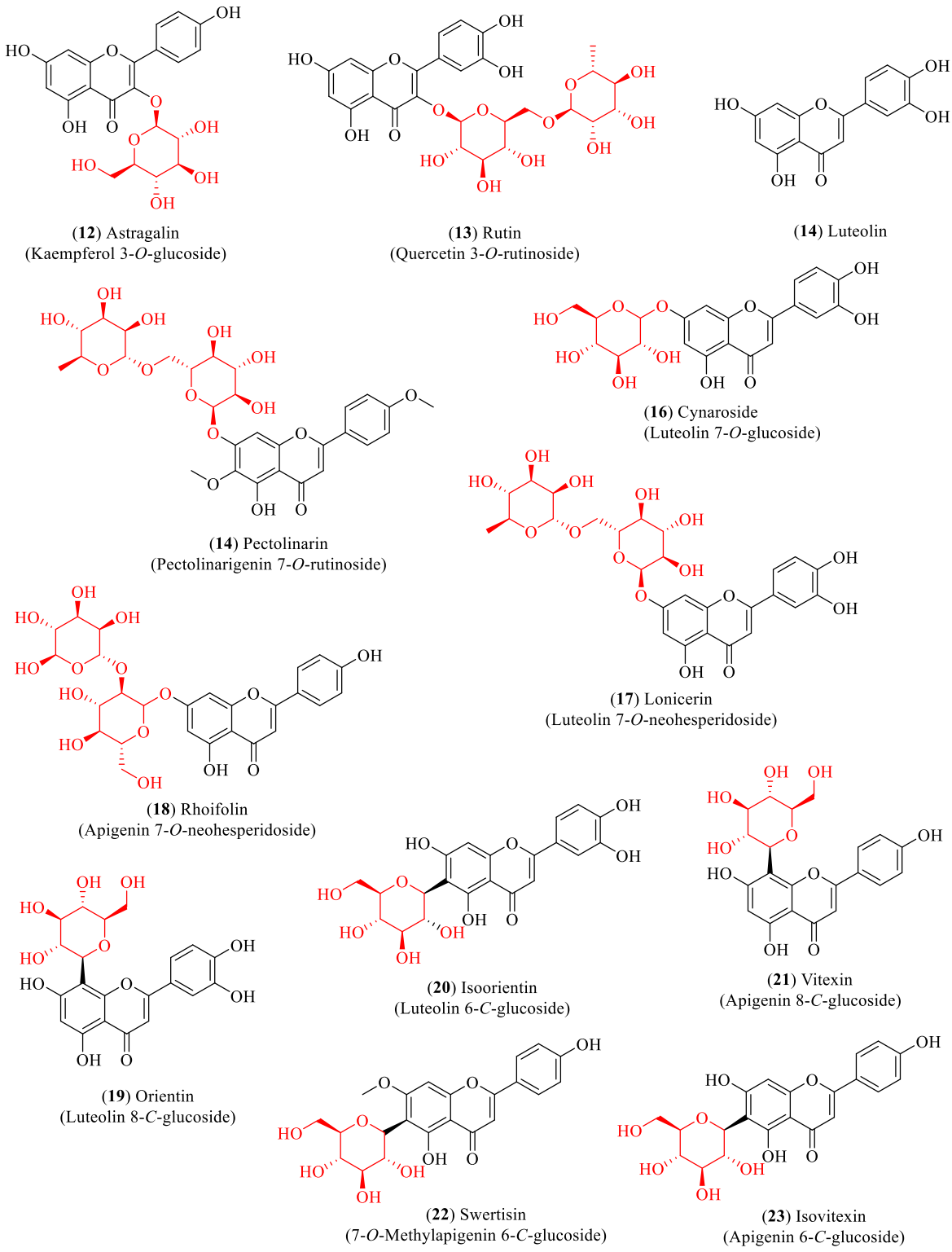

Figure 5. Antioxidant and antidiabetic flavonoids and glycosyl flavonoids.

1.2.2. Antiviral activity of flavonoids and glycosyl flavonoids

The traditional medicines are based on plants, and these are used in different parts of the world. A huge number of natural compounds, found in plants, belonging to different

chemical classes, have been identified as potential therapeutic agents. In the plant kingdom, flavonoids are one of the largest groups of polyphenolic compounds, with more than 9000 structures reported.[79] The antiviral properties of flavonoids were discovered in 1940s, being the quercetin (**1**) among these compounds.[80,81] Since then, flavonoids have been studied as possible therapeutic agents against many viruses. In fact, they can work through several different mechanisms, such as blocking the attachment and entry of the virus into host cells, interfering with various stages of viral replication processes or translation, and polyprotein processing to prevent the release of the viruses to infect other cells.[82]

Since glycosyl flavonoids are widely distributed in the plant kingdom, they also have been studied as antiviral agents. Indeed, several glycosyl flavonoids have demonstrated inhibitory effects against several viruses (**Figure 6, Table 1**).[83–97]

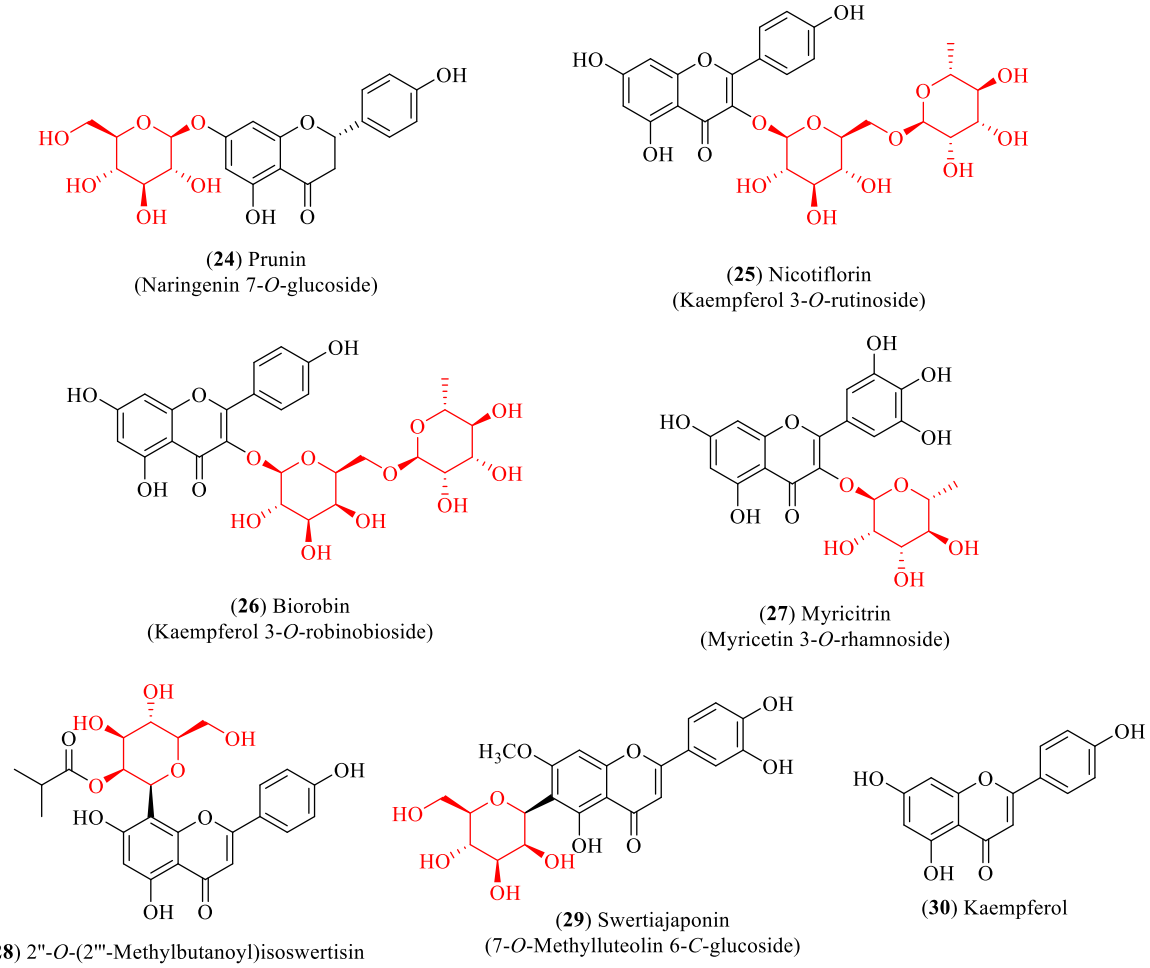

Figure 6. Antiviral flavonoid and glycosyl flavonoids.

Table 1. Antiviral activity of glycosyl flavonoids.

Virus	Compound	Source	IC_{50} (μM)[a]	Reference
Ebola virus	Isoquercitrin (**5**)	–	5.3	83
Enterovirus A71	Baicalin (**10**)	–	11.1	89
	Hesperidin (**8**)	–	–[b]	90
	Prunin (**24**)	–	–[b]	91
	Rutin (**13**)	–	109.6	85
Hepatitis B virus	Isovitexin (**23**)	*Swerbia yunnanensis*	–[b]	92
Herpes simplex virus	Rutin (**13**)	*Ficus benjamina*	–[b]	93
	Nicotiflorin (**25**)	*Ficus benjamina*	–[b]	93
	Biorobin (**26**)	*Ficus benjamina*	–[b]	93
Human immunodeficiency virus type 1	Baicalin (**10**)	*Scutellaria baicalensis*	–[b]	87
	Myricitrin (**27**)	*Marcetia taxifolia*	7.6	94
Influenza A virus	2’’-*O*-(2’’’-methylbutanoyl) isoswertisin (**28**)	*Trollius chinensis*	147.8	95
	Quercitrin (**6**)	*Houttuynia cordata*	–[b]	84
	Baicalin (**10**)	*Scutellaria baicalensis*	–[b]	88,96
Respiratory syncytial virus	Isoorientin (**20**)	*Lophoterum gracile*	12.7	97
	Swertisin (**22**)	*Lophoterum gracile*	112.0	97
	Isovitexin (**23**)	*Lophoterum gracile*	23.1	97
	Swertiajaponin (**30**)	*Lophoterum gracile*	27.1	97

[a] Although the IC_{50} values should be indicated with the error, this was not done because most of these values taken from the literature did not present the corresponding error.
[b] Not described

For example, several derivatives of quercetin, such as isoquercitrin (**5**) can protect mice from the *Ebola virus* infection when given prior to infection. Even though the mechanism of action is unknown, isoquercitrin targets the early steps of viral entry (IC_{50} 5.3μM).[83] Another quercetin glucoside, quercitrin (**6**) was found to inhibit the initial stage of virus replication in *influenza A virus* infection without direct interaction with the virus particles.[84] Moreover, glycosyl flavonoid rutin (**13**) inhibits *Enterovirus A71* 3C protease during the replication stage with an IC_{50} of 109.6 ± 1.1μM, significantly reducing viral plaque formation and the cytopathic effect.[85] This inhibition is associated with the

suppression of the MERK-ERK signaling pathway that is required for an efficient *Enterovirus A71* replication.[86]

Baicalin (**10**) is another glycosyl flavonoid known to be an antiviral agent against *human immunodeficiency virus type 1* (HIV-1), *influenza A virus*, and *Enterovirus A71* (**Table 1**). Baicalin can inhibit the entry of HIV-1 since it interferes with the interaction of the envelope proteins of the virus with the host immune cells.[87] Baicalin can increase the interferon-gamma (INF-γ) in human CD4+ and CD8+T lymphocytes (CTL) and natural killer (NK) during the *influenza A virus* infection. The induction of INF-γ leads to the activation of Janus Kinase/Signal Transducer and Activator of Transcription (JAK/STAT-1) signaling pathway, leading to the expression and secretion of INF-γ.[88] In addition, baicalin exhibits potent antiviral activity against *Enterovirus A71*. Regarding the mode of action, baicalin blocked the expression of mRNA and polymerase in early stages of infection, by decreasing the expressions of Fas ligand (FasL) and caspase-3 that inhibit the *Enterovirus A71* apoptosis in Rhabdomyosarcoma cells. Moreover, baicalin suppresses the NF-κB signaling pathway, decreasing the secretion of cytokines.[89]

1.3. Flavonoids and glycosyl flavonoids as anti-coronaviral agents

The COVID-19 epidemic caused by the novel coronavirus (SARS-CoV-2) infection is a public health emergency of international concern. Despite several vaccines having been approved, the infection is still spreading at an alarming rate. In the absence of confirmed effective treatments and due to public health emergency, it became crucial to study the possible effects of natural compounds or their synthetic analogues for the management of SARS-CoV-2.[98] Since the outbreak of SARS-CoV-2 in China, patients have been treated with a traditional Chinese medicine as a first-line drug.[99] In February 2020, the rate of this treatment was 87%, with only 5% of patients showing the worst clinical signs. The Qingfei Paidu Decoction, a formula consisting of 21 components including both herbs and mineral drugs, showed an effectiveness of 92% in patients at all stages of infection. Therefore, Yang *et al.* identified 129 constituents clustered into 14 groups, from which 45% were flavonoids.[100] These findings sparked interest in the study of flavonoids and glycosyl flavonoids as potential anti-SARS-CoV-2 agents.[101,102] In addition, several flavonoids have been identified to inhibit other CoVs, such as SARS and MERS.

The anti-coronaviral action of glycosyl flavonoids is in part due to the inhibition of the enzymatic activity of key targets involved in processes of virus replication, such as

SARS-CoV-2 $3CL^{pro}$, spike glycoprotein, SARS-CoV-2 PL^{pro}, and RdRp. On the other hand, during viral infection, changes in the body's antioxidant defense system lead to oxidative stress, which contributes to viral pathogenesis by stimulating inflammation, loss of immune function, and increased viral replication that may occur due to the activation of the NF-κB transcription pathway and may lead to a cytokine storm. The significant antioxidant action of flavonoids contributes to the reduction of reactive oxygen species (ROS) accumulation in the body, which might contribute to retard coronavirus-activated apoptotic signaling. Thus, the mechanism of oxidative stress can be a key mechanism for controlling inflammatory processes arising from the virus action.[103]

The $3CL^{pro}$ is involved in the replication and transcription of the viral RNA in the host cells. Since SARS-CoV and MERS-CoV proteases are very similar to SARS-CoV-2 protease, inhibitors of the first two viruses are expected to inhibit the replication and transcription of the genomic RNA of SARS-CoV-2. Flavonoids quercetin (**1**), epigallocatechin gallate (EGCG) (**33**) and gallocatechin gallate (GCG) (**34**) showed good inhibition of SARS-CoV $3CL^{pro}$ with IC_{50} values of 73 ± 4, 73 ± 2 and 47 ± 0.9 μM, respectively.[104] In a study to understand the interaction between the compounds and SARS-CoV $3CL^{pro}$, molecular docking simulations were used, and it was found that CGC displayed the lowest free binding energy. This compound interacts with the residues in the catalytic pocket of SARS-CoV $3CL^{pro}$ through seven hydrogen bonds, being four hydrogen bonds owed to the galloyl group interaction.[104] The quercetin glycoside isoquercitrin (**5**) was found to block the enzymatic activity of MERS-CoV $3CL^{pro}$. The docking study showed that the glucosyl moiety binds strongly to the S1 subsite of MERS-CoV $3CL^{pro}$, through a hydrogen bond.[105] Jo *et al.* found that pectolinarin (**14**) and rhoifolin (**18**) have an inhibitory activity towards SARS-CoV $3CL^{pro}$ with IC_{50} values of 37.78 and 27.45 μM, respectively (**Table 2**). The high binding affinity to the S1 and S2 subsites of SARS-CoV $3CL^{pro}$ is associated with the presence of sugar moieties.[106]

Su *et al*. described the anti-SARS-CoV-2 potential of the Shuanghuanglian preparation, a Chinese traditional patented medicine with a long history of treating respiratory tract infections in China and identified glycosyl flavonoid baicalin (**10**) as the major bioactive ingredient.[107] Baicalin was reported as an inhibitor of SARS-CoV-2 $3CL^{pro}$ through an enzymatic assay in combination with the ITC, ESI-MS, and X-ray protein crystallography. Although several other small molecules have been declared $3CL^{pro}$

inhibitors[108–111], this was the first report in which the binding with 3CL^{pro} was validated by ITC and complex structure. Thus, baicalin was tested by the FRET-based protease assay, showing an IC_{50} of 6.41 μM against SARS-CoV-2 3CL^{pro} (**Table 2**). To validate the binding of baicalin with 3CL^{pro} and exclude the possibility of the pan-assay interference compounds, their binding affinities with the protease were measured by ITC. The resulting K_d of baicalin binding with SARS-CoV-2 3CL^{pro} was 11.50 μM. The good correlation with the IC_{50} value demonstrated that the specific binding of baicalin with the enzyme was responsible for the antiviral activity. The antiviral efficacy of baicalin was further evaluated against a clinical isolate of SARS-CoV-2 in Vero E6 cells, showing dose-dependent inhibition of SARS-CoV-2 replication (EC_{50} = 27.87 μM). In a further study, both baicalin (**10**) and pectolinarin (**14**) revealed prominent inhibitory activity against SARS-CoV-2 3CL^{pro}, with measured IC_{50} values of 34.71 and 51.64 μM, respectively (**Table 2**).[112] To deduce the binding mode and binding affinity, Jo *et al.* performed an *in silico* docking study which showed fundamental differences in the binding of baicalin (**10**) as compared to pectolinarin (**14**). In pectolinarin, the sugar moiety occupies the S1 and S2 subsites of 3CL^{pro}, whereas the 4*H*-chromen-4-one moiety is in the S2 and S'3 subsites. In baicalin, the binding mode is severely influenced by the presence of the glucuronate sugar moiety. Thus, the important hydrogen bonds with Glu166 are formed by the 6-hydroxy group linked to the 4*H*-chromen-4-one moiety and also by the 5-hydroxy group attached to the glucuronate moiety.[112]

Table 2. Anti-coronaviral activity of glycosyl flavonoids.

Target	Compound	IC_{50} (μM)[a]	Reference
MERS-CoV 3CL^{pro}	Isoquercitrin (**5**)	– [b]	105
SARS-CoV 3CL^{pro}	Pectolinarin (**14**)	37.78	106
	Rhoifolin (**18**)	27.45	106
SARS-CoV-2 3CL^{pro}	Baicalin (**10**)	6.41	107
		34.71	112
	Pectolinarin (**14**)	51.64	112

[a] Although the IC_{50} values should be indicated with the error, this was not done because most of these values taken from the literature did not present the corresponding error.
[b] Not described

These findings prompted many studies on the inhibition of 3CL^{pro} by glycosyl flavonoids using molecular docking technology and simulation studies (**Table 3**). For

example, a computational study showed that narcissoside (**4**), a glycosyl flavonoid present in several wild plants, fits perfectly at the active site of 6W63, the experimental structure of SARS-CoV-2 $3CL^{pro}$.[113] Narcissoside (**4**) showed to be a potent inhibitor compared with a standard inhibitor X77 [(*R*)-*N*-(4-*tert*-butylphenyl)-*N*-(2-(cyclohexylamino)-2-oxo-1-(pyridin-3-yl)ethyl)-1*H*-imidazole-5-carboxamide], since it showed thirteen hydrogen bonds with nine amino acids in the active site pocket of 6W63, whereas X77 showed only four hydrogen bonds with four amino acids (**Table 3**).[113]

Recently, quercetin (**1**) was found to have the ability to inhibit the $3CL^{pro}$ of SARS-CoV-2 in an experimental *in vitro* molecular screening.[114] Despite being a potent *in vitro* inhibitor of $3CL^{pro}$, low *in vivo* bioavailability of quercetin hampers its potential as a therapeutic anti-coronaviral agent. To address this issue, Rizzuti *et al.* investigated the effect of glycosylation on quercetin binding to $3CL^{pro}$ by using rutin (**13**), a natural glycosylated conjugate of quercetin, as a model. Combining experimental (spectroscopy and calorimetry) and simulation techniques (docking and molecular dynamics simulations), it was found that the sugar adduct does not hamper rutin (**13**) binding to $3CL^{pro}$, and the conjugated compound preserves a high potency (inhibition constant in the low micromolar range, K_i = 11 μM). Such validation constitutes an important proof-of-concept that the presence of a sugar adduct allows the glycoside form to retain the key bioactive features of the aglycone lead compound.[115]

However, another molecular docking and simulation study showed that quercitrin (**7**), myricetin 3-*O*-rutinoside (**31**), and rutin (**13**) are potential drug candidates with high affinity to the active pocket of SARS-CoV-2 $3CL^{pro}$ (**Figure 7**).[116] This study also showed that flavonoids glycosylated at C-3 position bind with higher affinity.[116] The $3CL^{pro}$ inhibitory activity of rutin (**13**) was also confirmed in later studies.[117,118] Thus, a molecular docking approach demonstrated high affinity of rutin (**13**), nicotiflorin (**27**), and their human metabolites to SARS-CoV-2 $3CL^{pro}$ and also to RdRp.[117] Additionally, Agrawal *et al.* described that rutin matched very well with the 6GLU7 binding pocket of $3CL^{pro}$ and that it is able to form several hydrogen bonds and σ-π stacking interactions with various amino acids, suggesting that it may be a good inhibitor.[118] Furthermore, a docking study revealed scutellarin (**11**) as a potent candidate for targeting $3CL^{pro}$.[119]

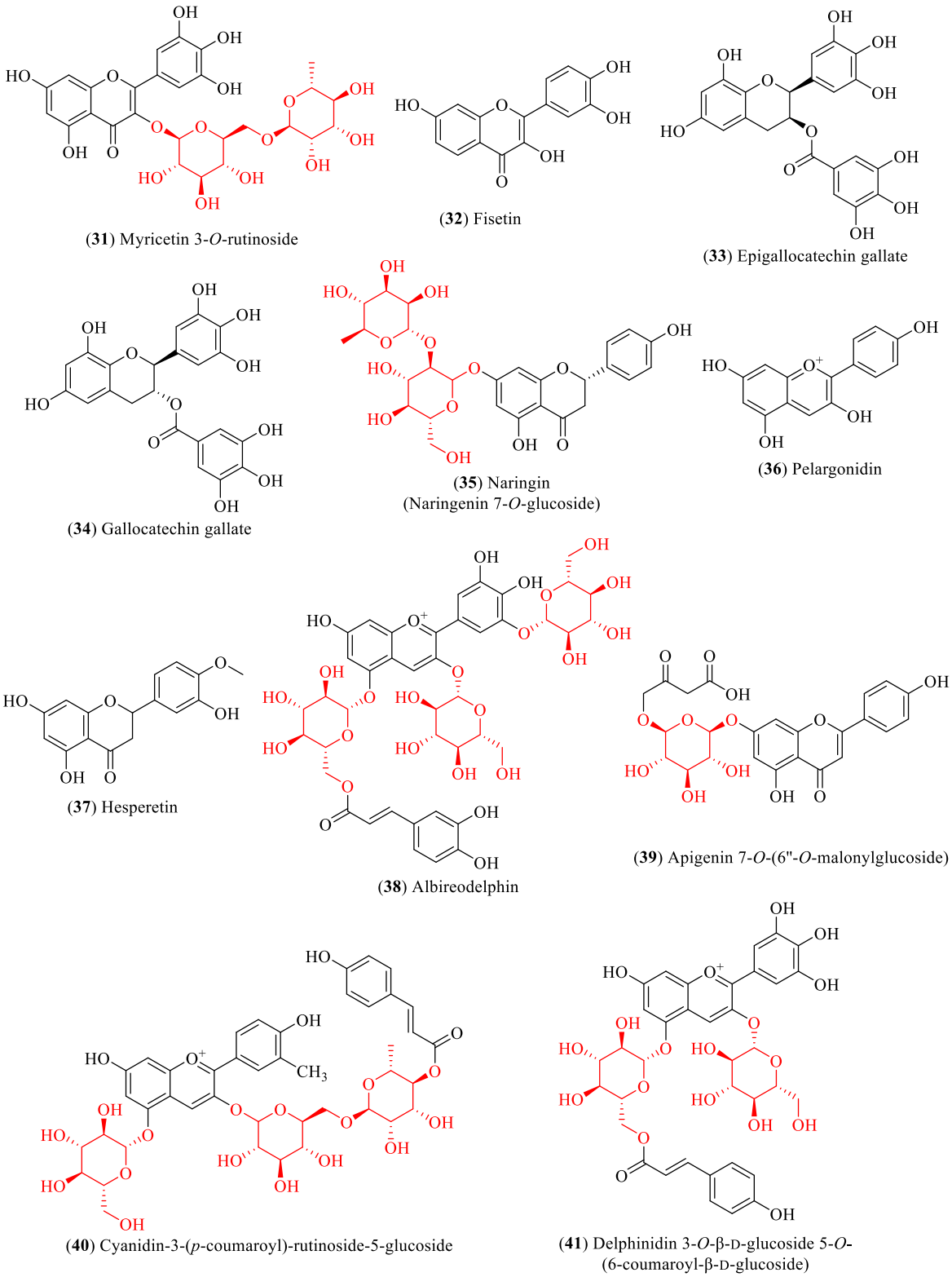

Figure 7. Anti-coronaviral flavonoids and glycosyl flavonoids.

In contrast, the Spike glycoprotein plays a crucial role in SARS-CoV-2 infection since it is involved in viral attachment, fusion and entry into host cells, thus promoting its

pathogenesis. This glycoprotein binds ACE2 receptor through hydrogen bonds and salt bridges with high affinity to enter in the host cell. Therefore, SARS-CoV-2 Spike glycoprotein is a potential therapeutic target, which has prompted many efforts to study the binding ability of natural compounds to the functional domains of this protein by means of molecular docking technology and simulation studies (**Table 3**). These computational studies provide valuable information for the discovery of the potential inhibitors of SARS-CoV-2; however, they have disadvantages such as low accuracy and high rate of false positive results. Despite these drawbacks, the biological evaluation of the potential anti-coronaviral agents identified through molecular docking can be useful, not only for the identification of novel pharmacological leads, but also for the improvement of screening accuracy.[101]

Pandley *et al.* reported that, according to the results obtained using molecular docking, flavonoids quercetin (**1**), kaempferol (**30**), and fisetin (**32**) bind to the Spike glycoprotein with a higher binding affinity than hydroxychloroquine[120], an analog of chloroquine that has received a lot of attention since it emerged as a potential therapeutic option against SARS-CoV-2.[121] Fisetin and quercetin exhibited a preference to bind to S2 domain of Spike glycoprotein through three and six hydrogen bonds, respectively, whereas kaempferol binds to S1 domain through three-four hydrogen bonds.[120] The same authors reported that baicalin (**10**) has a very high affinity to Spike glycoprotein, not only higher than standard drugs, like hydroxychloroquine and abacavir, but also higher than quercitrin (**6**) (**Table 3**).[122] Another *in silico* study that points to glycosyl flavonoids as effective antiviral agents was recently disclosed.[123] This study showed that glycosyl flavonoid naringin (**35**), widespread in citrus fruits, presented a high affinity to SARS-CoV-2 Spike glycoprotein, since it was able to stablish hydrogen bonds with the least binding energy.[123] These computational studies suggest that glycosyl flavonoids and spike glycoprotein could create stable complexes. The *in-silico* results have already been confirmed for several flavonoid derivatives. Thus, Biagioli *et al.* recently reported molecular docking studies suggesting that anthocyanidin pelargonidin (**36**) binds a fatty acid binding pocket to the receptor binding domain of the SARS-CoV-2 Spike glycoprotein. *In vitro* studies subsequently demonstrated that pelargonidin significantly reduces the binding of the SARS-CoV-2 Spike glycoprotein to ACE2, affecting the virus uptake and replication.[124] In a recent report about the inhibition effect of *Anatolian propolis* against SARS-CoV-2, *in-*

silico studies showed that several flavonoids bind stronger to the SARS-CoV-2 Spike glycoprotein than the reference molecule, hydroxychloroquine. Then, the ability of these flavonoids to inhibit the interaction of the SARS-CoV-2 S1 Spike glycoprotein and ACE2 was tested *in vitro*. Hesperidin aglycone hesperetin (**37**) was the best inhibitor against the SARS-CoV-2 S1 Spike glycoprotein and ACE2, with an IC_{50} value of 11.13 mM.[125]

Table 3. Molecular docking analysis of anti-coronaviral glycosyl flavonoids.

Target	Compound	Amino Acid Residues	Reference
SARS-CoV-2 3CL^{pro}	Narcissoside (**4**)	Arg188, Glu166, His164, Cys145, Asn14, Cys44, His41, Gln192, Thr190	113
	Rutin (1**3**)	Leu141, Thr26, Cys145, His41, Met49, Tyr54, Met165, Glu166	115–118
	Quercitrin (**6**)	Thr26, Phe140, Leu141, Gly143, His163, Arg188, Met49, Cys145	116
	Nicotiflorin (**27**)	Met49, Met165, Glu166, Thr190, Cys 145, His 41	117
	Myricetin 3-*O*-rutinoside (**31**)	Tyr54, His41, Met49, Met165, Thr26, Cys145, Ser144, Leu141, Gly143, Asn142, His163, Glu166	116
	Albireodelphin (**38**)	Lys5, Val125, Lys137, Ser139, Thr199, Glu288	126
	Apigenin 7-(6’’-malonyl-glucoside) (**39**)	Gln110, Thr111, Thr292, Asp295	126
	Cyanidin-3-(*p*-coumaroyl)-rutinoside-5-glucoside (**40**)	Thr111, Gln110, Asn151	126
	Delphinidin 3-*O*-β-D-glucoside 5-*O*-(6-coumaroyl-β-D-glucoside) (**41**)	Asp153, Asn151, Ser158, Thr111, Ile249	126
	Isoquercitrin (**5**)	Leu141, His163, Met165	127
Spike glycoprotein	Baicalin (**10**)	Lys964, Gln965, Leu962, Thr961, Ser1003, Ala958, Tyr1007, Gln1011, Gln1010, Arg1014	122
	Naringin (**35**)	Asn290, Ile291, His374, Leu370, Leu410, Ala413, Pro415, Phe438, Gln442, Asp367, Thr371, Lys441, Glu406, Ser409	123
	Albireodelphin (**38**)	Lys621, Asp623, Phe793, Lys798,	126

		Asp760, Asp761, Trp800, Glu811, Cys813, Ser814	
	Apigenin 7-(6''-malonyl-glucoside) (**39**)	Asp452, Trp617, Tyr619, Lys621, Asp760, Asp761, Trp800	126
	Cyanidin-3-(*p*-coumaroyl)-rutinoside-5-glucoside (**40**)	Asp164, Ile548, Ser549, Arg553, Arg555, Asp760, Asp761	126
	Delphinidin 3-*O*-β-D-glucoside 5-*O*-(6-coumaroyl-β-D-glucoside) (**41**)	Ser549, Arg553, Arg555, Thr556, Cys622, Asp623, Asp760, Asp761	126
	Isoquercitrin (**5**)	Thr998, Arg995, Asp994	127
RdRp	Rutin (**13**)	Tyr455, Arg553, Ala554, Asp452, Arg624, Asp623, Asn691, Ser759, Thr556, Asp760, Cys622	117
	Albireodelphin (**38**)	Arg348, Asp350, His378, Asp382, Phe390, Asn394, Asn397, Glu398, His401, Glu402, Arg514	126
	Apigenin 7-(6''-malonyl-glucoside) (**39**)	Als348, Asp350, His378, Asp382, Gly395, Asn394, His401	126
	Cyanidin-3-(*p*-coumaroyl)-rutinoside-5-glucoside (**40**)	Ser44, Asp206, Als348, Asp350, Asn397, Glu398, Ser511, Arg514	126
	Delphinidin 3-*O*-β-D-glucoside 5-*O*-(6-coumaroyl-β-D-glucoside) (**41**)	Try127, His345, Ala348, Asp350, Asp382, Tyr385, Asn394, Asn397, Arg401, His505, Arg514, Tyr515	126
	Isoquercitrin (**5**)	Ala125, His133	127
SARS-CoV-2 PL^{pro}	Isoquercitrin (**5**)	His74, Arg83, Tyr155, Asn157, His176	127

In order to identify the multiple target binding potential, Rameshkumar *et al.* screened a library of flavonoid compounds *in silico* against the two major targets of SARS-CoV-2 3CL^{pro} and Spike glycoprotein – as well as with the RdRp protein target.[126] The docking studies revealed that glycosyl flavonoids albireodelphin (**38**), apigenin 7-(6″-malonylglucoside) (**39**), cyanidin-3-(*p*-coumaroyl)-rutinoside-5-glucoside (**40**), and delphinidin 3-*O*-β-D-glucoside-5-*O*-(6-coumaroyl-β-D-glucoside) (**41**) had high binding energy values against all the three protein targets studied. In addition, a drug-likeness analysis revealed that these glycosyl flavonoids are non-carcinogenic and non-toxic,

suggesting that these phytocompounds can be potential therapeutic agents against SARS CoV-2.

Hiremath *et al.* studied *in silico* the ability of the phytochemicals present in *Phyllanthus amarus* and *Andrographis paniculata* to inhibit SARS-CoV-2 target proteins, including $3CL^{pro}$ and the Spike glycoprotein, as well as RdRp and PL^{pro}.[127] In this report, the glycosyl flavonoid isoquercitrin (**6**) showed good binding affinities with all the four SARS-CoV-2 target proteins. This suggests that isoquercitrin, which demonstrated multiple target binding abilities in the docking analysis and a higher dock score than remdesivir, can be a potential candidate for fighting SARS-CoV-2. However, *in vitro* evaluation is needed to authenticate the prediction studies.

1.4. Aims of this work

Several works have been done towards the study of glycosyl flavonoids as antiviral agents and anti-coronaviral agents. Based on the information previously presented, the aim of this work, in collaboration with the University of Oviedo (Spain), is the synthesis of *C*-glycosyl flavonoids, more specifically *C*-glycosyl flavones and *C*-glycosyl 2-styryl-4*H*-chromen-4-ones, with the glycosyl group linked at the C-3 position, and the structural characterization of the target compounds (**Figure 8**) in order to further evaluate the antiviral activity through the interaction with the virus $3CL^{pro}$ and Spike glycoprotein as well as with α-glucosidases.

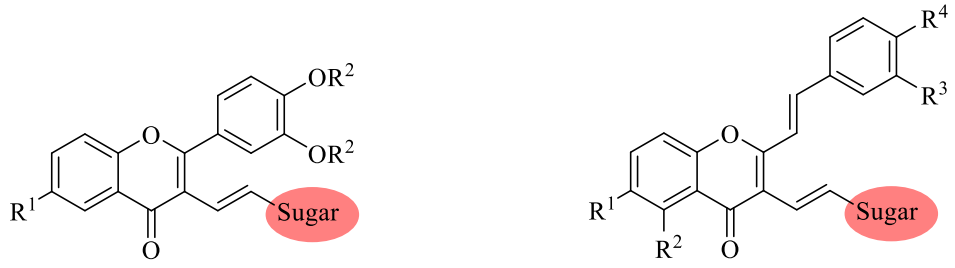

R^1 = H, Cl
R^2 = OBn, H

R^1 = H, Cl
R^2 = H, OCH_3, OH
R^3 = H, OBn, OCH_3, OH
R^4 = OBn, OCH_3, OH

Figure 8. *C*-Glycosyl flavonoids to be prepared in this work.

The first part of the work involves: i) the synthesis of several flavonoid aglycones decorated with substituents considered important for the antiviral and α-glucosidase

inhibitory activities and ii) the synthesis of sugar alkene as *C*-glycosylation agents. In a second part, the aglycone and the sugar unit will be linked to each other by a *C*-glycosidic bond through palladium mediated C-C coupling strategies, namely the Heck reaction, followed by cleavage of the glycosyl flavonoids protecting groups. All the compounds will be structurally characterized by mono- and two-dimensional nuclear magnetic resonance (NMR) techniques, mass spectrometry and high-resolution mass spectrometry in order to unequivocally confirm their structures.

Chapter 2: Synthesis of *C*-Glycosyl Flavonoids

2.1. Preamble

In this chapter, it will be described the synthetic methods that were adopted to prepare the target compounds. The nomenclature of the synthesized compounds will not be discussed since it is described in several works. In general, the compounds herein discussed follow the nomenclature recommended by IUPAC.

2.2. Synthesis of starting compounds

2.2.1. Synthesis of 1-(5-chloro-2-hydroxyphenyl)ethan-1-one

The synthesis of 1-(5-chloro-2-hydroxyphenyl)ethan-1-one involved two steps. The first step was the acetylation of the 4-chlorophenol (**42**) with acetyl chloride in dry pyridine. The reaction was stirred under nitrogen, at room temperature, for 5 hours (**Scheme 1**). After the reaction workup and purification by column chromatography, using dichloromethane as eluent, the expected 4-chlorophenyl acetate (**43**) was isolated in 83% yield. The second step involved a Fries rearrangement of the acetyl group of compound **43**, to convert the phenolic ester into the hydroxyaryl ketone **44** (**Scheme 1**). Thus, 4-chlorophenyl acetate (**43**) was heated at 150 °C for 2 hours in the presence of aluminium trichloride to afford, after purification by column chromatography, the expected 1-(5-chloro-2-hydroxyphenyl)ethan-1-one (**44**) in 89% yield.

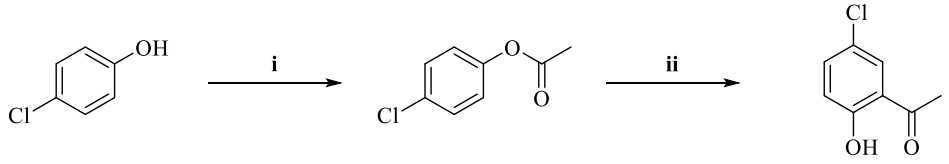

42 **43** (83%) **44** (89%)

i - CH_3COCl (1.2 equiv.), pyridine, r.t., 5 h
ii - $AlCl_3$ (2 equiv.), 150 °C, 2 h

Scheme 1. Synthesis of the 1-(5-chloro-2-hydroxyphenyl)ethan-1-one (**44**).

2.2.2. Synthesis of 3,4-bis(benzyloxy)benzoic acid and (E)-3-[3,4-bis(benzyloxy)phenyl]acrylic acid

The syntheses of 3,4-bis(benzyloxy)benzoic acid (**47a**) and (*E*)-3-[3,4-bis(benzyloxy)phenyl]acrylic acid (**47b**) were both achieved in two steps. The first step was the protection of the hydroxy groups of **45a** and **45b** using benzyl bromide following the procedure described in the literature.[128] The reaction mixture was stirred under

nitrogen, at room temperature, for 18 hours (**Scheme 2**). After the workup the compounds **46a** and **46b** were obtained with a yield of 89% and 90%, respectively.

Since the benzylation of the carboxylic acid also occurred in the first step, the following step involved the cleavage of the corresponding benzyl ester in basic conditions. A solution of the ester in methanol was refluxed at 70 °C for 3 hours in the presence of sodium hydroxide (**Scheme 2**). The reaction mixture was poured over ice and water and acidified. The precipitate formed was filtered and washed with water. After being dried, the 3,4-bis(benzyloxy)benzoic acid (**47a**) and (*E*)-3-[3,4-bis(benzyloxy)phenyl]acrylic acid (**47b**) were obtained with moderate to good yields (54% and 91%, respectively).

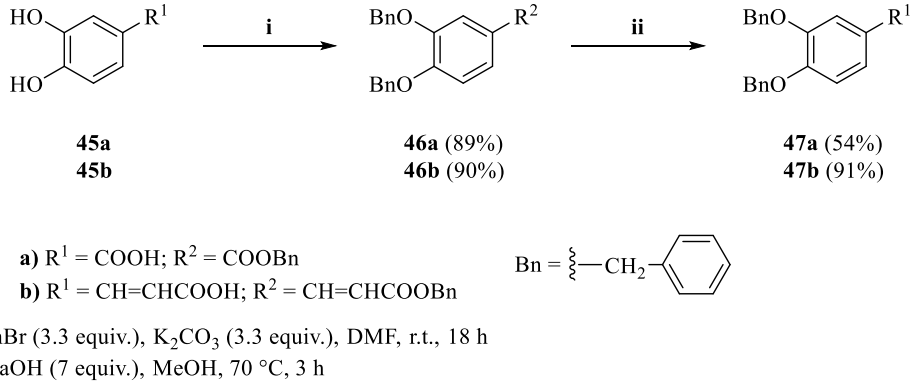

Scheme 2. Synthesis of 3,4-(bis-benzyloxy)benzoic acid (**47a**) and (*E*)-3-[3,4-bis(benzyloxy)phenyl]acrylic acid (**47b**).

2.3. Synthesis of 3-bromo-2-methyl-4*H*-chromen-4-one

The synthesis of 3-bromo-2-methyl-4*H*-chromen-4-one (**50**) consists of two steps. The first step is the formation of the diketone from 1-(2-hydroxyphenyl)ethan-1-one (**48**) (commonly named as 2'-hydroxyacetophenone) using metallic sodium in dry ethyl acetate (**Scheme 3**).[129] Under these conditions, the diketone **49**, which is in equilibrium with its enolic form **49'**, was formed. Then, the 3-bromo-2-methyl-4*H*-chromen-4-one (**50**) was synthesized following the method developed by Ibrahim, as described in the literature.[130] To a solution of the diketone (**49**) in ethanol, were added 1.5 equiv. of bromine and the mixture was left stirring at room temperature. After 2 hours, the mixture was acidified with hydrochloric acid and was refluxed for another 2 hours (**Scheme 3**). After the reaction workup and purification by column chromatography, using dichloromethane as eluent, the 3-bromo-2-methyl-4*H*-chromen-4-one was obtained in 31% yield.

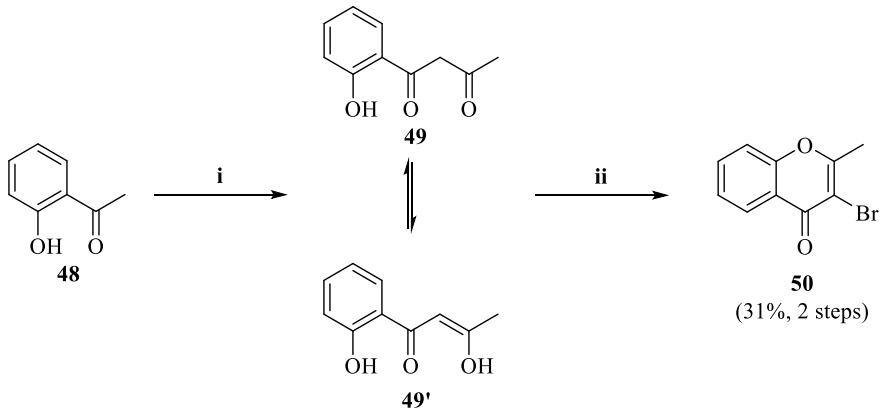

i - Metallic sodium (4 equiv.), dry ethyl acetate, r.t., 20 h
ii - 1. Br_2 (1.5 equiv.), EtOH, r.t., 2 h
2. HCl, reflux, 2 h

Scheme 3. Synthesis of 3-bromo-2-methyl-4*H*-chromen-4-one (**50**).

2.4. Synthesis of 3-bromo-2-aryl-4*H*-chromen-4-ones

The 3-bromoflavones that will be described in this section are derivatives of the 4*H*-chromen-4-ones that contain an aryl group at C-2 position and a bromo substituent at C-3 position. According to the IUPAC nomenclature these compounds are named as 3-bromo-2-aryl-4*H*-chromen-4-ones; however, for simplicity the name 3-bromoflavones will be frequently used along this work.

The first method attempted to obtain the 3-bromoflavone started with the aldol-type condensation, in basic conditions, of the 2'-hydroxyacetophenone (**48**) with the 3,4-bis(benzyloxy)benzaldehyde (**51**) (**Scheme 4**). The reaction was left stirring at room temperature for 20 hours. After that period, the reaction mixture was poured into ice and water and acidified. The organic layer was extracted with dichloromethane. After purification by column chromatography, both starting compounds **48** and **51** were recovered unaltered. The expected chalcone **52** was not formed probably due to the low reactivity of the 3,4-bis(benzyloxy)benzaldehyde (**51**), on account of the presence of electron donating groups in the 3 and 4 position of the aromatic ring. Since the chalcone **52** was not isolated it was not possible to proceed to the next step to obtain the flavone **53**.

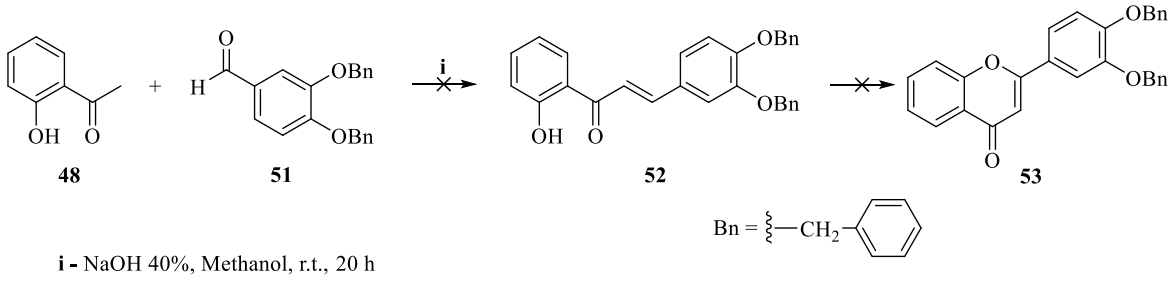

Scheme 4. Attempted synthesis of (*E*)-3-[3,4-bis(benzyloxy)phenyl]-1-(2-hydroxyphenyl)prop-2-en-1-one (**52**)/ 2-[3,4-bis(benzyloxy)phenyl]-4*H*-chromen-4-one (**53**).

In view of these unsatisfactory results, we investigated an alternative procedure to access 3-bromoflavones, based on the Baker-Venkataraman rearrangement of 2-acetylaryl benzoates **54** and **55**, followed by bromination and subsequent cyclization. Syntheses of benzoates **54** and **55** were achieved through cinnamoylation of the appropriate acetophenones **44** or **48** in the presence of 1.2 equiv. of 3,4-bis(benzyloxy)benzoic acid (**47a**), 1.2 equiv. of dicylclohexylcarbodiimide (DCC) and 0.12 equiv. of 4-pyrrolidinopyridine (4-PPy), the so-called "Steglich Esterification" (**Scheme 5**). The reaction was stirred under nitrogen for 6 days at room temperature, as described in the literature.[131] After purification of the reaction, by column chromatography, using dichloromethane as eluent, the target compound benzoate **54** was obtained in a quantitative yield. However, benzoate **55** was isolated in low yield (28%), so another esterification procedure, also developed by Steglich, was attempted.[132] Thus, to a solution of 3,4-bis(benzyloxy)benzoic acid (**47a**) and 0.1 equiv. of 4-PPy in dichloromethane, the appropriate acetophenone **44** or **48** was added. Then, DCC was added to the reaction mixture at 0 °C and it was left stirring for 30 minutes. After that period, the reaction was left stirring at room temperature for 3 hours (**Scheme 5**). After purification of the reaction, by column chromatography, using dichloromethane as eluent, benzoate **55** was isolated in 30% yield.

Both methods used to obtain the benzoate **55** gave low yields, probably due to the low reactivity of 3,4-bis(benzyloxy)benzoic acid (**47a**), since it possesses electron donating groups in the 3 and 4 positions of the aromatic ring. However, the second method described allows to obtain the target benzoate in a much shorter reaction time (3.5 hours).

The next step to achieve the 3-bromoflavones was the synthesis of the diketones **56** and **57**, through the Baker-Venkataraman rearrangement of the esters (**54** and **55**) under strong basic conditions (**Scheme 5**). The appropriate ester was dissolved in dimethyl

sulfoxide (DMSO) and 5 equiv. of potassium hydroxide were added. The reaction was stirred under nitrogen for 1 to 4 hours. After this period, the reaction was poured over ice and water and acidified. The formed precipitate was dissolved in dichloromethane, washed with water and the organic layer was evaporated to dryness. The expected diketones 1-[3,4-bis(benzyloxy)phenyl]-3-(5-chloro-2-hydroxyphenyl)propane-1,3-dione (**56**) and 1-[3,4-bis(benzyloxy)phenyl]-3-(2-hydroxyphenyl)propane-1,3-dione (**57**), which are in equilibrium with their enolic form **56'** and **57'**, respectively, were obtained in very good yields (90% and 99%, respectively).

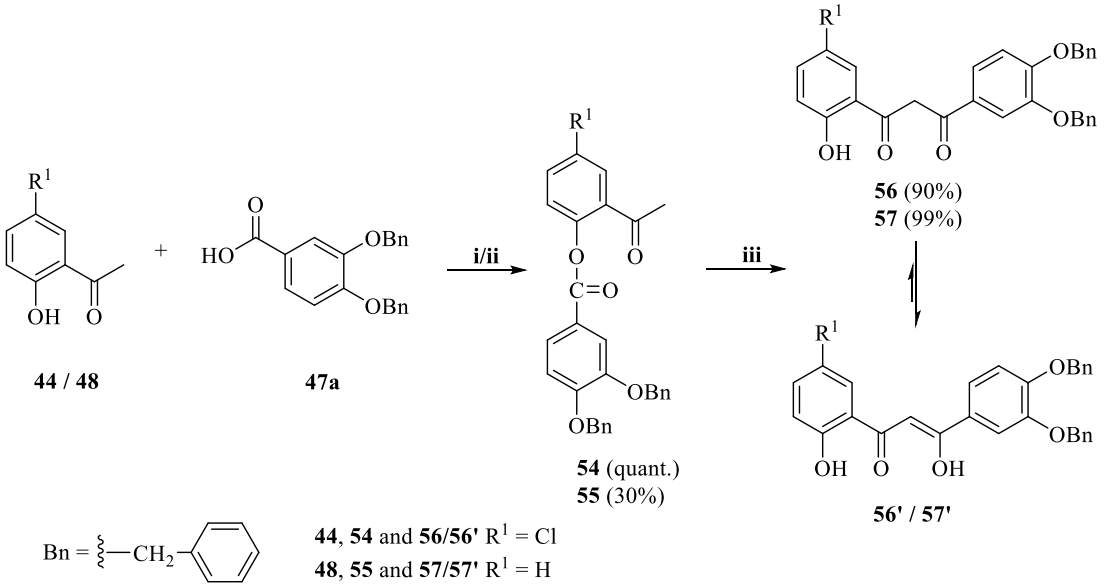

i - 47a (1.2 equiv.), DCC (1.2 equiv.), 4-PPy (0.12 equiv.), CH_2Cl_2, r.t., 6 days
ii - 44/48 (2 equiv.), DCC (1 equiv.), 4-PPy (0.1 equiv.), CH_2Cl_2, 35 min 0°C + 3 h r.t.
iii - KOH (5 equiv.), DMSO, r.t., 1-4 h

Scheme 5. Synthesis of diketones **56** and **57**.

For the synthesis of 3-bromoflavones through bromination and cyclization of the corresponding diketones, two different methods were tested (**Scheme 6**).

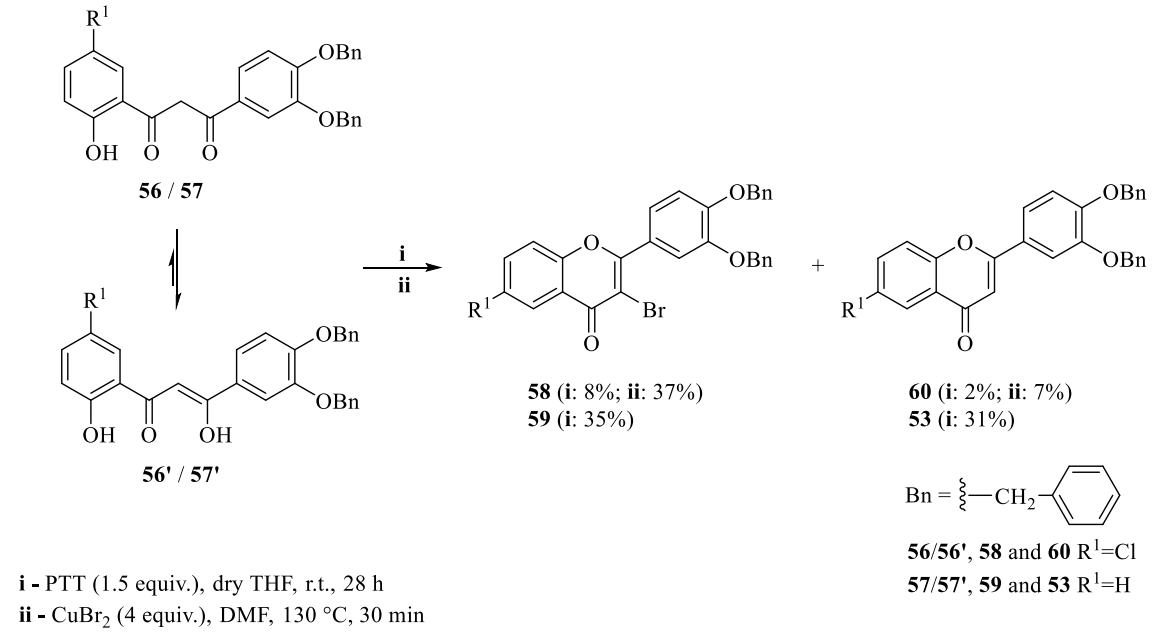

Scheme 6. Bromination and cyclization of 1-[3,4-bis(benzyloxy)phenyl]-3-(5-chloro-2-hydroxyphenyl)propane-1,3-dione (**56**) and 1-[3,4-bis(benzyloxy)phenyl]-3-(2-hydroxyphenyl)propane-1,3-dione (**57**)

The first attempted method is described in the literature and uses phenyltrimethylammonium tribromide (PTT) as bromination agent.[133,134] To a solution of **56** or **57** in dry tetrahydrofuran (THF) were added 1.5 equiv. of PTT and the mixture was left stirring at room temperature for 28 hours, protected from the light. After recrystallization, two products were obtained: the 3-bromoflavones **58** and **59** (8% and 35% yields, respectively) and the flavones **60** and **53** (2% and 31%, respectively) (**Scheme 6**).

The PTT is a selective brominating reagent since it is less electrophilic and less reactive towards aromatic rings and double bonds than bromine. When PTT is dissolved in THF, it can be a source of Br_3^- ions, which are stable in the solvent. Moreover, during the reaction hydrobromic acid is formed. The acid conditions catalyze the cyclization of the flavone before the bromination. To suppress this effect, THF is useful because it acts as a buffer, retarding the cyclization before the bromination. The presence of water in the reaction slows down the rate of bromination, which results in a decrease of selectivity, hence dry THF where Br_3^- is stable should be used.[135]

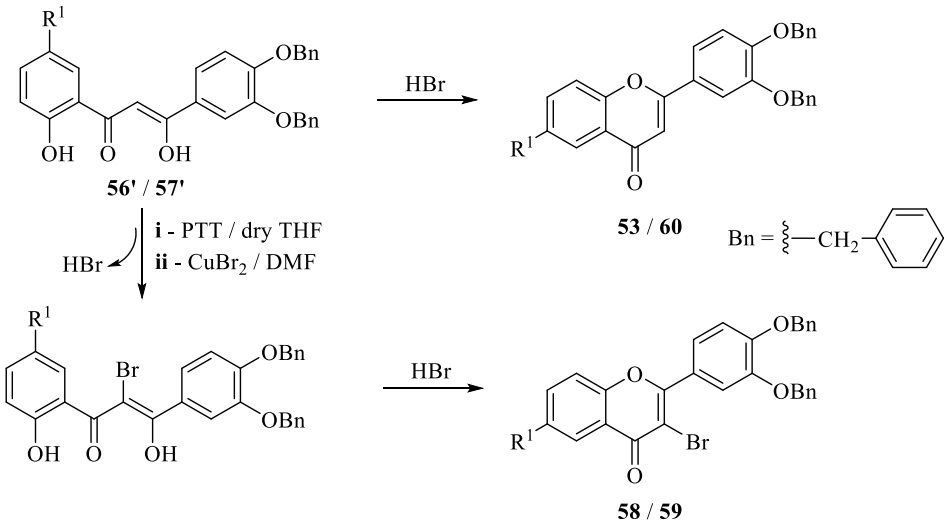

Scheme 7. The roles of the reagents and solvents towards the bromination and cyclization of compounds **56** and **57**. (Adapted from reference 136)

The other method tested to synthesize the target 3-bromoflavones, requires the use of copper(II) bromide, as described in the literature.[136] According to this method, to a solution of the diketone **56** in *N*,*N*-dimethylformamide (DMF), 4 equiv. of copper(II) bromide were added and the mixture was left stirring at 130 °C for 30 minutes. After the workup and purification, two products were isolated; the major product was 3-bromoflavone **58,** obtained in 37% yield, and the minor product was flavone **60**, isolated in 7% yield (**Scheme 6**).

Copper(II) bromide is a brominating reagent used for the bromination of diketones. This chemoselective reagent reacts with aromatic diketones, giving the α-bromoketones without affecting the aromatic rings. As stated above, during the reaction hydrobromic acid is formed which promotes the cyclization of the diketone before the bromination (**Scheme 7**). The role of DMF is to trap the H^+ ions, in order to moderately suppress the acid-catalyzed cyclization.[136]

Both methods used to brominate and cyclize the diketones **56** and **57** present advantages and disadvantages. The method that uses PTT requires a reaction time of 28 hours, whereas the other that uses copper(II) bromide needs 30 minutes. However, this second method uses DMF as solvent that causes reproductive toxicity and is difficult to eliminate during the reaction workup. Therefore, dry THF is safer and more practical to use than DMF.[137]

A plausible mechanism for the bromination and cyclization of the diketones **56** and **57** is depicted in **Scheme 8**.[138]

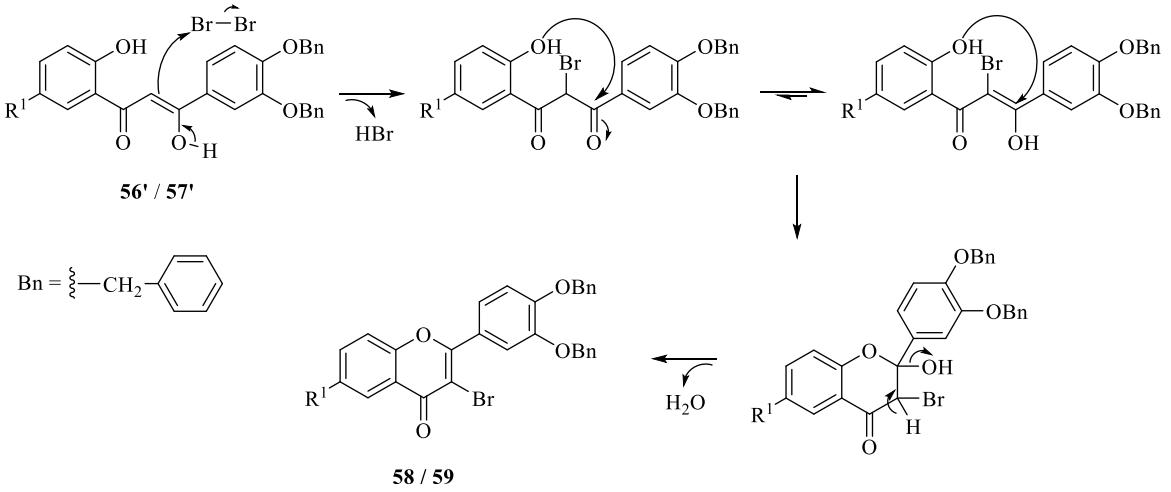

Scheme 8. Plausible mechanism for the formation of the 3-bromoflavones **58** and **59**. (Adapted from reference 138)

As an alternative for the preparation of 3-bromoflavones, direct bromination of flavones was also attempted. Firstly, for the synthesis of the starting flavone **53**, the cyclization of the diketone **57** was carried out using 0.5 equiv. of *p*-toluene-sulfonic acid (*p*-TSA) and DMSO as solvent. The reaction was left stirring at 90 °C under nitrogen for 24 hours and the flavone **53** was obtained in 99% yield (**Scheme 9**).

For the bromination of flavone **53**, two different methods were investigated. In the first one, 3 equiv. of tetrabutylammonium bromide (TBAB) and 3 equiv. of (diacetoxyiodo)benzene ($PhI(OAc)_2$) in dichloromethane where left stirring for 30 minutes. After this period, the flavone **53** was added to the previous mixture and left stirring for 24 hours, at room temperature. After the reaction workup and purification, only the starting flavone **53** was recovered (**Scheme 9**). [139]

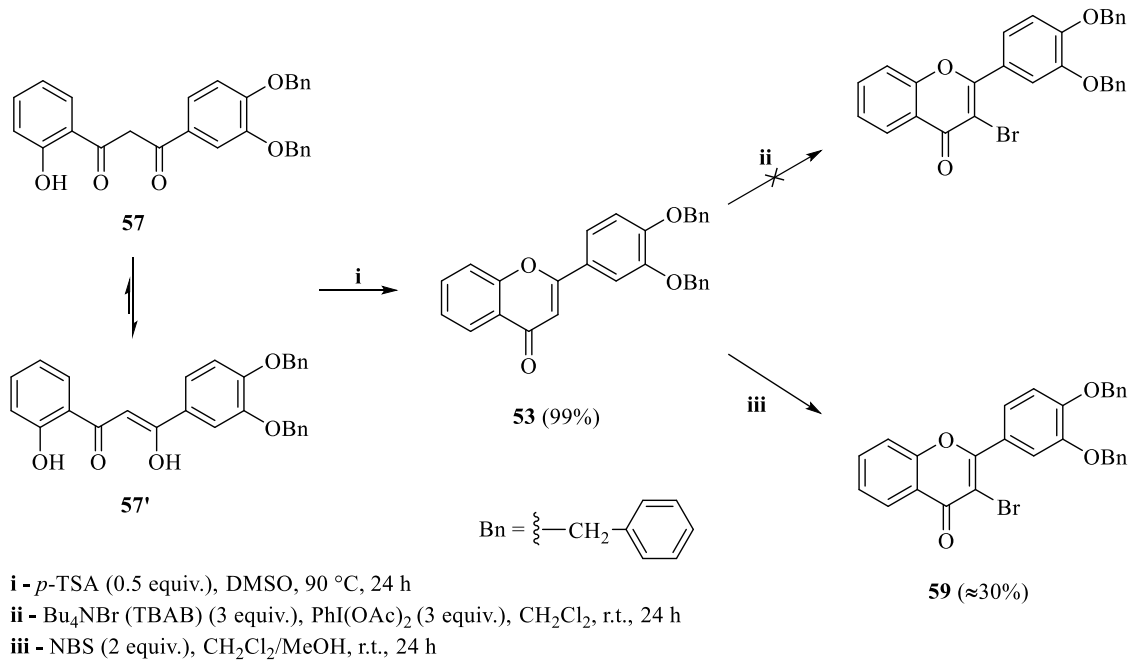

Scheme 9. Cyclization of diketone **57**/**57'** followed by bromination at C-3 position of flavone **53**.

In view of these unsatisfactory results, an alternative method that uses *N*-bromo succinimide (NBS) was investigated (**Scheme 9**).[140] To a solution of the flavone **53** in dichloromethane and methanol, were added 2 equiv. of NBS. The reaction was left stirring at room temperature for 24 hours. After evaporation to dryness and recrystallization in ethanol, the 3-bromoflavone **59** was obtained, albeit in low purity and limited yield (≈30%).

2.5. Synthesis of (*E*)-3-bromo-2-styryl-4*H*-chromen-4-ones

For the preparation of (*E*)-3-bromo 2-styryl-4*H*-chromen-4-ones, a straightforward synthesis was first attempted, which involved the condensation of the 3-bromo-2-methyl-4*H*-chromen-4-one (**50**) with benzaldehyde **51** (**Scheme 10**). Thus, 4*H*-chromen-4-one (**50**) was added to a solution of 4 equiv. of metallic sodium in ethanol. Then, 1.2 equiv. of benzaldehyde **51** were added to the reaction mixture, and it was left stirring at room temperature for 24 hours. However, the desired (*E*)-3-bromo-2-styryl-4*H*-chromen-4-one **61** was not isolated. This result can be explained by the low reactivity of 3,4-bis(benzyloxy)benzaldehyde (**51**), due to the presence of electron donating groups in the 3 and 4 position of the aromatic ring.

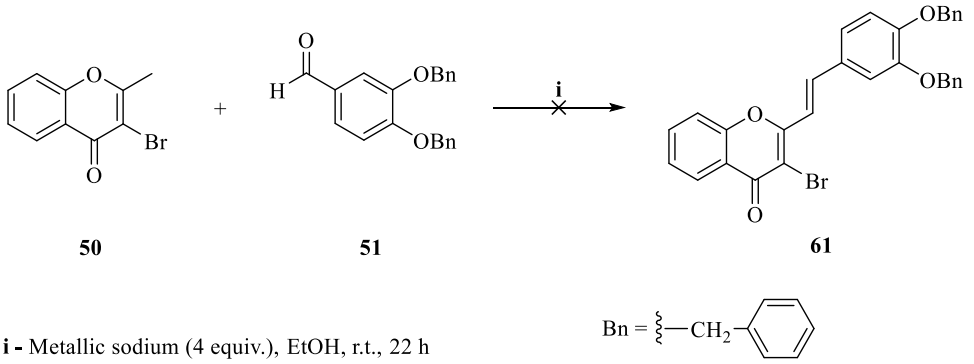

Scheme 10. Attempted synthesis of (*E*)-2-[3,4-bis(benzyloxy)styryl]-3-bromo-4*H*-chromen-4-one (**61**).

Since the previously described method failed, the synthesis of the (*E*)-3-bromo-2-styryl-4*H*-chromen-4-ones **66** and **61** was carried out following a similar method to that used for the synthesis of the 3-bromoflavones **58** and **59**. It started with the "Steglich Esterification" of the appropriate acetophenone **44** or **48** with the (*E*)-3-(3,4-dihydroxyphenyl)acrylic acid (**47b**). To a mixture of 1 equiv. of the acrylic acid **47b** and 0.1 equiv. of 4-PPy in dichloromethane, were added 2 equiv. of the acetophenone **44** or **48**. Then 1 equiv. of DCC was added to the reaction mixture at 0 °C and it was left stirring for 30 minutes. After that period, the reaction was left stirring at room temperature for 3 hours (**Scheme 11**). After the reaction workup and purification by column chromatography, using dichloromethane as eluent, 2-acetyl-4-chlorophenyl (*E*)-3-[3,4-bis(benzyloxy)phenyl]acrylate (**62**) and 2-acetylphenyl (*E*)-3-[3,4-bis(benzyloxy)phenyl]acrylate (**63**) were both isolated in moderate yields (58%).

In the next step, compounds **62** and **63** underwent a Baker-Venkataraman rearrangement under strong basic conditions (**Scheme 11**) by treatment with 5 equiv. of potassium hydroxide in DMSO for 1-4 hours at room temperature. The expected (*E*)-5-[3,4-bis(benzyloxy)phenyl]-1-(5-chloro-2-hydroxyphenyl)pent-4-ene-1,3-dione (**64**) and (*E*)-5-[3,4-bis(benzyloxy)phenyl]-1-(2-hydroxyphenyl)pent-4-ene-1,3-dione (**65**), which are in equilibrium with their corresponding enolic form **64'** and **65'**, were obtained with good yields (95% and 99%, respectively).

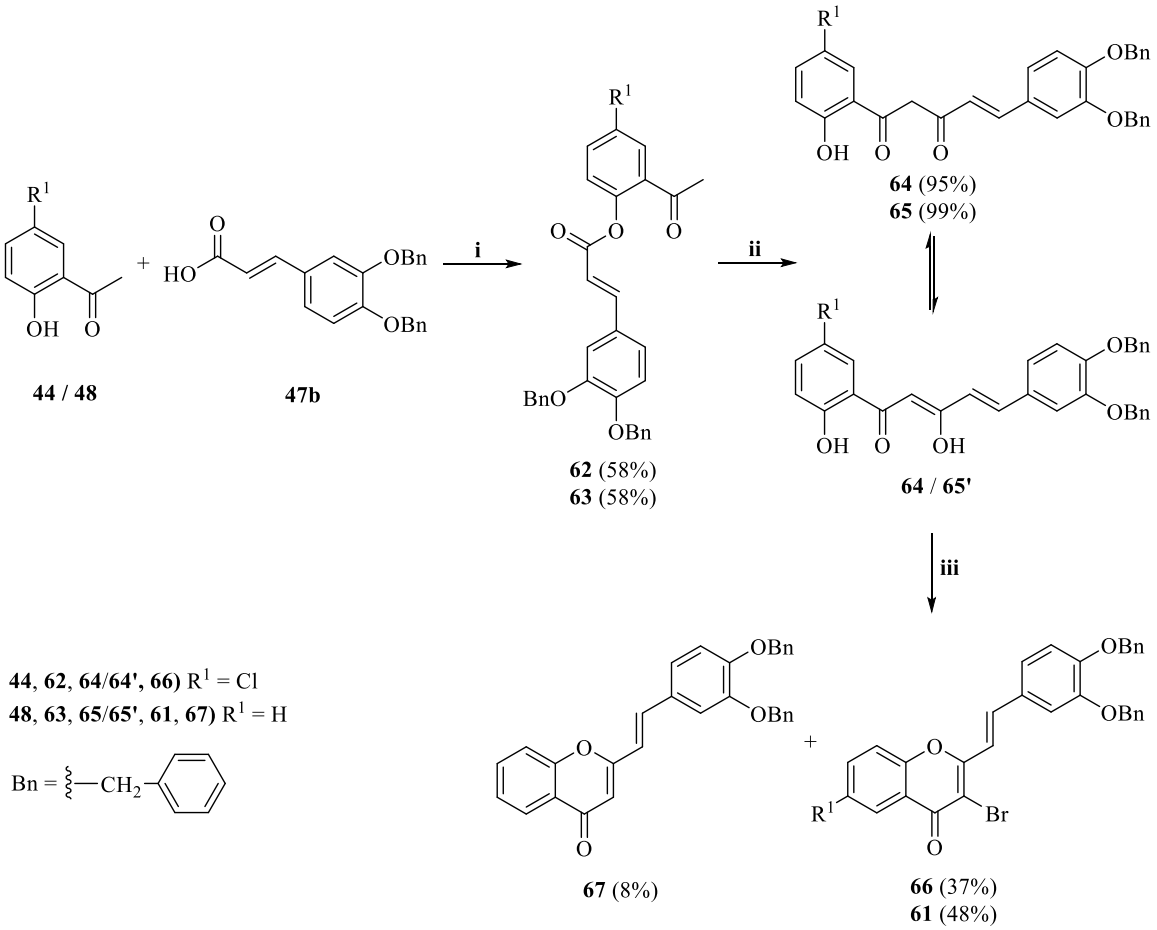

i - 44/48 (2 equiv.), DCC (1 equiv.), 4-PPy (0.1 equiv.), CH_2Cl_2, 30 min 0°C + 3 h r.t.
ii - KOH (5 equiv.), DMSO, r.t., 1-4 h
iii - $CuBr_2$ (4 equiv.), DMF, 130°C, 30 min

Scheme 11. Synthesis strategy followed to obtain the (*E*)-2-[3,4-bis(benzyloxy)styryl]-3-bromo-6-chloro-4*H*-chromen-4-one (**66**) and (*E*)-2-[3,4-bis(benzyloxy)styryl]-3-bromo-4*H*-chromen-4-one (**61**).

For the bromination-cyclization step, copper(II) bromide was used (section 2.1.3). Thus, to a solution of diketone **64** or **65** in DMF, 4 equiv. of copper(II) bromide were added. The reaction was stirred at 130 °C for 30 minutes. After workup and purification, two products were isolated: (*E*)-3-bromo-2-styryl-4*H*-chromen-4-ones **66** or **61** as the major products (37% and 48% yields, respectively) and (*E*)-2-styryl-4*H*-chromen-4-one (**67**) as the minor product (8% yield).

Other (*E*)-3-bromo-2-styryl-4*H*-chromen-4-ones **70** and **71** bearing methoxy protecting groups were also synthesized from diketones **68** and **69** already available in the research group (**Scheme 12**).

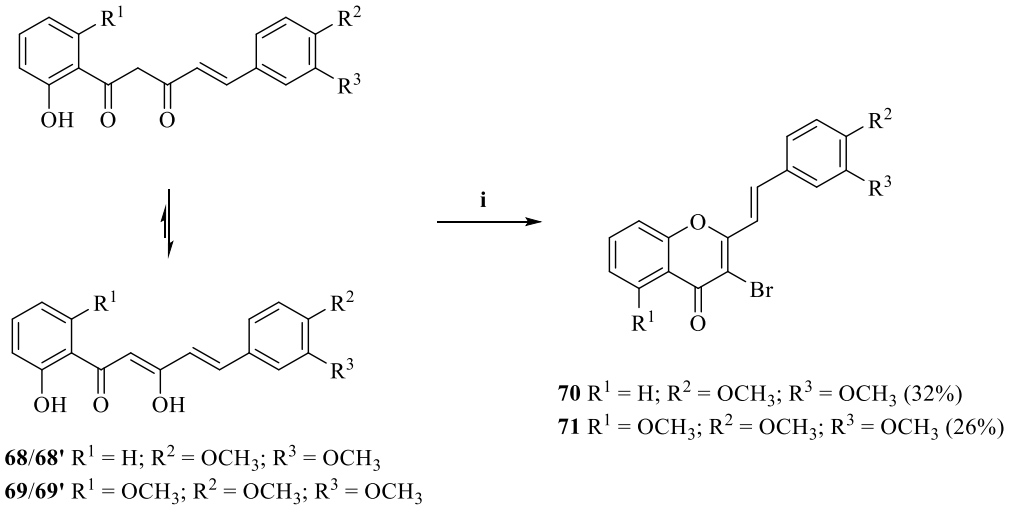

68/**68'** R^1 = H; R^2 = OCH_3; R^3 = OCH_3
69/**69'** R^1 = OCH_3; R^2 = OCH_3; R^3 = OCH_3

70 R^1 = H; R^2 = OCH_3; R^3 = OCH_3 (32%)
71 R^1 = OCH_3; R^2 = OCH_3; R^3 = OCH_3 (26%)

i - PTT (1.5 equiv.), dry THF, r.t., 42 h

Scheme 12. Bromination and cyclization of diketones **68** and **69**.

For the bromination-cyclization step, PTT was used as reagent. Thus, to a solution of 1 equiv. of the diketone **68** or **69** in dry THF, 1.5 equiv. of PTT were added. The reaction mixture was left stirring at room temperature for 42 hours, protected from the light (**Scheme 12**). After recrystallization, the desired (*E*)-3-bromo-2-styryl-4*H*-chromen-4-one **70** and **71** were obtained in low yields (32% and 26%, respectively).

2.6. Synthesis of the sugar alkene

The synthesis pathway of the sugar alkene 6,7-dideoxy-1,2:3,4-di-*O*-isopropylidene-α-D-*galacto*-hept-6-enopyranose (**74**) is described in **scheme 13**.

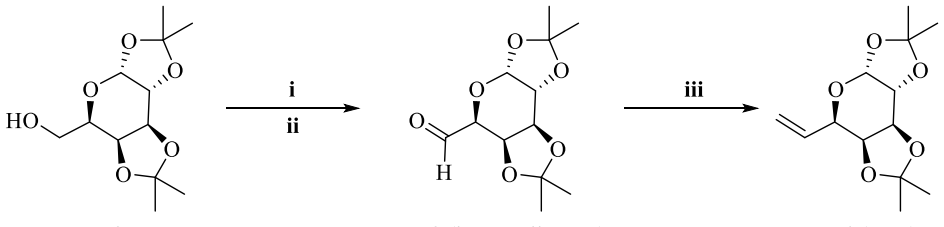

72 **73** (**i**: 65%; **ii**: 73%) **74** (81%)

i - DMP (2 equiv.), CH_2Cl_2, r.t., 3 h
ii - $C_2O_2Cl_2$ (1.35 equiv.), DMSO (1.8 equiv.), $N(C_2H_5)_3$ (2.9 equiv.), CH_2Cl_2, -78 °C to r.t., 1 h 30 min
iii - NaH (2 equiv.), $CH_3P^+Ph_3Br^-$ (2.4 equiv.), dry THF, 1 h sonication + 3 h r.t.

Scheme 13. Synthesis pathway of the sugar alkene (**74**).

The first step consists in the oxidation of the protected D-galactose derivative **72** to the corresponding sugar aldehyde **73**. For this purpose, a Dess-Martin periodinane

oxidation was used.[141] Thus, to a solution of commercially available 1,2:3,4-di-*O*-isopropylidene-α-D-galactopyranose (**72**) in dichloromethane, 2 equiv. of Dess-Martin periodinane (DMP) dissolved in dichloromethane were added dropwise at 0 °C. The reaction mixture was stirred at room temperature for 3 hours and then, it was diluted with diethyl ether and quenched with a solution of sodium thiosulfate in aqueous saturated sodium bicarbonate to remove both the iodine and the acetic acid generated on the course of the oxidation reaction. After purification by column chromatography, using ethyl acetate:hexane (1:2), the sugar aldehyde **73** was obtained in 65% yield. The reaction mechanism is depicted in **scheme 14**.

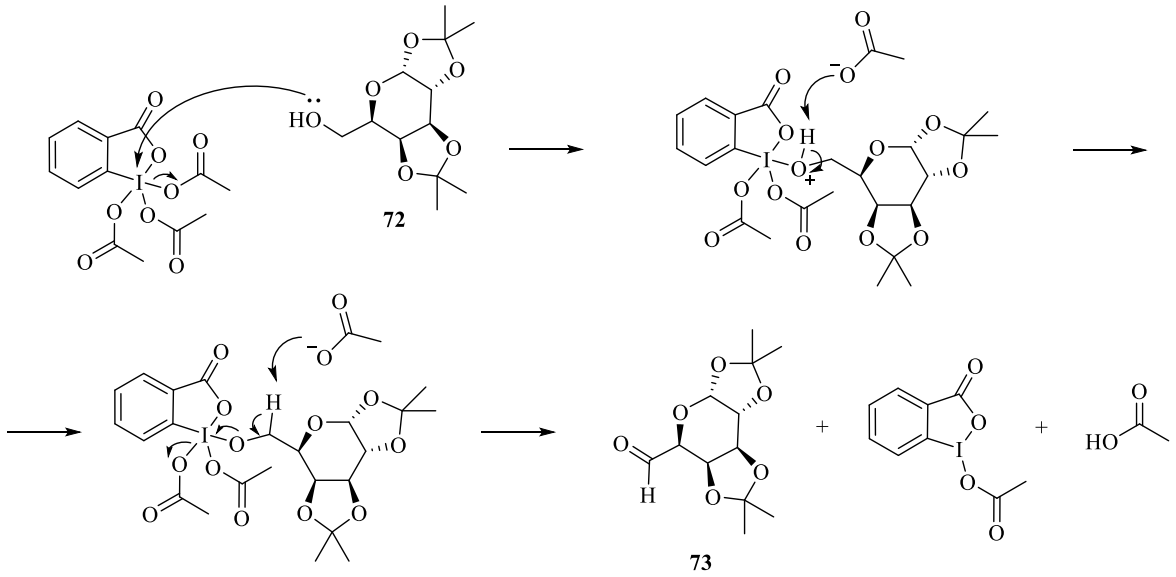

Scheme 14. Reaction mechanism towards the sugar aldehyde **73**.

The main drawback of this procedure is the relatively high cost of DMP. Alternatively, a Swern oxidation was employed.[142] To a solution of 1.35 equiv. of oxalyl chloride in dichloromethane, it was added 1.8 equiv. of DMSO at -78 °C. After a period of 15 minutes, a solution of sugar alcohol **72** in dichloromethane was added, and left stirring for 30 minutes at -78 °C until the addition of 2.9 equiv. of triethylamine. The reaction mixture was allowed to reach the room temperature under stirring for 45 minutes. After the workup, the sugar aldehyde **73** was obtained in 73% yield.

For the conversion of the sugar aldehyde **73** into the sugar alkene **74**, a Wittig reaction was used.[143] Thus, reaction of sugar aldehyde **73** with methyltriphenylphosphorane, prepared *in situ* by the reaction of 2.4 equiv. of methyltriphenylphosphonium bromide and and 2 equiv. of sodium hydride 60% dispersion

in mineral oil, was carried out. The aimed sugar alkene **74** was isolated in 81% yield. The reaction mechanism is depicted in the **scheme 15**.

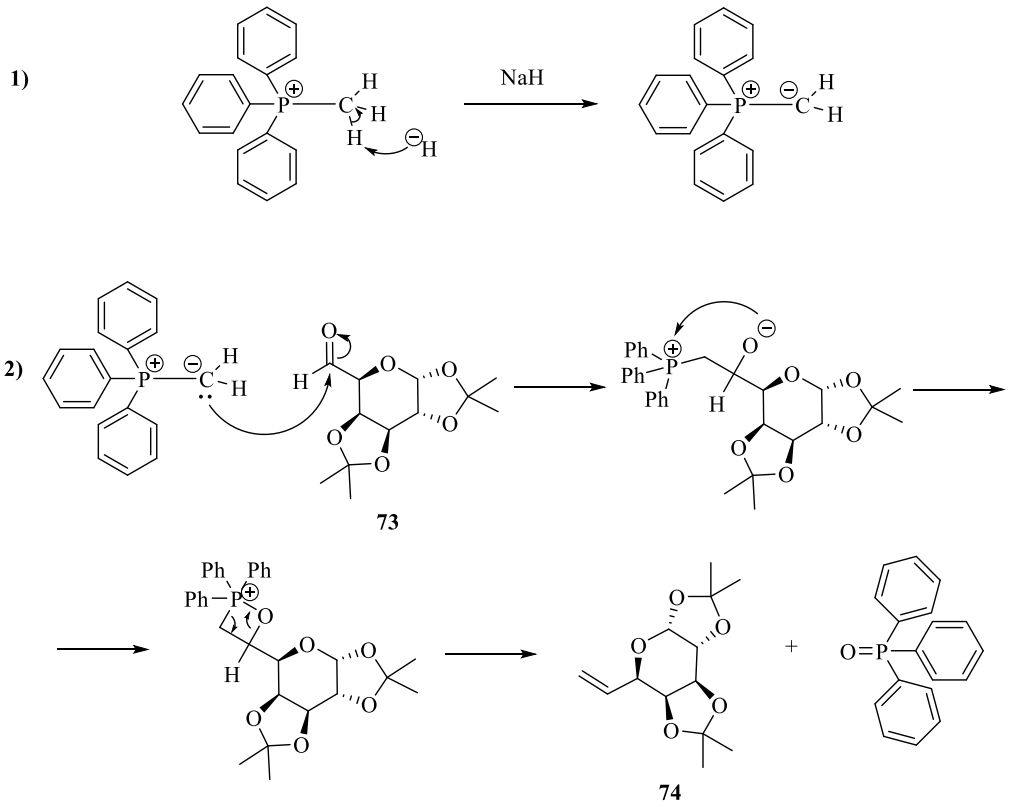

Scheme 15. Reaction mechanism towards the sugar alkene **74**. 1) Formation of ylide; 2) The Wittig reaction.

2.7. *C*-Glycosylation of flavonoid derivatives

The methodology used for the synthesis of the *C*-glycosyl flavonoid derivatives involved the palladium catalyzed Heck cross-coupling of the corresponding 3-bromoflavonoid derivatives (3-bromoflavone **58** and **59** or (*E*)-3-bromo-2-styryl-4*H*-chromen-4-one **61**, **66**, **70**, **71** and **75**) with the sugar alkene **74**.

2.7.1. Palladium-catalyzed cross-coupling reactions for the synthesis of *C*-glycosyl flavonoids

As Organic Synthesis concerns the preparation of complex molecules from simple derivatives, it is evident that one of the most relevant aspects is the formation of C–C bonds. Transition metal-catalyzed cross-coupling reactions exemplify one of the most powerful and popular method for the formation of carbon–carbon bonds.[144] Among all transition metals used to perform cross-coupling reactions, palladium (Pd) is the most

common for the variety of reactions that can catalyze, the range of functional groups tolerated, and the excellent chemo- and regioselectivity attained. Most palladium catalyzed reactions are believed to follow a similar catalytic cycle (**Scheme 16**). [145,146]

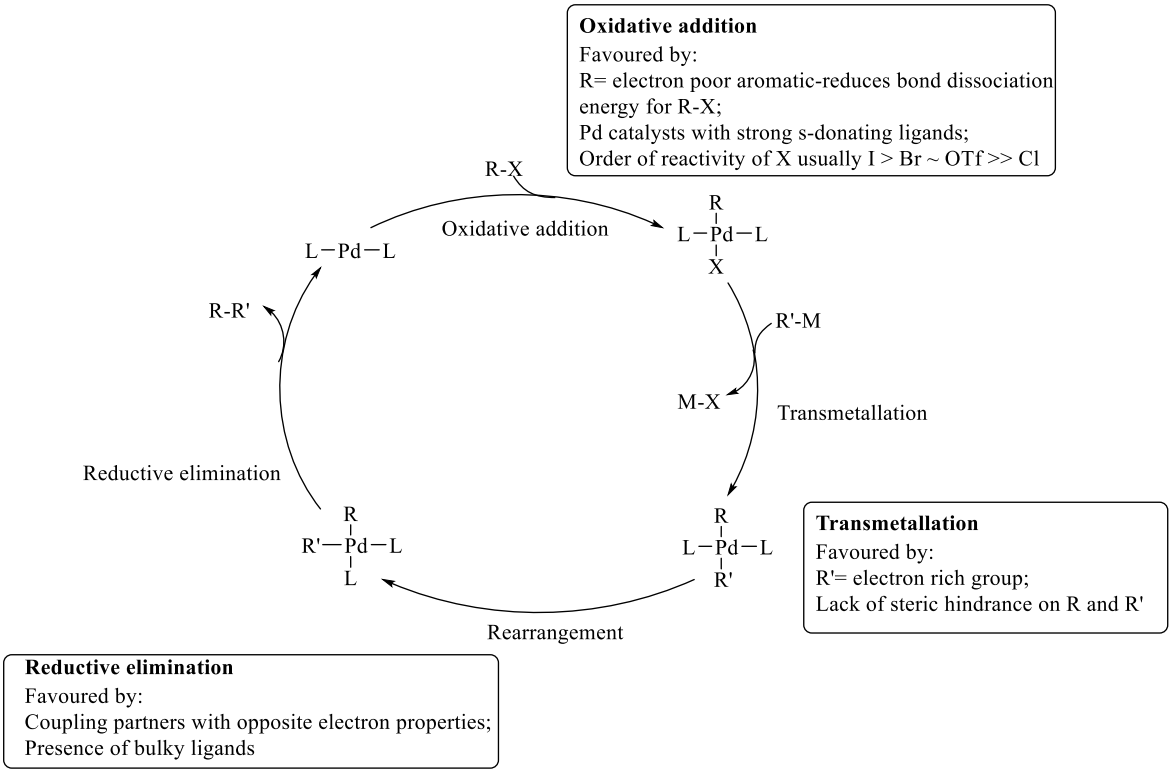

Scheme 16. Palladium cycle in cross coupling reactions.

Pd(0) catalyst is required to promote the palladium cycle, which can be obtained commercially or through Pd(II) stable catalyst precursors. This Pd(II) precursors must be pre-activated *in situ* by reduction of the palladium to the zero-oxidation state. There are two ways to activate the Pd(II) catalysts, which are the phosphine-assisted approach and the phosphine-free approach. The classical methodology is the phosphine-assisted approach, a well-established method known for the excellent results. However, there have been developed phosphine-free approaches to overcome the problems associated to the phosphine ligands that are expensive, toxic, and unrecoverable. Therefore, the reduction of Pd(II) can be alternatively done with amines, olefins, and by quaternary ammonium and phosphonium salts.[147]

Among the palladium catalyzed cross-coupling reactions, the Heck reaction (also named Mizoroki-Heck reaction) is particularly useful to access *C*-aryl glycosides. The cross-coupling Heck reaction involves the reaction of organohalides with alkenes.[144] This

reaction is performed with a slight excess of alkene and a base in the presence of $Pd(OAc)_2$/triarylphosphine catalyst system under inert atmosphere. The most common base used is triethylamine, yet other organic and inorganic bases such as NaOAc, $NaHCO_3$ and K_2CO_3 have been used. The temperature of the reaction can vary between 60 to 150 °C, since it can depends on the reactivity of the reagents used; for example, aryl chlorides are usually unreactive at temperatures below 120 °C, whereas reactions with aryl iodides can be carried out at room temperature.[148]

The Heck catalytic cycle, after the catalytic active Pd(0) is generated, is divided in four main steps: oxidative addition, migratory insertion, β-hydride elimination-dissociation and reductive elimination. The first step is the **oxidative addition**, where the $L_2Pd(0)$ is inserted into the R-X bond. The rupture of R-X bond is fast; however, the rate depends on the X nature, which follows an order of reactivity: R–I >> R–OTf > R–Br >> R–Cl. The second step is the **migratory insertion**, where the C-C bond is formed. The palladium forms a complex with the alkene, where the geometry is a key point since the insertion requires a coplanar assembly of the metal, ethylene, and the hydride. The insertion occurs in a *syn*-manner and the stereoselectivity is determined in this step, where it tends for a *trans*-coupling (*E*-isomer). After this insertion, the C-C bond suffers an internal rotation, that brings to the third step. The **β-hydride elimination-dissociation** is also stereoselective and occurs in a *syn*-manner, where the efficiency is associated to the dissociation. The β-hydride elimination occurs, forming an alkene-palladium complex, which is an unstable intermediate. This process can be reversible, and a slower dissociation of the palladium from the alkene can generate the formation of different products. Although, the *E*-isomer is thermodynamically favorable, the formation of the *Z*-isomer can still occur. The last and fourth step is the **reductive elimination** where the regeneration of $L_2Pd(0)$ occurs. In this step, the presence of a base is necessary to regenerate the $L_2Pd(0)$.[147,149]

Regarding the solvents used in the Heck reaction, the more commonly used are the dipolar aprotic solvents, such as DMF, DMSO, *N*-methylpyrrolidone (NMP) and acetonitrile. A classic variation of the Heck reaction is the Jeffery's protocol, which occurs under phase-transfer conditions. "Jeffery conditions" involve the simple palladium salts, inorganic bases, and tetraalkylammonium salts in anhydrous solvents.[148,150]

2.7.2. Heck reaction for the synthesis of *C*-glycosyl flavonoids

As stated above, the Heck reaction was the elected tool to synthesize *C*-glycosyl flavonoids. Heck reaction has been extensively used for the *C*-glycosylation of arenes.[145,151] In this section, several relevant examples will be presented.

Xiong and co-workers developed a Pd(II)-catalyzed oxidative Heck type reaction of pyranoid glycals with arylboronic acids, 3-keto *C*-aryl glycosides (**Scheme 17**). The cross-coupling reaction proceeded with high regioselectivity and stereoselectivity.[152]

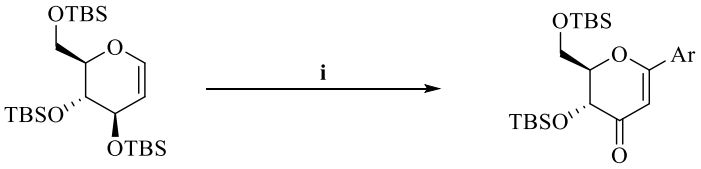

76

Ar = *p*-MeOPh **77a**
p-CF_3Ph **77b**

i - $Pd(OAc)_2$ (0.1 equiv.), $ArB(OH)_2$ (2.0 equiv.), DDQ (2.0 equiv.), CH_3CN, 30-40 °C

Scheme 17. Pd(II)-catalyzed Heck reaction to prepare enone-type *C*-glycosides.

Li and Ye reported a simple, mild, and efficient procedure for the Heck *C*-glycosylation of pyranoid glycals, using aryl iodides in the presence of Ag_2CO_3, $Cu(OAc)_2$ and catalytic $Pd(OAc)_2$ (**Scheme 18**).[153] The Heck glycosylation took place via *syn*-β-hydride elimination affording a single enol ether coupling product **80**. This methodology showed to be highly regioselective, as single anomer was obtained. The configuration of the newly introduced aryl group at the anomeric position is opposite to the C_3-*O*-substituent of the starting glycal **78**, indicating a *syn*-addition due to steric hindrance.

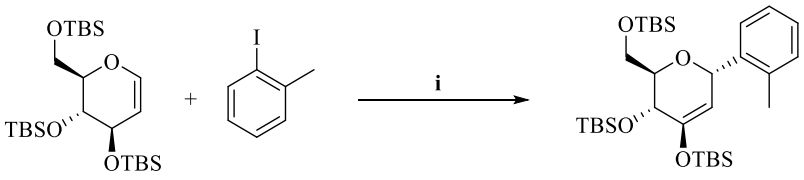

78 **79** **80**

i - $Pd(OAc)_2$ (10 mol%), Ag_2CO_3 (0.6 equiv.), $Cu(OAc)_2$ (2.0 equiv.), MeCN, under air, 40 °C, 24 h

Scheme 18. Pd(II)-catalyzed Heck reaction of pyranoid glycal **78** with aryl iodide **79** to form pyranoid aryl *C*-glycoside **80**.

Singh *et al.* developed an efficient palladium-catalyzed Heck type coupling of glycals and boronic acids for the synthesis of 2-deoxy-aryl-*C*-glycosides (**Scheme 19**).

This methodology proceeded in a stereoselective and regioselective manner and the expected compounds **84** were obtained in very good yields (up to 90% yield).[154]

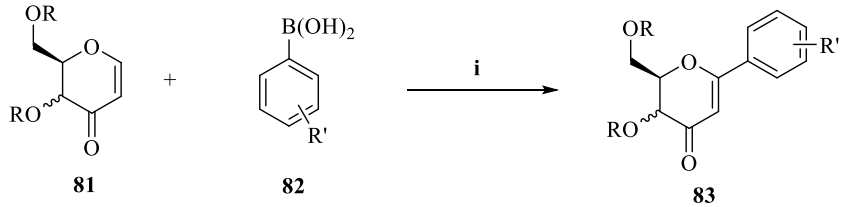

81 **82** **83**

R = Bn, Ac, Bz, Piv, MOM and TBDPS
R' = Alkyl, Aryl, Halogens, NO_2, CHO

i - $Pd(OAc)_2$ (10 mol%), 1,10-Phen (20 mol%), DMF, O_2, 100 °C

Scheme 19. Reaction of glycal enones **81** with arylboronic acids **82**.

The Heck reaction between aryl groups and sugar alkenes, using the "Jeffery conditions" were also described by Patonay *et al.* in 2016. These studies showed the synthesis of *C*-glycosyl flavonoids using as key step a Heck reaction of bromoflavonoids and sugar alkenes, under a palladium-catalyzed phosphine free approach (**Scheme 20**).[155,156] In a first study the reaction of bromochromones and/or bromoflavones **84** with 1-allyl-β-D-ribofuranose derivatives **85** gave the aimed *C*-glycosyl flavones/chromones **86** in excellent yields (up to 92% yield).[155] In a second study, the reaction of 5,6-dideoxy-1,2-*O*-isopropylidene-α-D-xylo-hex-5-enofuranose with bromochromones, bromoflavones, bromochromanones and bromoflavanones gave the aimed *C*-glycosyl compounds in yields up to 86%.[156]

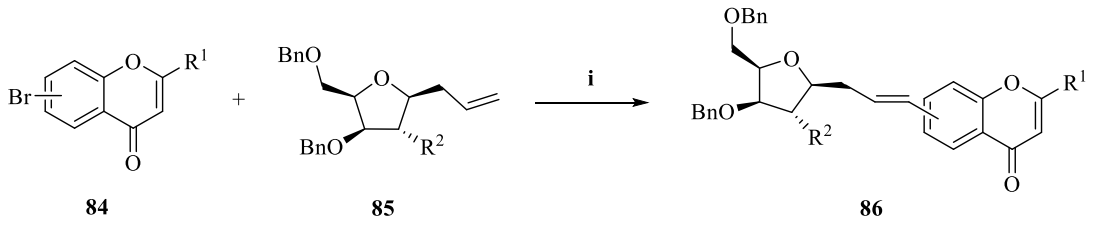

84 **85** **86**

R^1 = Ph, H
R^2 =H, OBn
i - $Pd(OAc)_2$ (6 mol%), K_2CO_3 (1.5 equiv.), KCl (1 equiv.), Bu_4NBr (2 equiv.), anhyd DMF, 110 °C, 2h

Scheme 20. Synthesis of flavonoid-β-D-ribofuranose derivatives **86**.

2.7.3. Synthesis of *C*-glycosyl flavonoid-type compounds

Based on the work of Patonay *et al.*, the C-C coupling reactions of sugar alkene **74** with different bromoflavonoids (3-bromoflavones **58** and **59** and (*E*)-3-bromo-2-styryl-4*H*-chromen-4-ones **61**, **66**, **70**, **71** and **75**) were carried out under phosphine-free approach

"Jeffery conditions". Thus, to a solution of 1 equiv. of the 3-bromoflavonoid (**58**, **59**, **61**, **66**, **70**, **71** and **75**) and 1.2 equiv. of sugar alkene **76** in dry DMF, were added 1 equiv. of K_2CO_3, 0.1 equiv. of TBAB and 0.05 equiv. of $Pd(OAc)_2$. In all cases, the reaction was left stirring overnight at 110°C (**Scheme 21**).

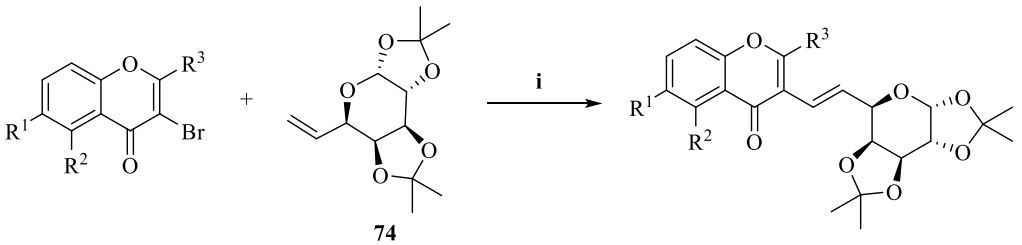

58 R^1 = Cl; R^2 = H; R^3 = 3,4-bis(benzyloxy)phenyl
59 R^1 = H; R^2 = H; R^3 = 3,4-bis(benzyloxy)phenyl
61 R^1 = H; R^2 = H; R^3 = 3,4-bis(benzyloxy)styryl
66 R^1 = Cl; R^2 = H; R^3 = 3,4-bis(benzyloxy)styryl
70 R^1 = H; R^2 = H; R^3 = 3,4-dimethoxystyryl
71 R^1 = H; R^2 = OCH_3; R^3 = 3,4-dimethoxystyryl
75 R^1 = H; R^2 = H; R^3 = 4-methoxystyryl

87 R^1 = Cl; R^2 = H; R^3 = 3,4-bis(benzyloxy)phenyl
88 R^1 = H; R^2 = H; R^3 = 3,4-bis(benzyloxy)phenyl
89 R^1 = H; R^2 = H; R^3 = 3,4-bis(benzyloxy)styryl (62%)
90 R^1 = Cl; R^2 = H; R^3 = 3,4-bis(benzyloxy)styryl (72%)
91 R^1 = H; R^2 = H; R^3 = 3,4-dimethoxystyryl (74%)
92 R^1 = H; R^2 = OCH_3; R^3 = 3,4-dimethoxystyryl (48%)
93 R^1 = H; R^2 = H; R^3 = 4-methoxystyryl (53%)

i - 74 (1.2 equiv.), K_2CO_3 (1 equiv.), Bu_4NBr (TBAB) (0.1 equiv.), $Pd(OAc)_2$ (0.05 equiv.), dry DMF, 110 °C, overnight

Scheme 21. Synthesis of *C*-glycosyl flavonoids **87**-**93**.

The C-C cross coupling Heck reaction of 3-bromoflavones was unsuccessful, and the starting 3-bromoflavones **58** and **59** were recovered unaltered. These unsatisfactory results could be explained by the steric hindrance caused by the presence of an aryl group in the C-2 position of the 3-bromoflavone. Therefore, the C-C cross-coupling was attempted with other less hindered flavonoids, more specifically the 3-bromo-2-styryl-4*H*-chromen-4-ones. The Heck reaction of sugar alkene **74** and 3-bromo-2-styryl-4*H*-chromen-4-ones **61**, **66**, **70**, **71** and **75** afforded in all cases the expected *C*-glycosyl 2-styryl-4*H*-chromen-4-ones **89**, **90**, **91**, **92** and **93** in moderate to good yields (48 – 72%). This result show that the steric hindrance was surpassed due to the addition of the styryl group in the C-2 position instead of the aryl group. When analyzing the ^{1}H NMR spectra of the *C*-glycosyl 2-styryl-4*H*-chromen-4-one **89** it was possible to identify the presence of two major isomers, which were impossible to separate after several attempts with different eluents. However, in the *C*-glycosyl 2-styryl-4*H*-chromen-4-ones **90**, **91**, **92** and **93** the presence of four isomers was detected, by integration of the anomeric protons in 48:30:16:6 proportion. It was impossible to purify this mixture, since only one spot in the Thin-Layer Chromatography (TLC) plate was observed with the different eluents tested.

2.8. Hydrogenation of *C*-glycosyl 2-styryl-4*H*-chromen-4-ones

The presence of isomers in the *C*-glycosyl 2-styryl-4*H*-chromen-4-ones could be attributed to the isomerization of the exocyclic double bond C-α=C-β of the styryl moiety and to the presence of both *E* and *Z* isomers of the newly formed alkenyl bond as a result of the Heck reaction. We hypothesized that the deprotection of the benzyl groups by catalytic hydrogenation, would occur with concomitant reduction of both ethenyl moieties to the ethanyl groups, thus overcoming the problem of the presence of *E*/*Z* isomers.

The hydrogenation carried out with *in situ* generated hydrogen was performed on the *C*-glycosyl 2-styryl-4*H*-chromen-4-one **61**. To 1 equiv. of compound **61** and palladium on carbon suspended in dry ethyl acetate, 5 equiv. of triethylsilane were added. The mixture was left stirring overnight at room temperature, under nitrogen atmosphere. After the workup and purification, it was not possible to isolate the target compound. Through ^{1}H NMR spectrum it was not possible to identify the compound **94** and it was observed degradation of the *C*-glycosyl 2-styryl-4*H*-chromen-4-one **61**.

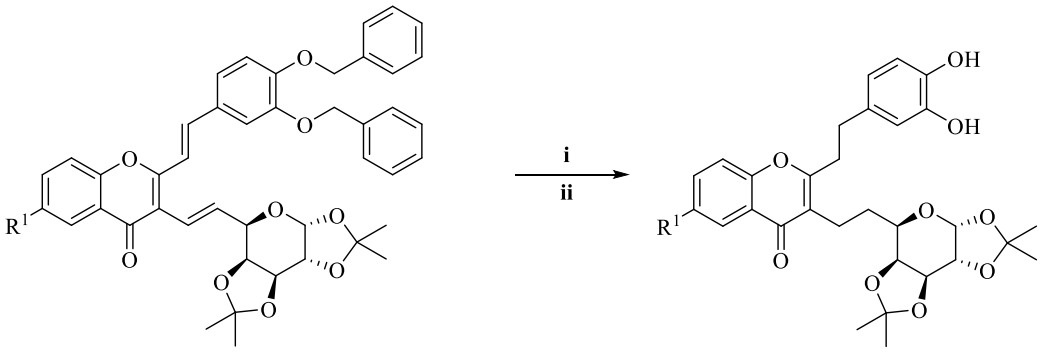

61
66

94 R^1 = H
95 R^1 = Cl

i - Pd/C (0.6 equiv.), triethylsilane (5 equiv.), dry ethyl acetate, r.t., 20 h
ii - Pd/C, ethanol, H_2 atm, 6 h

Scheme 22. Attempted hydrogenation of *C*-glycosyl 2-styryl-4*H*-chromen-4-ones **61** and **66**.

Because of these unsatisfactory results, the hydrogenation of *C*-glycosyl 2-styryl-4*H*-chromen-4-one **66** was performed with hydrogen gas. Thus, a degassed mixture of compound **66** and palladium on carbon in ethanol was stirred overnight under hydrogen atmosphere. However, a complex mixture was obtained from which the aimed compound **95** could not be isolated.

Chapter 3: Structural Characterization of the Synthesized Compounds

3.1. Preamble

In this section, the structural characterization of the most relevant compounds will be presented and discussed. All the compounds were characterized by mono-(^{1}H and ^{13}C) and two-(HSQC and HMBC, and NOESY and COSY whenever necessary) dimensional NMR techniques, as well as by mass spectrometry (ESI^{+}) and high-resolution mass spectrometry (HRMS). The combination of these techniques allows to unequivocally confirm the structure of the synthesized compounds.

3.2. Structural characterization of the 3-bromo-2-methyl-4*H*-chromen-4-one, 3-bromoflavones, (*E*)-3-bromo-2-styryl-4*H*-chromen-4-ones

3.2.1. Characterization of 3-bromo-2-methyl-4*H*-chromen-4-one

The structure and numbering of 3-bromo-2-methyl-4*H*-chromen-4-one (**50**) is presented in **figure 9**.

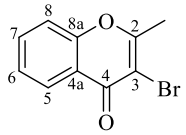

Figure 9. Structure and numbering of 3-bromo-2-methyl-4*H*-chromen-4-one (**50**).

The analysis of the ^{1}H NMR spectrum of compound **50** (**Figure 10**) allowed the unequivocal assignment of all the protons of the structure.

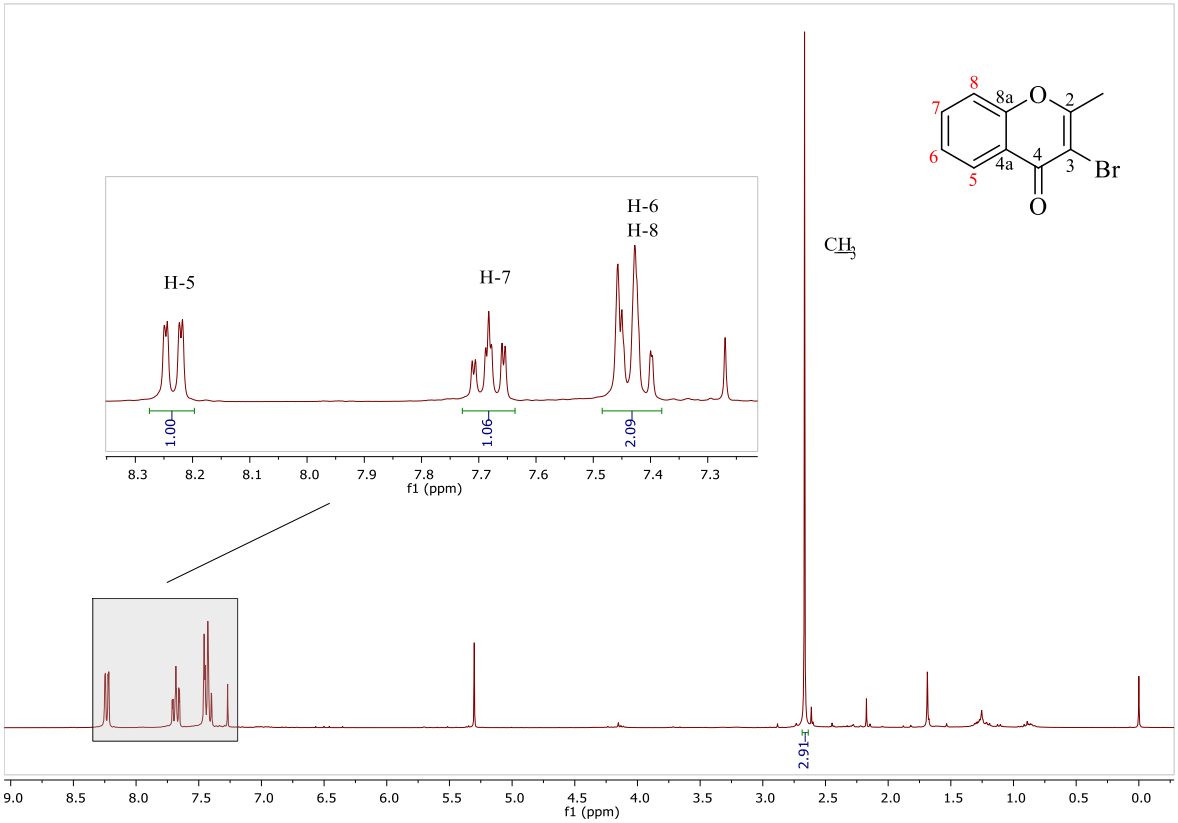

Figure 10. ^{1}H NMR spectrum and expansion of the aromatic region with assignments of protons of the 3-bromo-2-methyl-4*H*-chromen-4-one (**50**) (300.13 MHz, $CDCl_3$).

As can be seen in **Figure 10**, the most important peaks in the ^{1}H NMR spectrum of compound **50** are:

- The singlet at δ_H = 2.67 ppm corresponding to the resonance of the protons of the methyl group.
- The doublet of doublets (dd) due to the resonance of H-5 and the double of doublets of doublets (ddd) assigned to H-7 in the aromatic region (δ_H = 8.23 ppm and δ_H = 7.68 ppm, respectively). The signal corresponding to the resonance of H-5 proton appears at the highest frequency values due to both the mesomeric and anisotropic deshielding effect of the carbonyl group. The H-7 is more deshielded than H-6 and H-8 due to the mesomeric effect. The multiplicity of the signal of H-5, which appears as a dd, is justified by the coupling of H-5 with H-6 (^{3}J = 8.0 Hz) and with H-7 (^{4}J = 1.7 Hz) at a longer distance, whereas the multiplicity of the signal of H-7

is justified by the coupling of H-7 with H-6 and H-8 (^3J = 8.6, 7.1 Hz) and with H-5 at a longer distance (^4J = 1.7 Hz) (**Figure 10**).

- The multiplet (m) at δ_H = 7.39 – 7.46 ppm, corresponding to two protons, was assigned to the resonances of H-6 and H-8.

Considering the ^{13}C NMR spectrum (**Figure 11**), it was possible to assign all the carbons and identify the non-protonated carbons on the structure. The five protonated carbons were easily assigned based on the correlations observed in the heteronuclear single quantum correlation (HSQC) spectrum (**Figure 12**) at δ_C = 21.7 ppm ($\underline{C}H_3$), δ_C = 126.4 ppm (C-5), δ_C = 125.5 ppm (C-6), δ_C = 133.8 ppm (C-7), δ_C = 117.6 ppm (C-8).

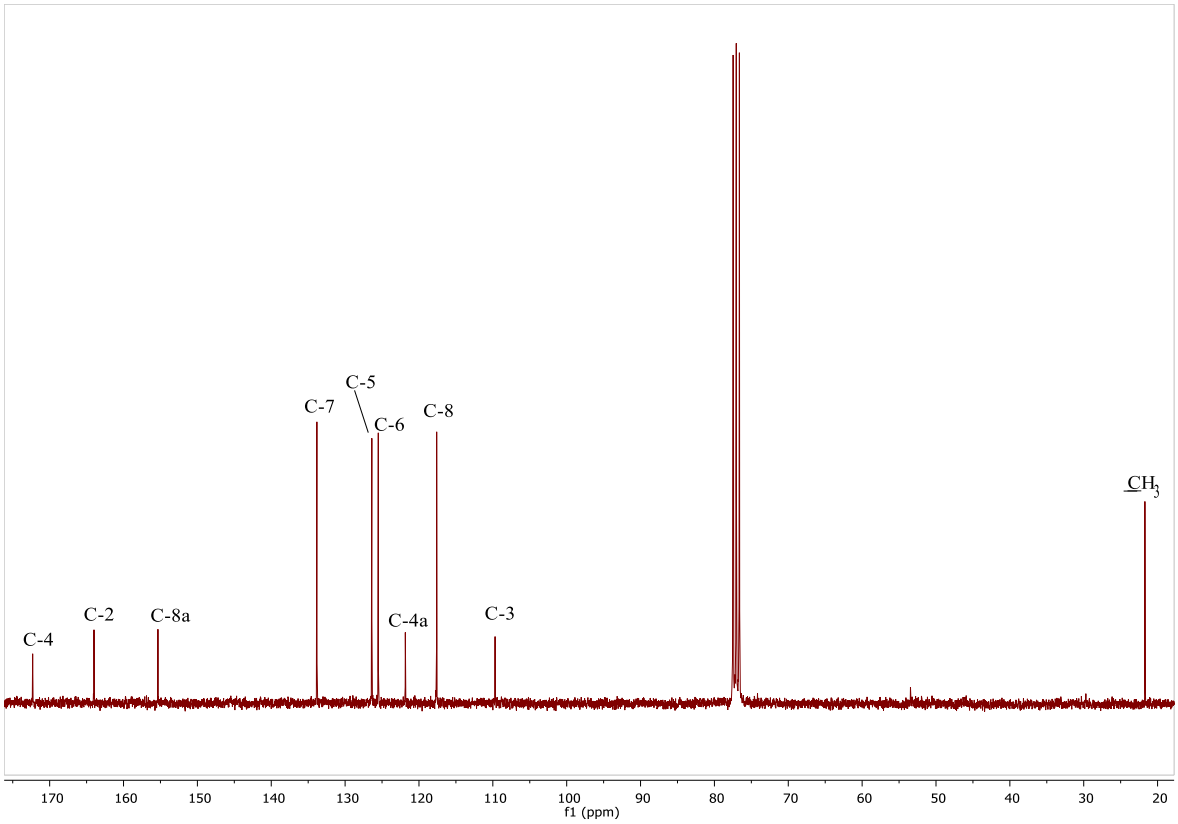

Figure 11. ^{13}C NMR spectrum of 3-bromo-2-methyl-4*H*-chromen-4-one (**50**) (75.47 MHz, $CDCl_3$).

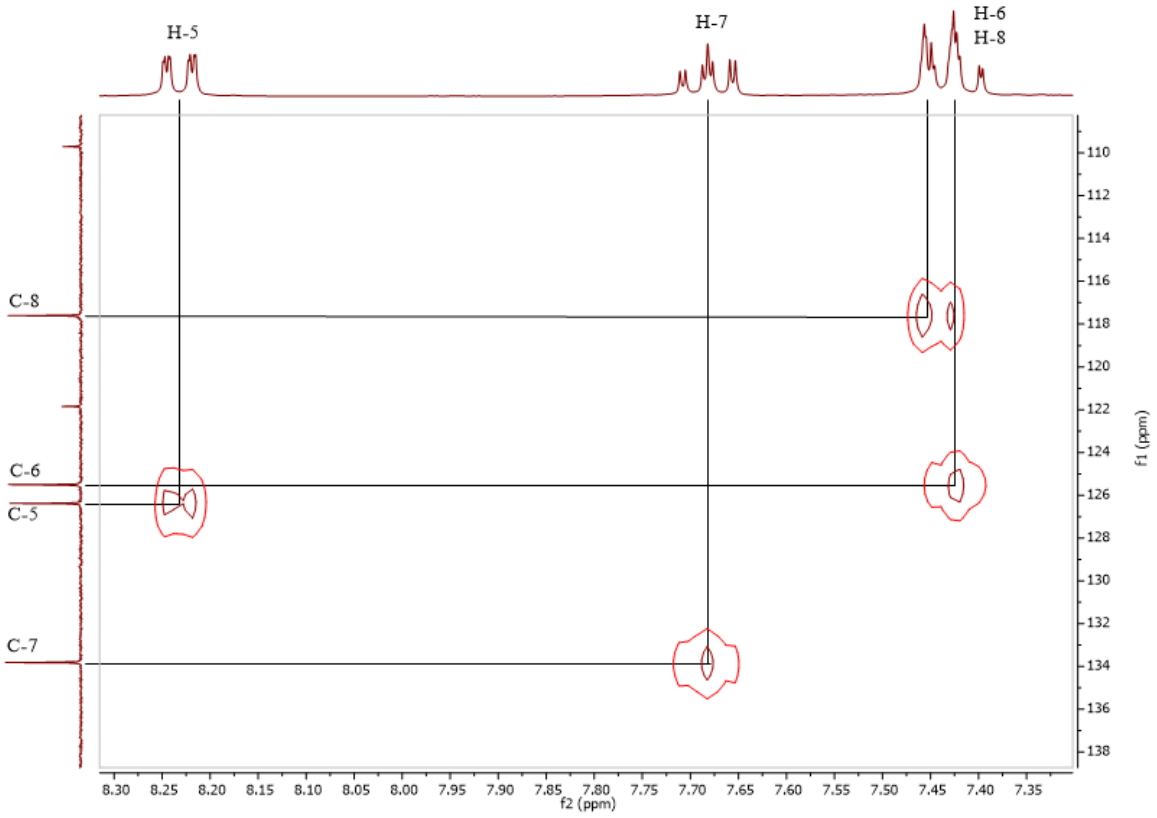

Figure 12. Expansion of the HSQC spectrum of 3-bromo-2-methyl-4*H*-chromen-4-one (**50**).

The non-protonated carbons were assigned based on the correlations observed in the heteronuclear multiple bond correlation (HMBC) spectrum (**Figure 13**), namely H-5→C-4 (δ_C = 172.3 ppm); H-6, H-8→C-4a (δ_C = 121.9 ppm); H-5, H-7, H-8→C8a (δ_C = 155.3 ppm). Moreover, the correlations observed for the protons of the methyl group, allowed the assignment of carbons C-2 and C-3: C$\underline{H}_3$→C-2 (δ_C = 164.0 ppm) and C$\underline{H}_3$→C-3 (δ_C = 109.7 ppm).

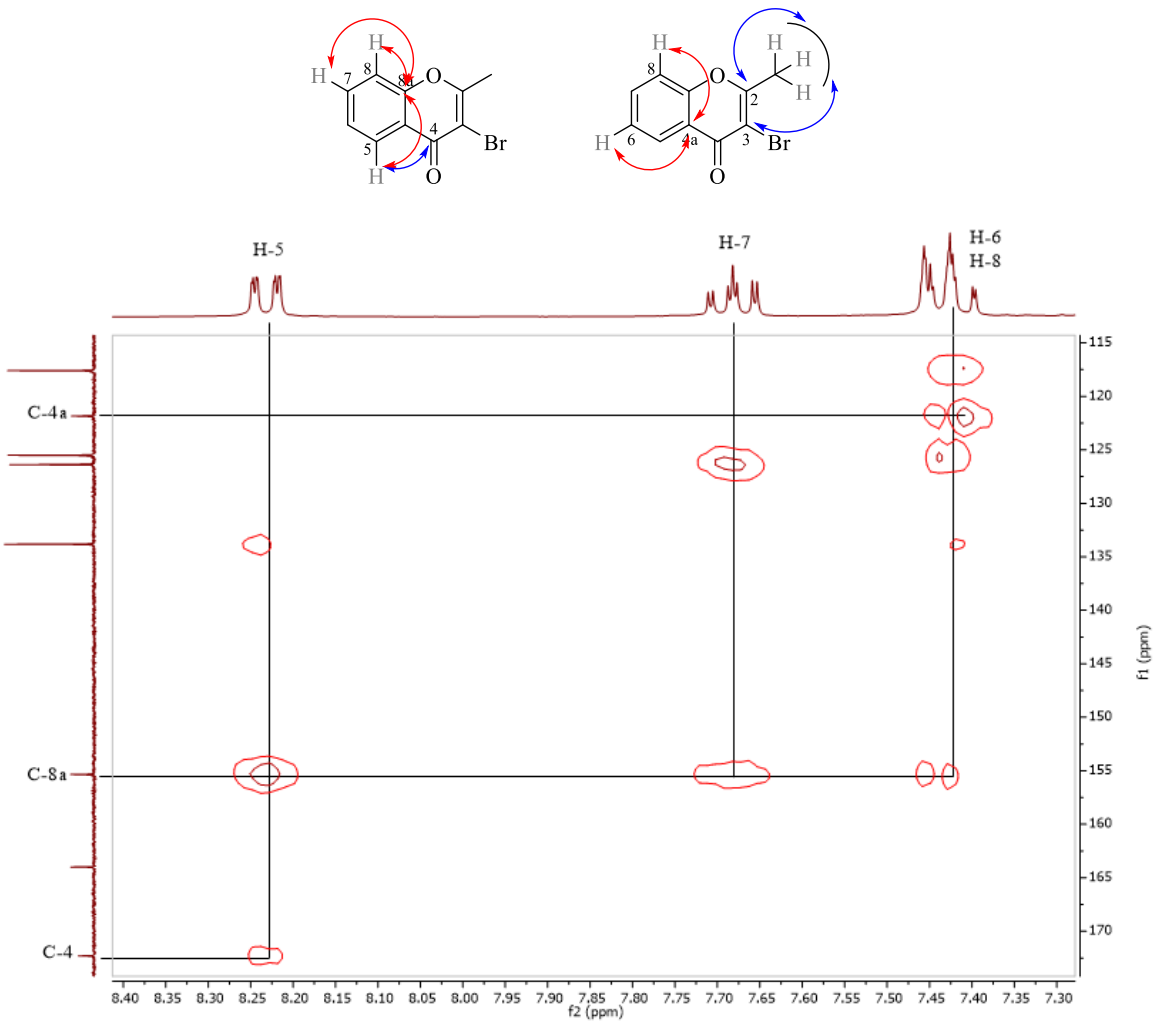

Figure 13. Expansion of the HMBC spectrum of 3-bromo-2-methyl-4*H*-chromen-4-one (**50**) and most relevant correlations observed therein.

3.2.2. Characterization of 3-bromoflavones

The structure and numbering of 3-bromoflavones (**58** and **59**) whose structural characterization will be discussed in this section are presented in **figure 14**. For sake of simplicity the protons and carbons of the benzyloxy groups in the C-3' and C-4' positions were not numbered.

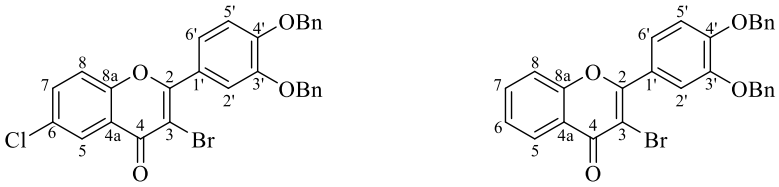

58 **59**

Figure 14. Structure and numbering of 2-[3,4-bis(benzyloxy)phenyl]-3-bromo-6-chloro-4*H*-chromen-4-one (**58**) and 2-[3,4-bis(benzyloxy)phenyl]-3-bromo-4*H*-chromen-4-one (**59**).

The ^{1}H NMR spectrum was obtained using deuterated chloroform as solvent, but in the aromatic region it was impossible to unequivocally assign all the protons. Thus, the ^{1}H NMR spectrum was obtained again using deuterated acetone (**Figure 15**).

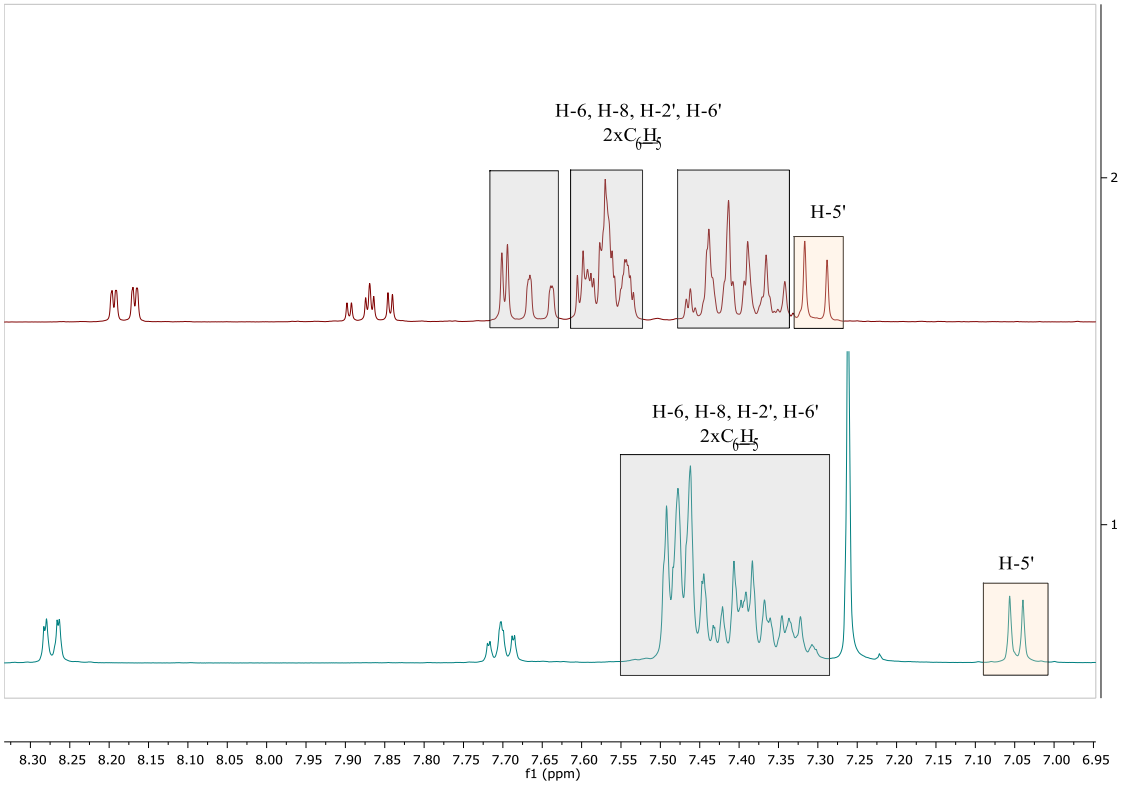

Figure 15. Comparison of the ^{1}H NMR spectra of compound **59** obtained with different solvents: 1- 300.13 MHz, $CDCl_3$; 2- 300.13 MHz, $(CD_3)_2CO$.

Based on the analysis of the ^{1}H NMR spectra of compounds **58** and **59**, it was possible to assign all the protons in their structures. The analysis of compound **59** (**Figure 16**) is presented as an example.

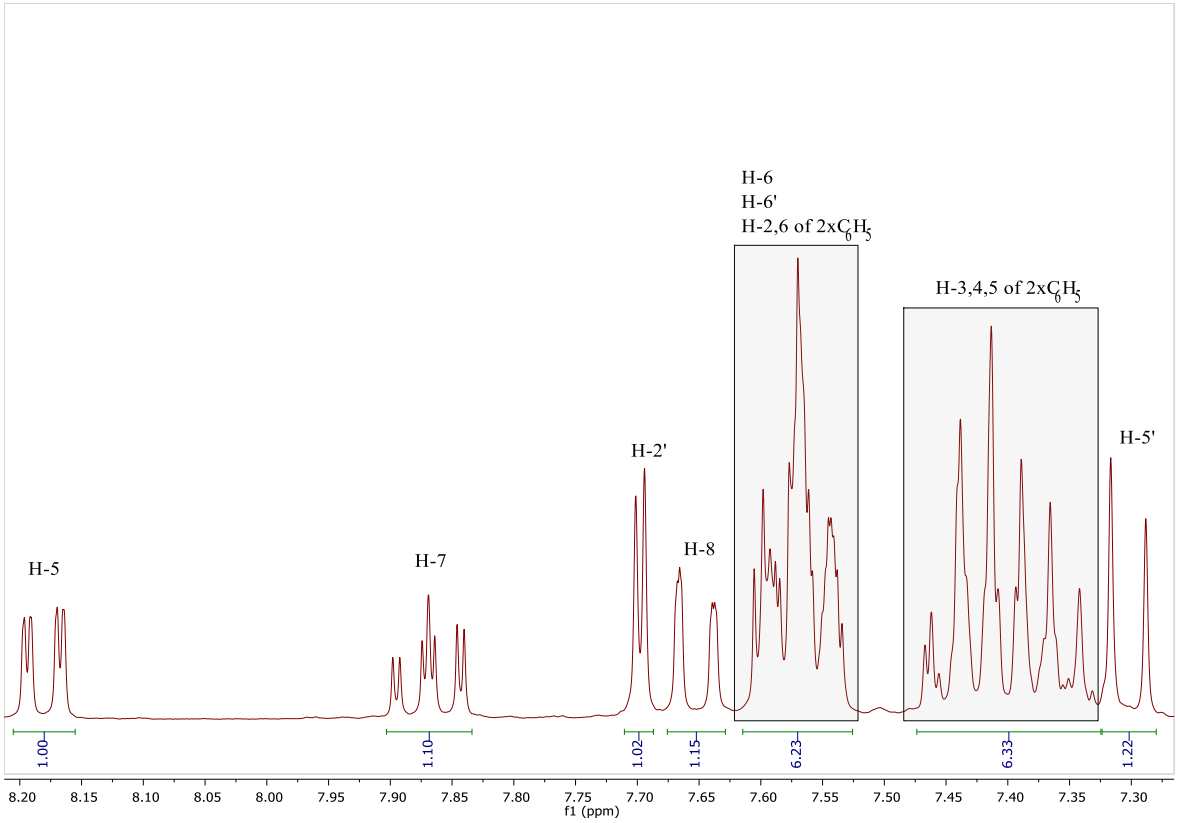

Figure 16. Expansion of the aromatic region of the ^{1}H NMR spectrum of compound **59** (300.13 MHz, $(CD_3)_2CO$).

The most important signals observed in the ^{1}H NMR spectrum of compound **59** are:

- Two singlets at δ_H = 5.30 ppm and δ_H = 5.34 ppm corresponding to the resonance of the protons of the two C$\underline{H}_2$ of the benzyloxy groups at the C-3' and C-4' position, respectively. Based on the analysis of the Nuclear Overhauser Effect Spectroscopy (NOESY) spectrum it was possible to see the correlation between the doublet at δ_H = 7.70 ppm assigned to H-2' and the singlet at δ_H = 5.30 ppm, which corresponds to the C$\underline{H}_2$ at C-3' position. The NOESY correlation between the doublet at δ_H = 7.30 ppm assigned to H-5' with the singlet at δ_H = 5.34 ppm, allowed its attribution to the C$\underline{H}_2$ at C-4' position (**Figure 17**).

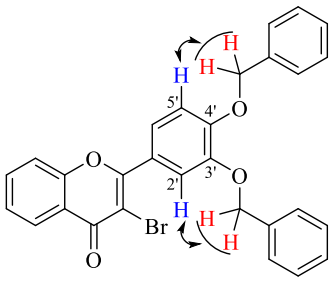

Figure 17. Important correlations observed in the NOESY spectrum of compound **59** between the two C<u>H</u>$_2$ with H-5' and H-2'.

- A doublet (d) due to the resonance of H-5' at δ_H = 7.30 ppm. The multiplicity of this signal is justified by the coupling of H-5' with H-6' (^3J = 8.5 Hz).
- The multiplet (m) at δ_H = 7.32 – 7.47 ppm corresponding to the resonance of six protons, namely H-3,4,5 of 3',4'-OCH$_2$C$_6$<u>H</u>$_5$.
- The multiplet at δ_H = 7.52 – 7.62 ppm corresponding to the resonance of six protons, namely H-6, H-6' and H-2,6 of 3',4'-OCH$_2$C$_6$<u>H</u>$_5$.
- A doublet of doublets at δ_H = 7.65 ppm due to the resonance of H-8. The multiplicity of this signal is justified by the coupling of H-8 with H-7 (^3J = 8.7 Hz) and with H-6 at long distance (^4J = 0.5 Hz).
- A doublet corresponding to the resonance of H-2' at δ_H = 7.70 ppm. The multiplicity of this signal is due to the coupling of H-2' with H-6' at a long distance (^4J = 2.2 Hz).
- A double of doublets of doublets at δ_H = 7.87 ppm due to the resonance of H-7, which is coupling with H-8 (^3J = 8.7 Hz) and H-6 (^3J = 7.1 Hz) and at a long distance with H-5 (^4J = 1.7 Hz).
- A doublet of doublets at δ_H = 8.18 ppm, due to resonance of H-5, which is coupling with H-6 (^3J = 8.0 Hz) and at a long distance with H-7 (^4J = 1.7 Hz). This signal appears at a higher frequency value due to both the mesomeric and anisotropic deshielding effect of the carbonyl group.

The same analysis was performed to assign all the protons of the compound **58**, where the only variation seen is the presence of a chloro in the C-6 position (**Table 4**). The presence of the halogen does not significantly affect the chemical shifts of the other protons.

Table 4. Chemical shifts (δ, ppm), multiplicities and coupling constants (J, Hz) of the signals observed in the ^{1}H NMR spectra of 3-bromoflavones **58** and **59**.

^{1}H NMR	58	59
H-5	δ 8.10 d, J = 2.6 Hz	δ 8.18 dd, J = 8.0, 1.7 Hz
H-6	–	δ 7.52 – 7.61 m
H-7	δ 7.86 dd, J = 9.1, 2.6 Hz	δ 7.87 ddd, J = 8.7, 7.1, 1.7 Hz
H-8	δ 7.72 d, J = 9.1 Hz	δ 7.65 dd, J = 8.7, 0.5 Hz
H-2'	δ 7.70 d, J = 2.1 Hz	δ 7.70 d, J = 2.2 Hz
H-5'	δ 7.30 d, J = 8.5 Hz	δ 7.30 d, J = 8.5 Hz
H-6'	δ 7.59 dd, J = 8.5, 2.1 Hz	δ 7.52 – 7.61 m
C$\underline{H}_2$	δ 5.29, s (3'-OC$\underline{H}_2$-Ph) δ 5.33, s (4'-OC$\underline{H}_2$-Ph)	δ 5.30, s (3'-OC$\underline{H}_2$-Ph) δ 5.34, s (4'-OC$\underline{H}_2$-Ph)
C$_6\underline{H}_5$	δ 7.52 –7.62 (H-2,6), m δ 7.33 – 7.47 (H-3,4,5), m	δ 7.52 – 7.61 (H-2,6), m δ 7.32 – 7.47 (H-3,4,5), m

Considering the ^{13}C NMR it was possible to unequivocal assign all the carbons in the structure of compound **59**. The total of carbons in the structure is 29, however, only 25 peaks appear in the ^{13}C NMR spectrum due to the equivalence of some carbons that have the same chemical environment (**Figure 18**).

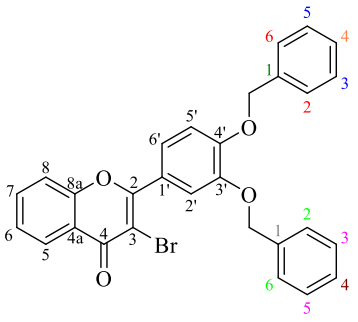

Figure 18. Carbon numbering of compound **59** with colors representing the carbons with similar chemical environments.

The nineteen protonated carbons were easily assigned based on the correlations observed in the HSQC spectrum (**Figure 19**) at δ_C = 125.8 ppm (C-5), δ_C = 125.5 ppm (C-6), δ_C = 134.3 ppm (C-7), δ_C = 118.2 ppm (C-8), δ_C = 116.1 ppm (C-2'), δ_C = 113.4 ppm (C-5'), δ_C = 123.5 ppm (C-6'). As for the carbons on the benzyloxy groups in the C-3' and C-4' positions, they were also assigned at δ_C = 70.9 ppm (3'-OC<u>H</u>$_2$Ph), δ_C = 70.4 ppm (4'-OC<u>H</u>$_2$Ph), δ_C = 127.8, 127.9, 128.4, 128.5 ppm (C-3, C-4, C-5) and δ_C =127.5 and 127.6 ppm (C-2 and C-6).

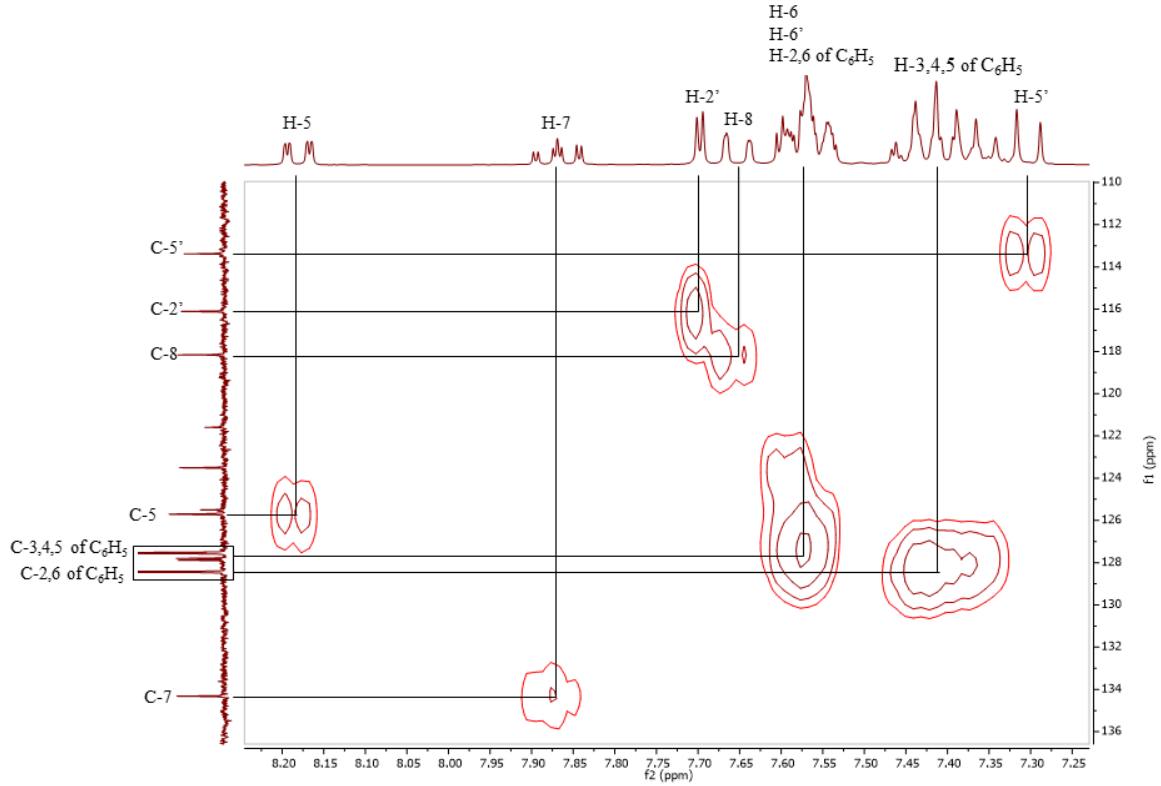

Figure 19. Expansion of the HSQC spectrum of compound **59**.

The non-protonated carbons were assigned based on the correlations observed in the HMBC spectrum (**Figure 20**), namely H-2'→C-2 (δ_C = 161.7 ppm); C-3 cannot be detected by any proton (δ_C = 108.1 ppm); H-5→C-4 (δ_C = 172.1 ppm); H-8, H-6→C4a (δ_C = 121.6 ppm); H-5, H-7, H-8→C-8a (δ_C = 155.6 ppm); H-5'→C-1' (δ_C = 125.7 ppm); H-5', 3'-OC<u>H</u>$_2$Ph, H-2'→C3' and (δ_C = 148.1 ppm); H-2', H-6', 4'-OC<u>H</u>$_2$Ph, H-5'→C4' and (δ_C = 151.4 ppm). As for the quaternary carbons (C-1) of the benzyloxy groups at C-3' and C-4' positions, they were assigned at δ_C = 137.2 ppm and δ_C = 137.3 ppm.

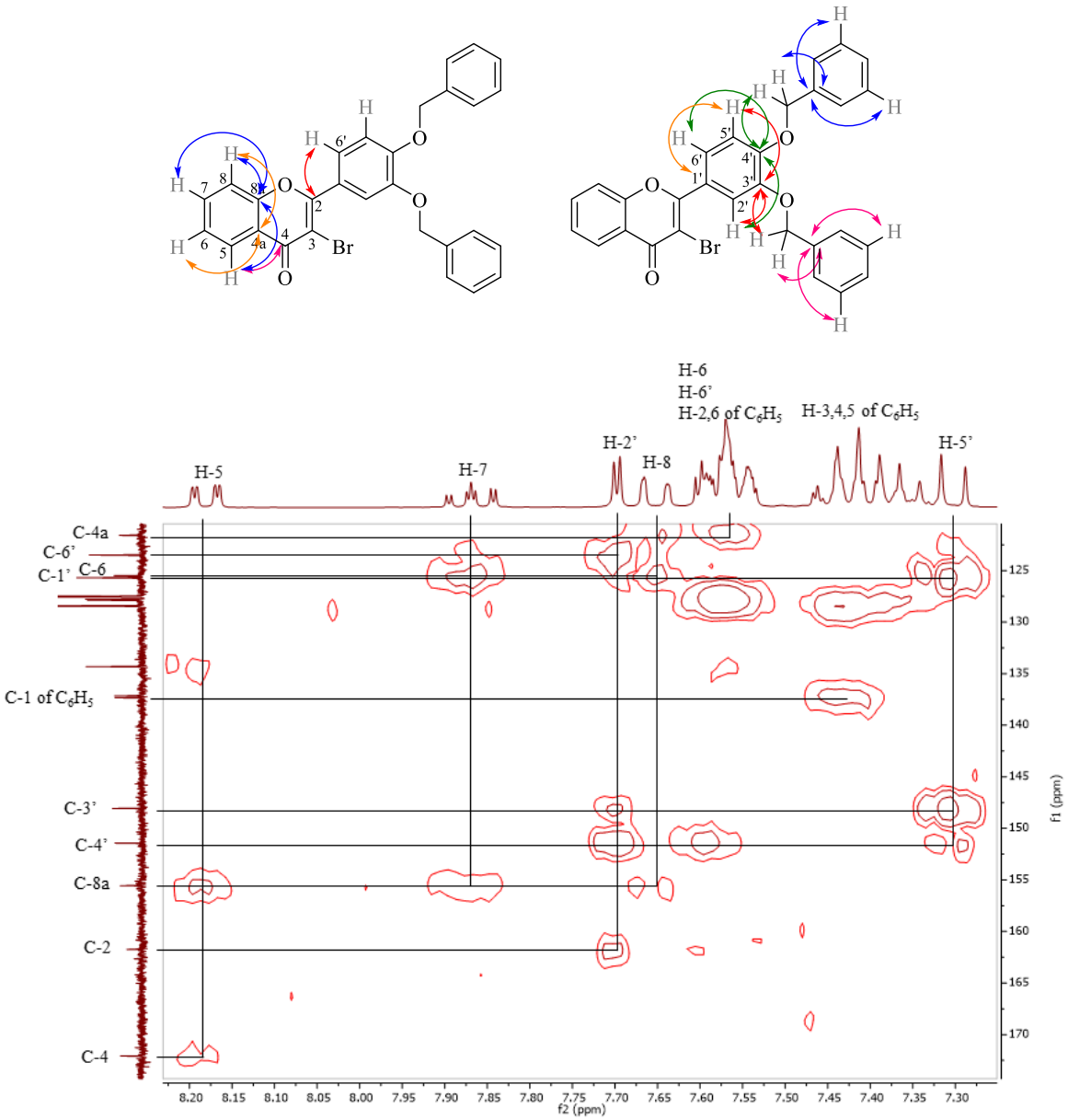

Figure 20. HMBC correlations and expansion of the HMBC spectrum of compound **59**.

The same analysis was performed to assign all the carbons of the compound **58**, based on the analysis of the HSQC and HMBC spectra (**Table 5**).

Table 5. Chemical shifts (δ, ppm) of the signals identified in the ^{13}C NMR spectra of 3-bromoflavones **58** and **59**.

^{13}C NMR	**58**	**59**
C-2	162.0	161.7
C-3	107.9	108.1
C-4	171.2	172.1
C-4a	122.6	121.6
C-5	124.7	125.7
C-6	130.8	125.5
C-7	134.3	134.3
C-8	120.6	118.2
C-8a	154.1	155.6
C-1'	125.1	125.7
C-2'	116.1	116.1
C-3'	148.1	148.1
C-4'	151.6	151.4
C-5'	113.4	113.4
C-6'	123.6	123.5
$\underline{C}H_2$	70.9 (3'-O$\underline{C}$H$_2$Ph) 70.4 (4'-O$\underline{C}$H$_2$Ph)	70.9 (3'-O$\underline{C}$H$_2$Ph) 70.4 (4'-O$\underline{C}$H$_2$Ph)
$C_6\underline{H}_5$	137.1 and 137.3 (C-1) 127.5 and 127.6 (C-2,6) 127.8, 127.9, 128.4 and 128.5 (C-3,4,5)	137.2 and 137.3 (C-1) 127.5 and 127.6 (C-2,6) 127.8, 127.9, 128.4 and 128.5 (C-3,4,5)

3.2.3. Characterization of (*E*)-3-bromo-2-styryl-4*H*-chromen-4-ones

The structures and numbering of (*E*)-3-bromo-2-styryl-4*H*-chromen-4-ones (**61**, **66**, **70** and **71**) are presented in **figure 21**. The protons and carbons of the benzyloxy and methoxy groups were not numbered for sake of simplicity.

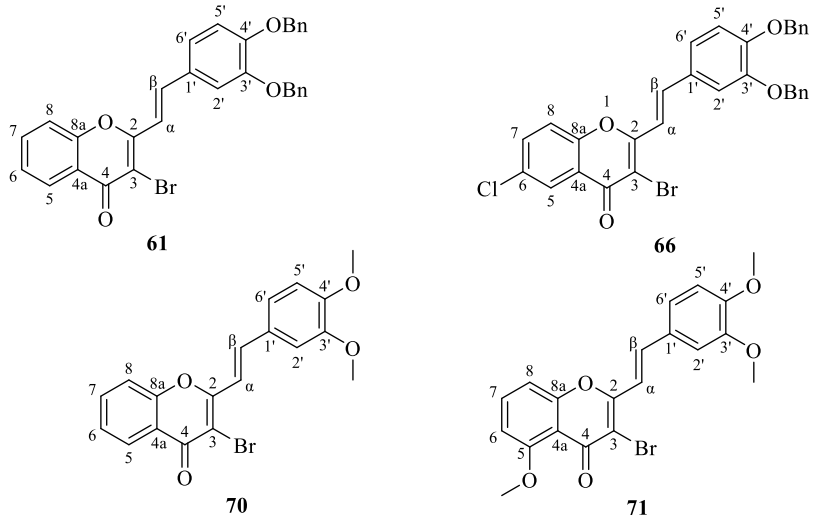

Figure 21. Structure and numbering of (*E*)-3-bromo-2-styryl-4*H*-chromen-4-ones **61**, **66**, **70** and **71**.

Based on the analysis of the ^{1}H NMR spectra (**Figure 22**), it was possible to assign all the protons of all the structures. The analysis of compound **61** is presented as an example.

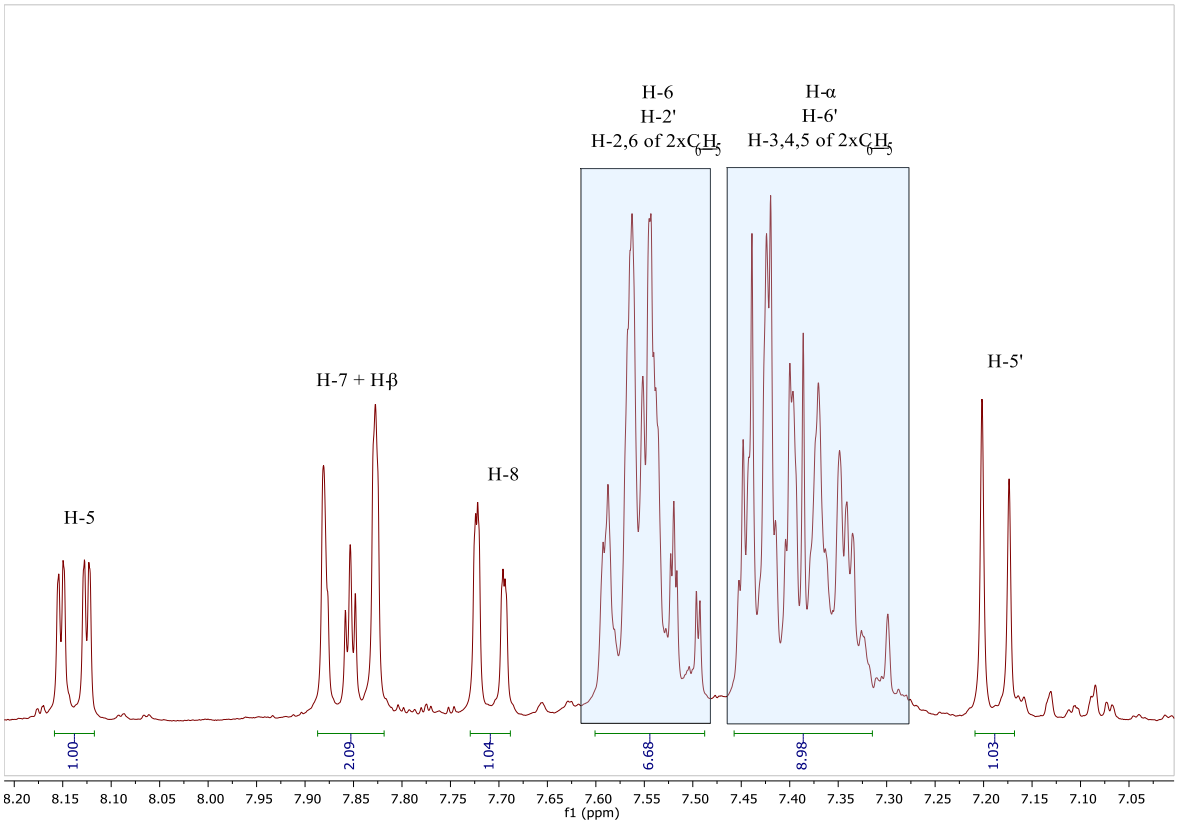

Figure 22. Expansion of the aromatic region of the ^{1}H NMR spectrum of compound **61** (300.13 MHz, $(CD_3)_2CO$).

As can be seen in **Figure 22**, the most important peaks in the ^{1}H NMR spectrum of compound **61** are:

- Two singlets at δ_H = 5.28 ppm and δ_H = 5.30 ppm corresponding to the resonance of the protons of the two C$\underline{H}_2$ of the benzyloxy groups at the C-4' and C-3' positions, respectively (although, these singlets are not shown in **Figure 22**). Based on the analysis of the NOESY spectrum it was possible to see the correlation between the H-2' at δ_H = 7.48 – 7.61 ppm and the singlet at δ_H = 5.30 ppm, which corresponds to the C$\underline{H}_2$ at C-3' position. The NOESY correlation between the doublet at δ_H = 7.19 ppm assigned to H-5' with the singlet at δ_H = 5.28 ppm, allowed its attribution to the C$\underline{H}_2$ at C-4' position.
- A doublet at δ_H = 7.19 ppm due to the resonance of H-5'. The multiplicity of this signal is justified by the coupling of H-5' with H-6' (^{3}J = 8.4 Hz).
- The multiplet (m) at δ_H = 7.28 – 7.47 ppm corresponding to the resonance of eight protons, namely H-α, H-6' and H-3,4,5 of 3',4'-OCH$_2$C$_6\underline{H}_5$.
- The multiplet at δ_H = 7.48 – 7.61 ppm corresponding to the resonance of six protons, namely H-6, H-2' and H-2,6 of 3',4'-OCH$_2$C$_6\underline{H}_5$.
- A doublet of doublets at δ_H = 7.72 ppm due to the resonance of H-8. The multiplicity of this signal is justified by the coupling of H-8 with H-7 (^{3}J = 8.5 Hz) and with H-6 at long distance (^{4}J = 1.0 Hz).
- The multiplet at δ_H = 7.82 – 7.90 ppm corresponding to the resonance of two protons, namely H-7 and H-β. The proton H-β appeared at δ_H = 7.86 ppm, and its multiplicity is justified by the coupling oh H-β with H-α (^{3}J = 16.0 Hz).
- The doublet of doublets corresponding to the resonance of H-5 proton appears at the highest frequency values, δ_H = 8.23 ppm, due to both the mesomeric and anisotropic deshielding effect of the carbonyl group. The multiplicity of this proton H-5 is due to the coupling with H-6 (^{3}J = 7.8 Hz) and with H-7 at a long distance (^{4}J = 1.8 Hz).

The same analysis was performed to assign all the protons of the compounds **61**, **66**, **70** and **71** (**Table 6**). The variation of the protecting groups in the 3' and 4' position

observed between the compounds **61**, **66** and the compounds **70**,**71** does not significantly affect the signals of the protons in the 2-styryl group. However, in the compound **71**, the presence of the methoxy group in the 5 position causes a shielding of the protons H-6, H-7 and H-8. Moreover, it is possible to distinguish the compounds **70**,**71** from the compounds **61**, **66** in the ^{1}H NMR due to loss of the singlets of the C<u>H</u>$_2$ of the benzyloxy groups at the C-4' and C-3' positions (δ_H = 5.22 – 5.30 ppm) and the appearance the characteristic singlets of the CH_3 of the methoxy groups at the C-4', C-3' and C-5 positions (δ_H = 3.94 – 3.99 ppm).

Table 6. Chemical shifts (δ, ppm), multiplicities and coupling constants (J, Hz) of the signals observed in the ^{1}H NMR spectra of (*E*)-3-bromo-2-styryl-4*H*-chromen-4-ones **61**, **66**, **70** and **71**.

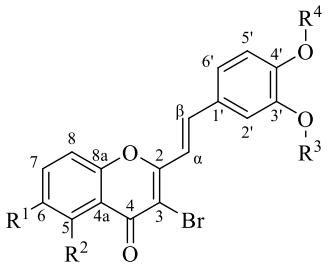

^{1}H NMR	61	66	70	71
H-5	δ 8.14 dd, J = 7.8, 1.8 Hz	δ 8.16 d, J = 2.6 Hz	δ 8.25 dd, J = 8.1, 1.7 Hz	–
H-6	δ 7.48 – 7.61 m	–	δ 7.43 ddd, J = 8.1, 7.1, 1.1 Hz	δ 6.82 dd, J = 8.3, 0.9 Hz
H-7	δ 7.82 – 7.90 m	δ 7.61 dd, J = 8.9, 2.6 Hz	δ 7.71 ddd, J = 8.7, 7.1, 1.7 Hz	δ 7.57 t, J = 8.3 Hz
H-8	δ 7.72 dd, J = 8.5, 1.0 Hz	δ 7.29 – 7.52 m	δ 7.55 dd, J = 8.7, 1.1 Hz	δ 7.09 dd, J = 8.3, 0.9 Hz
H-α	δ 7.28 – 7.47 m	δ 7.21 d, J = 15.9 Hz	δ 7.36 d, J = 16.0 Hz	δ 7.26 d, J = 16.0 Hz
H-β	δ 7.86 d, J = 16.0 Hz	δ 7.56 d, J = 15.9 Hz	δ 7.68 d, J = 16.0 Hz	δ 7.57 d, J = 16.0 Hz
H-2'	δ 7.48 – 7.61 m	δ 7.20 d, J = 2.1 Hz	δ 7.16 d, J = 2.0 Hz	δ 7.12 d, J = 1.9 Hz
H-5'	δ 7.19 d, J = 8.4 Hz	δ 6.95 d, J = 8.4 Hz	δ 6.93 d, J = 8.4 Hz	δ 6.91 d, J = 8.3 Hz

H-6'	δ 7.28 – 7.47 m	δ 7.16 dd, J = 8.4, 2.1 Hz	δ 7.25 dd, J = 8.4, 2.1 Hz	δ 7.21 dd, J = 8.3, 1.9 Hz
R^2 = OC<u>H</u>$_3$	–	–	–	δ 3.98, s
R^3, R^4 = OC<u>H</u>$_3$	–	–	δ 3.95, s (4'-OC<u>H</u>$_3$) δ 3.99, s (3'-OC<u>H</u>$_3$)	δ 3.94, s δ 3.97, s
R^3, R^4 = OBn				
C<u>H</u>$_2$	δ 5.30, s (3'-OC<u>H</u>$_2$) δ 5.28, s (4'-OC<u>H</u>$_2$)	δ 5.22, s δ 5.23, s	–	–
C$_6$<u>H</u>$_5$	δ 7.48 –7.61 (H-2,6), m δ 7.28 – 7.47 (H-3,4,5), m	δ 7.29 – 7.52 m		

Considering the ^{13}C NMR (**Figure 23**) it was possible to assign all the carbons in the structure of compound **61**, with support of the HSQC and HMBC spectra. The total of carbons in the structure is 31, however, only 27 peaks appear in the ^{13}C NMR spectrum due to the equivalence of some carbons that have the same chemical environment.

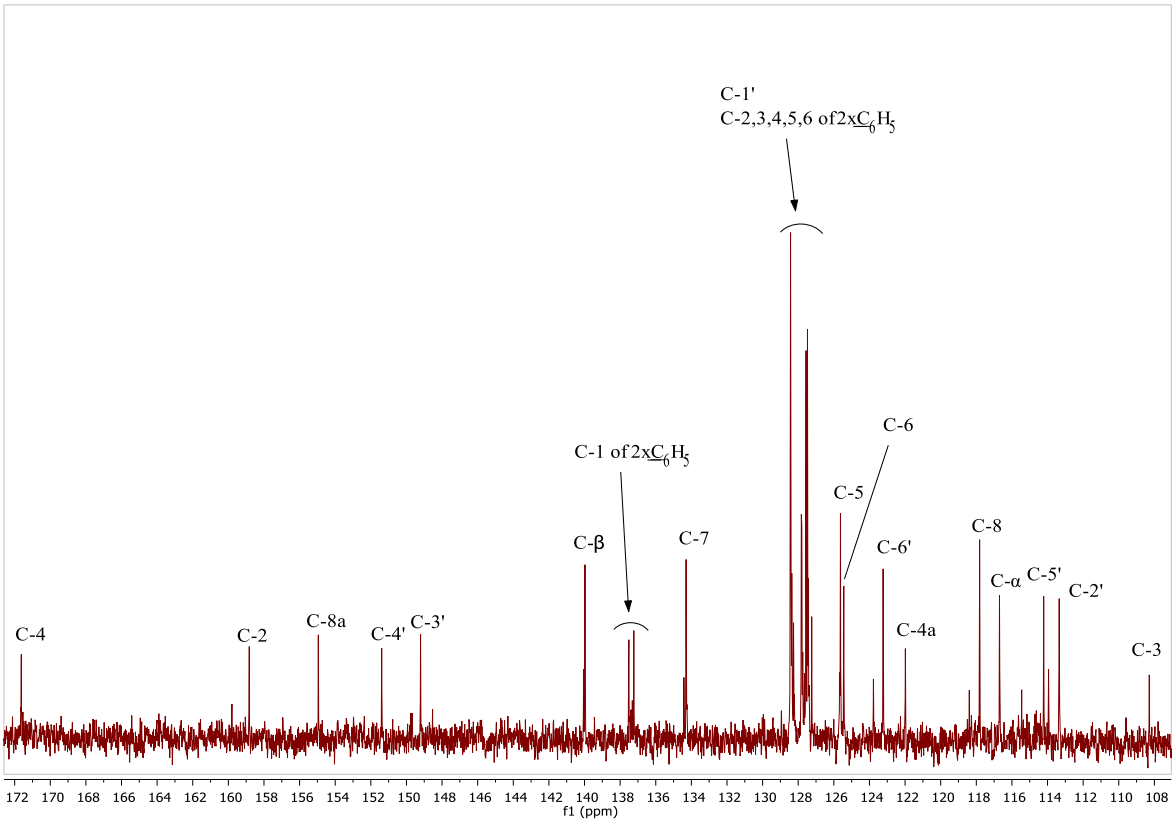

Figure 23. Expansion of the ^{13}C NMR spectrum of compound **61** (75.47 MHz, $(CD_3)_2CO$).

The twenty-one protonated carbons were easily assigned based on the correlations observed in the HSQC spectrum (**Figure 24**) at δ_C = 125.6 ppm (C-5), δ_C = 125.4 ppm (C-6), δ_C = 134.3 ppm (C-7), δ_C = 117.8 ppm (C-8), δ_C = 116.7 ppm (C-α), δ_C = 140.0 ppm (C-β), δ_C = 113.3 ppm (C-2'), δ_C = 114.2 ppm (C-5'), δ_C = 123.2 ppm (C-6'). As for the carbons on the benzyloxy groups in the C-3' and C-4' positions, they were also assigned at δ_C = 70.7 ppm (3'-OC<u>H</u>$_2$Ph), δ_C = 70.4 ppm (4'-OC<u>H</u>$_2$Ph), δ_C =127.5 and 127.6 ppm (C-2 and C-6) and δ_C = 127.80, 127.83, 128.41, 128.43 ppm (C-3, C-4, C-5).

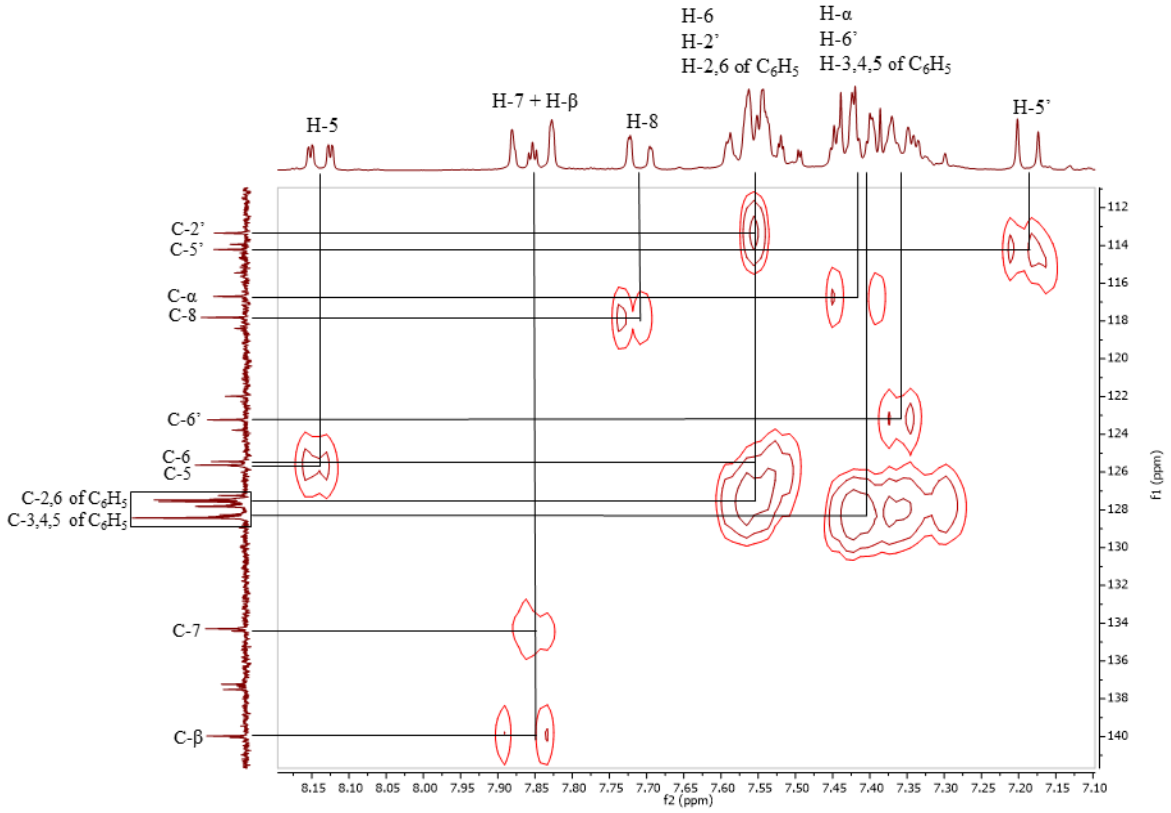

Figure 24. Expansion of the HSQC spectrum of compound **61**.

The non-protonated carbons were assigned based on the correlations observed in the HMBC spectrum (**Figure 25**), namely H-β, H-α→C-2 (δ_C = 158.8 ppm); H-α→C-3 (δ_C = 108.3 ppm); H-5→C-4 (δ_C = 171.6 ppm); H-8, H-6→C4a (δ_C = 122.0 ppm); H-5, H-7, H-8→C-8a (δ_C = 155.0 ppm); H-5'→C-1' (δ_C = 128.4 ppm); H-5', 3'-OC<u>H</u>$_2$Ph→C3' and (δ_C = 149.2 ppm); H-2', H-6', 4'-OC<u>H</u>$_2$Ph→C4' and (δ_C = 151.4 ppm). As for the quaternary carbons (C-1) of the benzyloxy groups at C-3' and C-4' positions, they were assigned at δ_C = 137.2 ppm and δ_C = 137.5 ppm.

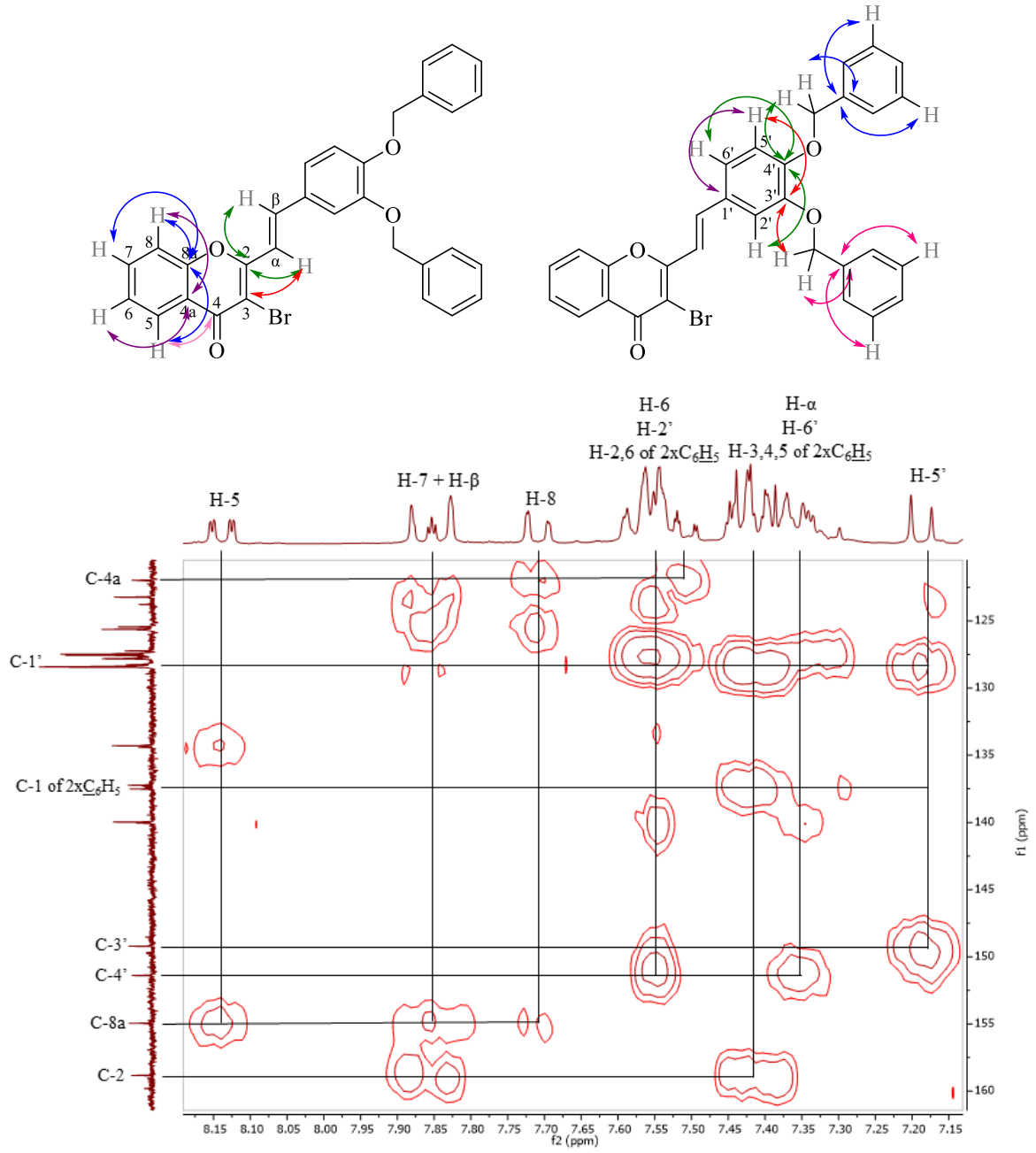

Figure 25. HMBC correlations and expansion of the HMBC spectrum of compound **61**.

The same analysis was performed to assign all the carbons of the compounds **70** and **71**, based on the analysis of the HSQC and HMBC spectra (**Table 7**). For compound **66** this analysis was not performed due to the low purity of the compound.

Table 7. Chemical shifts (δ, ppm) of the signals identified in the ^{13}C NMR spectra of (*E*)-3-bromo 2-styryl-4*H*-chromen-4-ones **61**, **70** and **71**.

^{13}C NMR	**61**	**70**	**71**
C-2	158.8	158.8	156.9
C-3	108.3	109.1	110.7
C-4	171.6	172.7	171.4
C-4a	122.0	122.2	112.9
C-5	125.6	126.5	159.8
C-6	125.4	125.3	106.5
C-7	134.3	134.0	134.0
C-8	117.8	117.5	109.4
C-8a	155.0	154.9	156.8
C-α	116.7	117.0	116.9
C-β	140.0	139.6	138.8
C-1'	128.4	128.0	128.1
C-2'	113.3	109.7	109.7
C-3'	149.2	149.4	149.3
C-4'	151.4	151.3	151.1
C-5'	114.2	111.2	111.2
C-6'	123.2	122.7	122.4
R^2 = O<u>C</u>H$_3$	–	–	56.0
R^3, R^4 = O<u>C</u>H$_3$	–	56.0 (4'-OC<u>H</u>$_3$) 56.1 (3'-OC<u>H</u>$_3$)	56.5
R^3, R^4 = OBn			
<u>C</u>H$_2$	70.7 (3'-O<u>C</u>H$_2$) 70.4 (4'-O<u>C</u>H$_2$)	–	–
<u>C</u>$_6$H$_5$	137.2 and 137.5 (C-1) 127.5 and 127.6 (C-2,6) 127.80, 127.83, 128.41 and 128.43 (C-3,4,5)		

3.3. Structural characterization of sugar alkene

The structure and numbering of sugar alkene **74** are presented in **figure 26**. Based on the analysis of the ^{1}H NMR spectra (**Figure 27**), it was possible to identify the sugar alkene and assign all the protons of the structure.

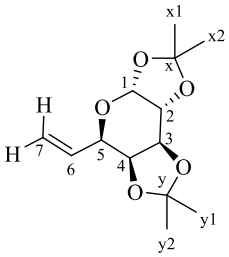

Figure 26. Structure and numbering of 6,7-dideoxy-1,2:3,4-di-*O*-isopropylidene-α-D-*galacto*-hept-6-enopyranose (**74**).

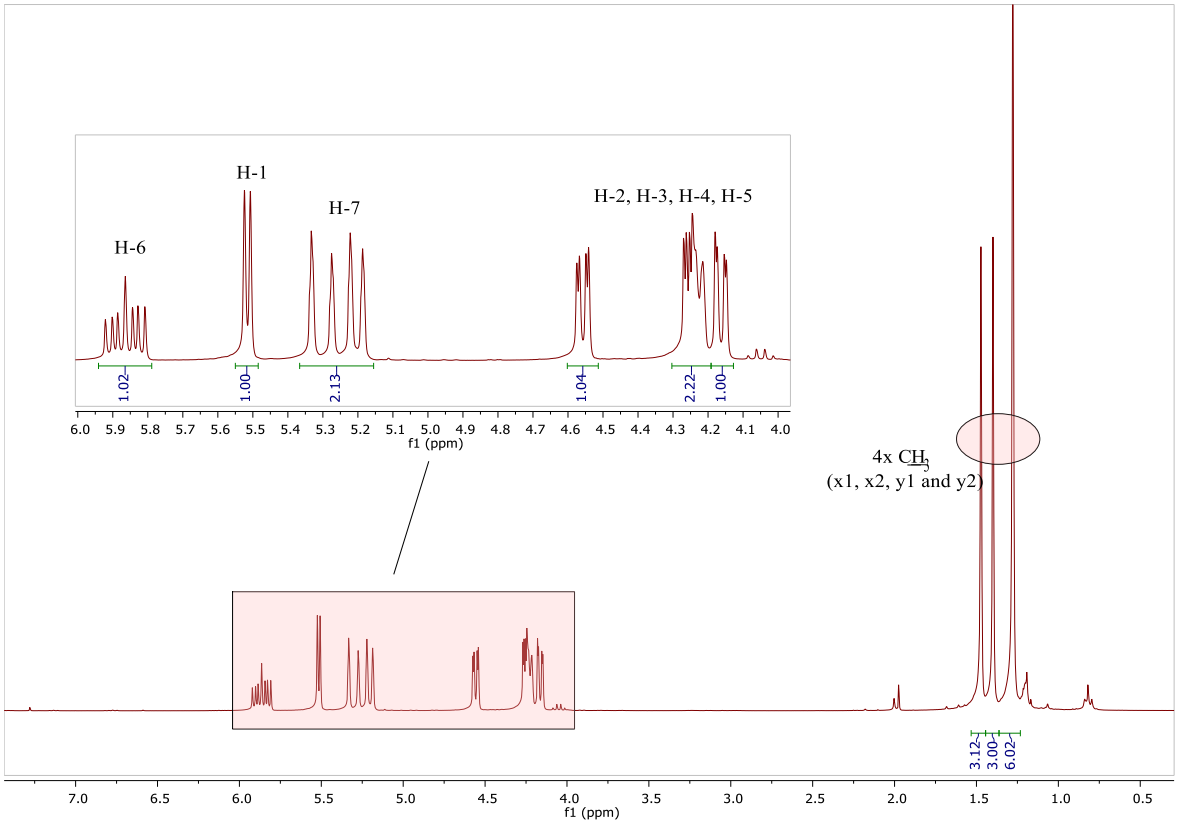

Figure 27. ^{1}H NMR spectrum with assignments of protons of the sugar alkene **74** (300.13 MHz, $CDCl_3$).

The most important signals observed in the ^{1}H NMR spectrum of compound **74**, are:

- Three singlets at δ_H = 1.28 ppm, δ_H = 1.40 ppm and δ_H = 1.47 ppm corresponding to the resonances of the protons of the four CH_3 of the protecting groups (x1, x2, y1 and y2).
- A doublet of doublets at δ_H = 4.16 ppm (J = 7.8, 1.9 Hz), the multiplet at δ_H = 4.20 – 4.30 ppm and the doublet of doublets at δ_H = 4.56 ppm (J = 7.9, 2.4 Hz), which corresponds to four protons, namely H-2, H-3, H-4, and H-5.

- The multiplet at δ_H = 5.16 – 5.37 ppm corresponding to the resonance of two protons, namely H-7.
- A doublet at δ_H = 5.52 ppm due to the resonance of H-1, which is coupling with H-2 (^3J = 5.2 Hz).
- A double of doublets of doublets at δ_H = 5.86 ppm due to the resonance of H-6, which is coupling with the two protons H-7 and with H-5.

3.4. Structural characterization of the *C*-glycosyl 2-styryl-4*H*-chromen-4-ones

The structures and numbering of *C*-glycosyl 2-styryl-4*H*-chromen-4-ones (**89**, **90**, **91**, **92** and **93**) are presented in **figure 28**. The protons and carbons of the benzyloxy and methoxy groups were not numbered for sake of simplicity.

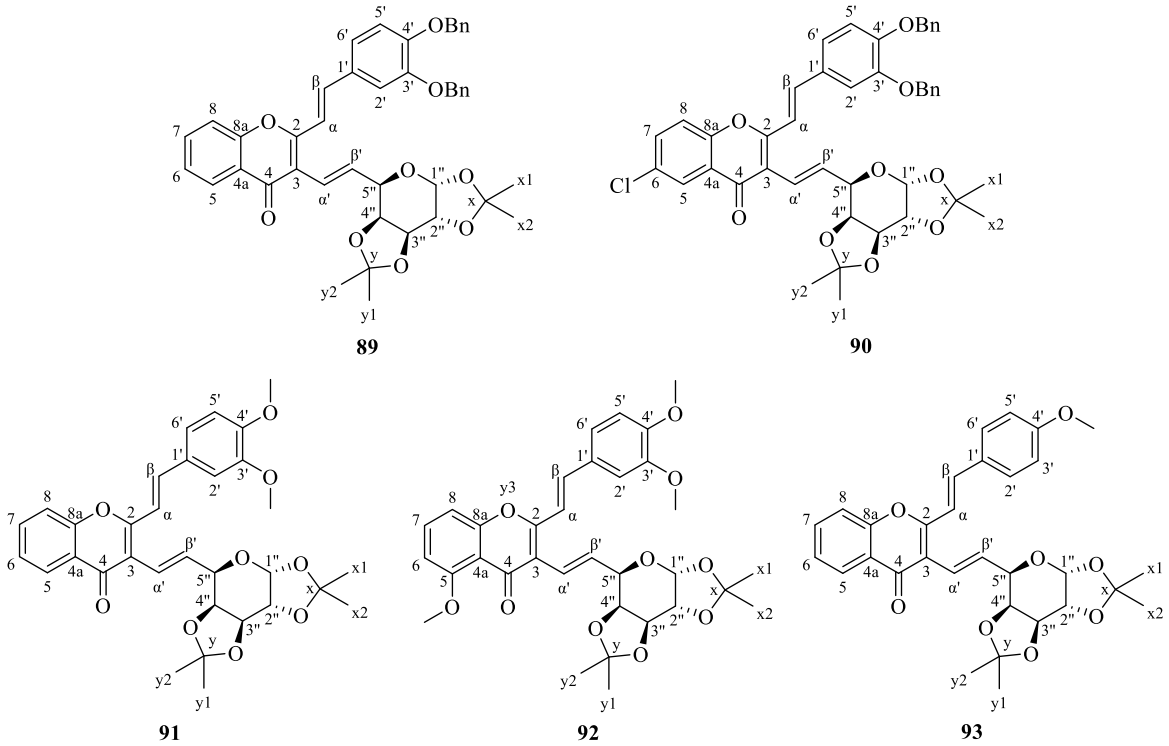

Figure 28. Structure and numbering of the *C*-glycosyl 2-styryl-4*H*-chromen-4-ones **89**-**93**.

Based on the analysis of the ^{1}H NMR spectra (**Figure 29**), it was possible to identify the presence of isomers in all the target compounds. For the compound **89** it was possible to identify two major isomers, whereas for the compounds **90**, **91**, **92** and **93** it was observed the presence of four isomers, which the unequivocal assignments were not possible to be done. Thus, the discussion of the compound **89** will be presented in this section.

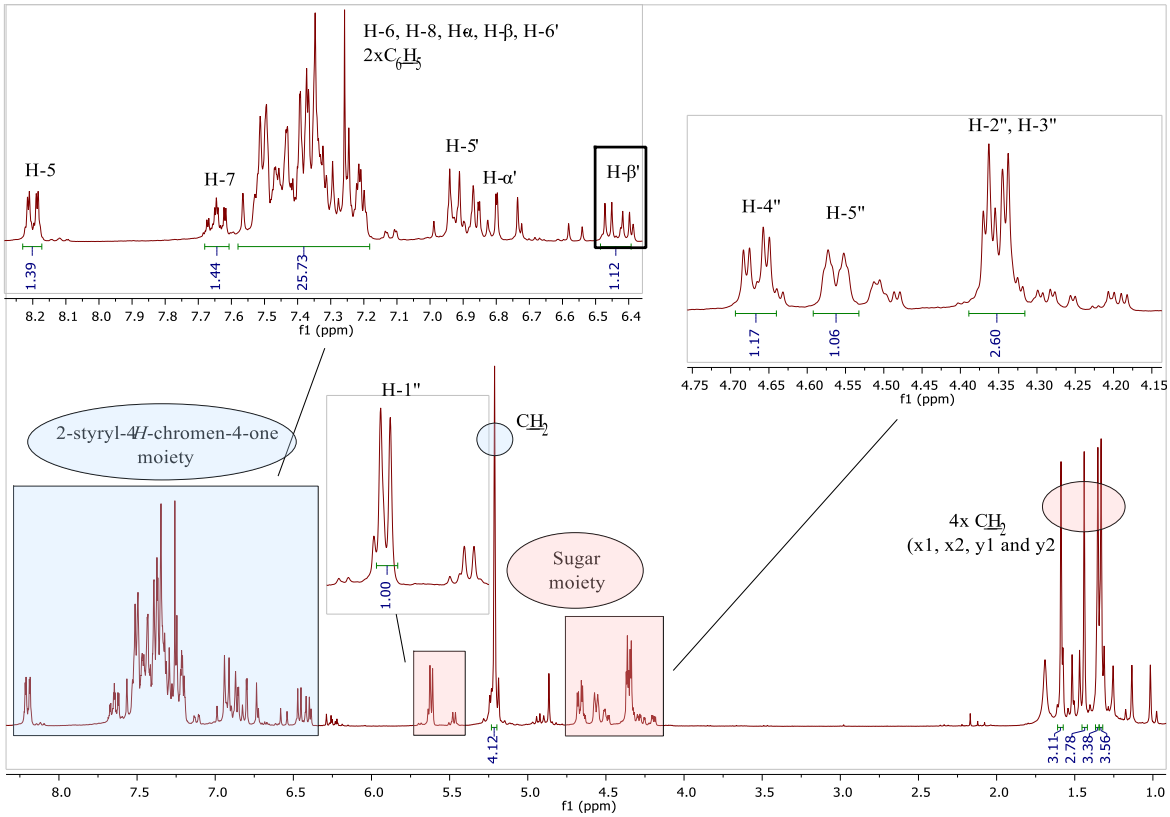

Figure 29. ^{1}H NMR spectrum with assignments of the protons of compound **89** (300.13 MHz, ($CDCl_3$).

As can be seen in **Figure 29**, it is possible to conclude that the coupling of the 3-bromo 2-styryl-4*H*-chromen-4-one **61** with the sugar alkene **74** was achieved due to the resonance of the proton H-β' at δ_H = 6.43 ppm. The multiplicity of this signal is due to the coupling of H-β' with H-α' (^{3}J = 16.1 Hz) and with H-5'' (^{3}J = 6.1 Hz). Also, the coupling is also supported by the absence of the double of doublets of doublets observed in the sugar alkene **74** regarding the H-6 (δ_H = 5.86 ppm) in the ^{1}H NMR spectrum of compound **89**. Moreover, the presence of isomers is corroborated by the signals of the proton H-1''; the doublet at δ_H = 5.62 ppm corresponds to the major isomer whose multiplicity is due to the coupling of H-1'' with H-2'' (J = 5.1 Hz).

Although most of the signals observed in the ^{1}H NMR spectrum are difficult to observe, there are some that were possible to assign to the *C*-glycosyl 2-styryl-4*H*-chromen-4-one **89** mainly:

- Two singlets at δ_H = 1.33 ppm, δ_H = 1.44 ppm corresponding to the resonance of the protons H-y1 and H-y2 and other two singlets at δ_H = 1.35

ppm and δ_H = 1.49 ppm corresponding to the resonance of the protons H-x1 and H-x2 of the protecting groups of the sugar moiety.

- A multiplet at δ_H = 4.32 – 4.38 ppm, corresponding to the resonance of two protons of H-2'' and H-3'' and the multiplet at δ_H = 4.53 – 4.59 ppm corresponding to H-5''. The doublet of doublets at δ_H = 4.67 ppm due to the resonance of H-4'' (J = 7.8, 2.4 Hz).
- A singlet at δ_H = 5.21 ppm corresponding to the resonance of the protons of the two C<u>H</u>$_2$ of the benzyloxy groups at the C-3' and C-4' position of the 2-styryl-4*H*-chromen-4-one.
- A doublet of doublets at δ_H = 6.83 ppm corresponding to the resonance of the proton H-α' was confirmed by the COSY correlations between the protons H-β' and H-α'. The multiplicity of this signal is due to the coupling of H- α' with H-β' (^3J = 16.1 Hz) and with H-5'' at long distance (^4J = 1.4 Hz).
- A doublet at δ_H = 6.93 ppm due to the resonance of the proton of H-5', which is coupling with H-6' (^3J = 8.6 Hz).
- A doublet of doublets of doublets at δ_H = 7.65 ppm due to the resonance of H-7, which is coupling with H-8 and H-6 (^3J = 8.6, 7.0 Hz) and at long distance with H-5 (^4J = 1.8 Hz).
- A doublet of doublets at a higher frequency value, δ_H = 8.20 ppm, due to resonance of H-5, which is coupling with H-6 (^3J = 8.0 Hz) and at a long distance with H-7 (^4J = 1.8 Hz).

Considering the ^{13}C NMR it was possible to assign some of the carbons of the *C*-glycosyl 2-styryl-4*H*-chromen-4-one **89**, with support of the HSQC and HMBC spectra (**Figures 30, 31 and 32**). The carbons bearing the previous identified protons were easily assigned based on the correlations observed in the HSQC spectrum (**Figures 30** and **31**) at δ_C = 24.5, 24.9, 26.1 and 26.2 ppm (C-x1, C-x2, C-y1 and C-y2), δ_C = 69.2 ppm (C-5''), δ_C = 70.4 and 73.7 ppm (C-2'' and C-3''), δ_C = 71.0 and 71.4 ppm (3', 4'-O<u>C</u>H$_2$Ph), δ_C = 71.1 ppm (C-4''), δ_C = 96.5 ppm (C-1''), δ_C = 114.6 ppm (C-5'), δ_C = 122.5 ppm (C-α'), δ_C = 126.0 ppm (C-5), 133.2 ppm (C-β'), δ_C = 133.5 ppm (C-7), δ_C = 136.6 ppm (C-β).

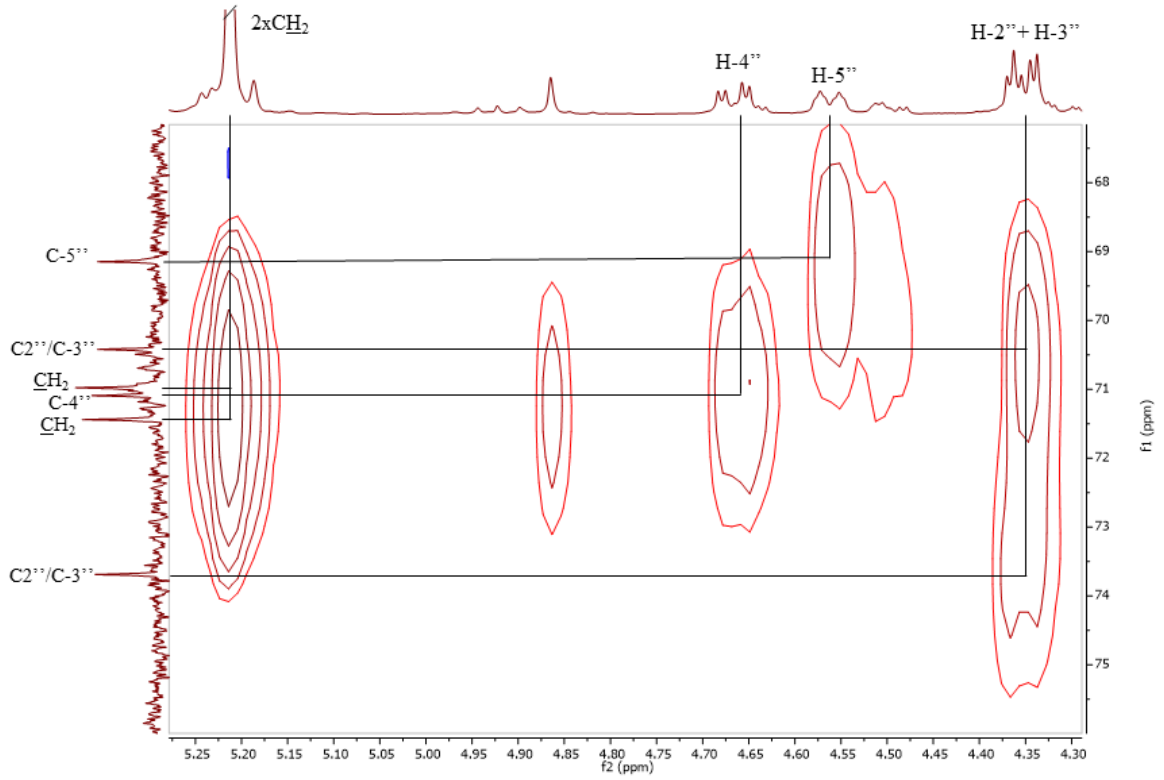

Figure 30. Expansion of HSQC spectrum of compound **89**.

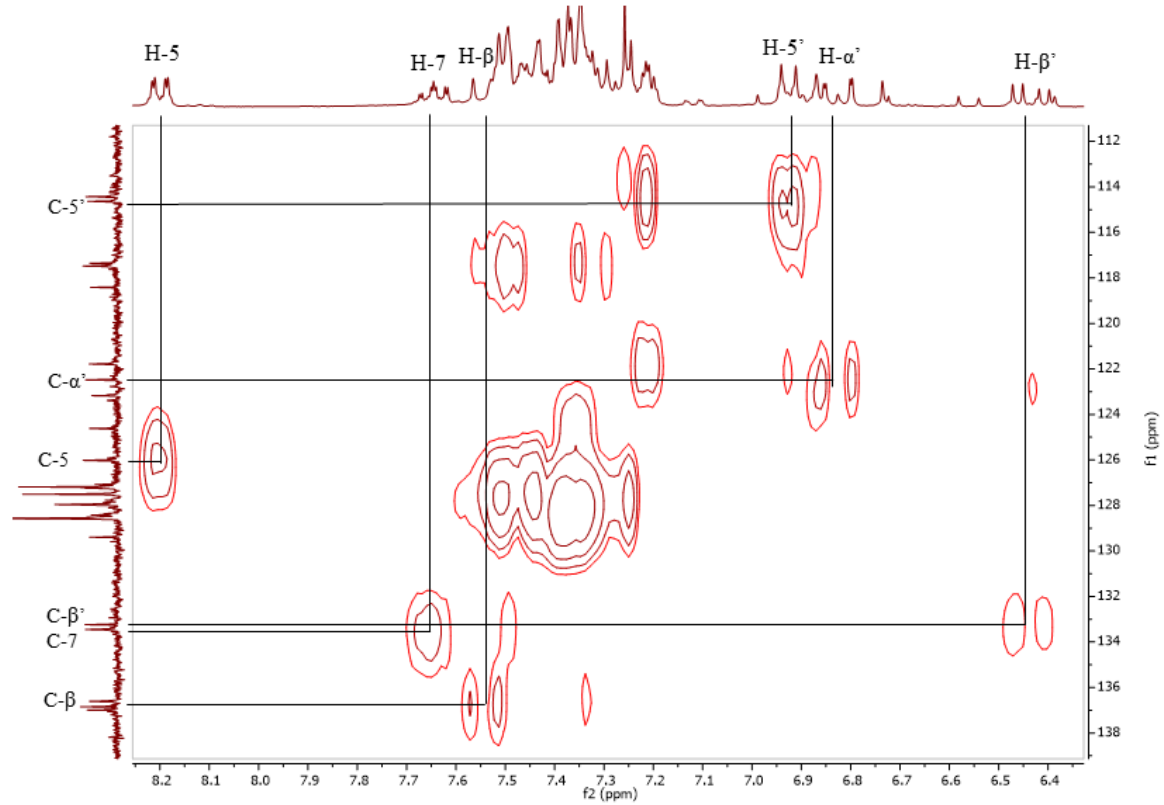

Figure 31. Expansion of HSQC spectrum of compound **89**.

Some non-protonated carbons were assigned based on the HMBC correlations (**Figure 32**): H-β, H-α'→C-2 (δ_C = 158.7 ppm); H-β'→C-3 (δ_C = 118.4 ppm); H-5, H-α'→C-4 (δ_C = 177.4 ppm); H-5, H-7→C8a (δ_C = 155.1 ppm); H-5', 3'-OC<u>H</u>$_2$Ph→C-3' (δ_C = 149.0 ppm); H-2', H-6', 4'-OC<u>H</u>$_2$Ph→C-4' (δ_C = 150.4 ppm); 3',4'-OC<u>H</u>$_2$C$_6$<u>H</u>$_5$→C-1 of the benzyloxy groups at C-3' and C-4' positions (δ_C = 136.9 and 137.0 ppm); H-x1, H-x2, H-1''→C-x (δ_C = 108.6 ppm); H-y1 and H-y2→C-y (δ_C = 109.3 ppm).

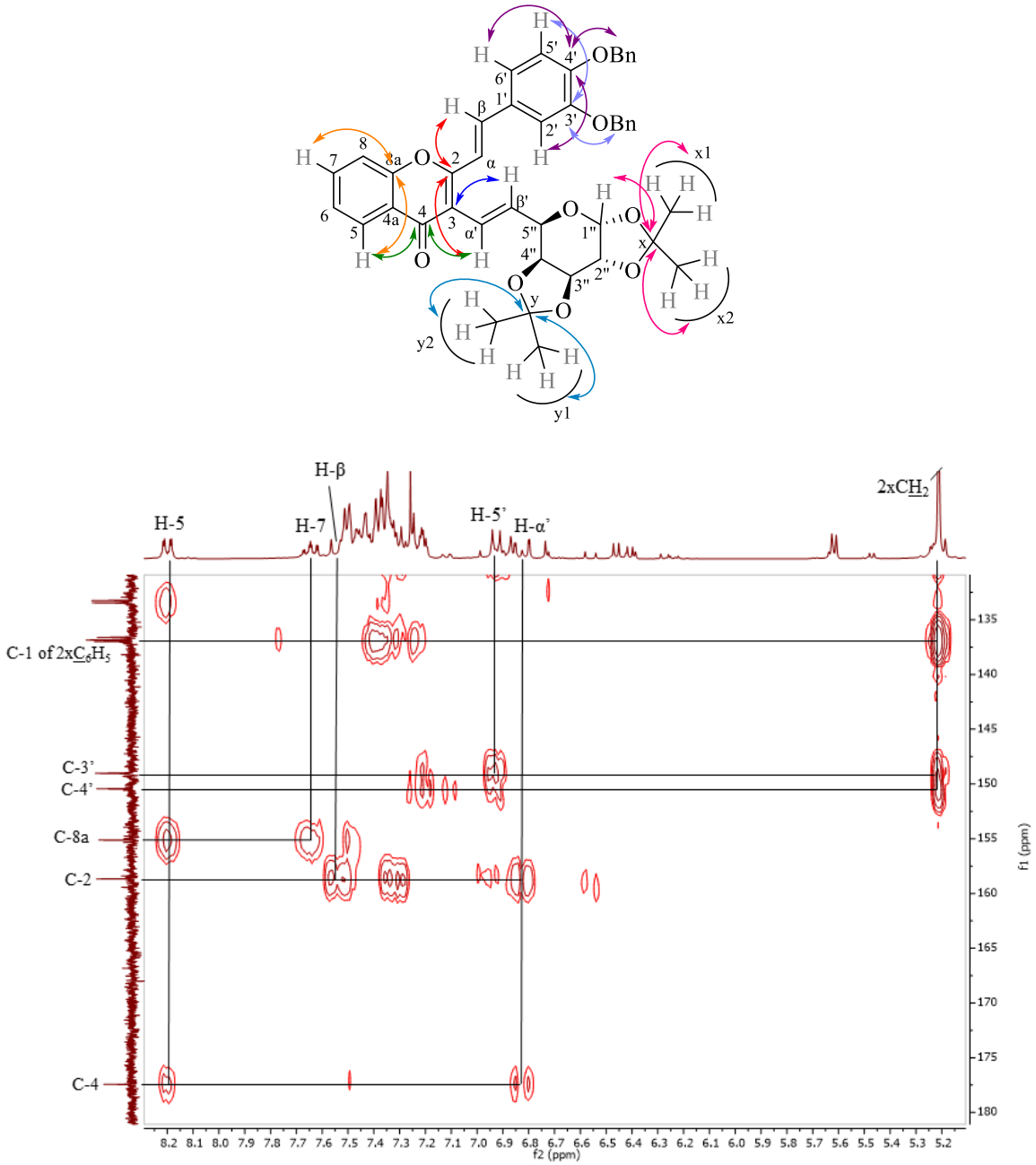

Figure 32. HMBC correlations and expansion of HMBC spectrum of compound **89**.

Chapter 4: Conclusions and future perspectives

4.1. Conclusions

In this work a new family of *C*-glycosyl flavonoids was synthesized. To achieve this aim three types of bromoflavonoids were first prepared, a 3-bromo-2-methyl-4*H*-chromen-4-one (**50**), 3-bromoflavones (**58** and **59**) and 3-bromo-2-styryl-4*H*-chromen-4-ones (**61**, **66**, **70** and **71**). The methodology adopted to obtain these compounds involved the bromination and cyclization of the respective diketone precursors. Also, sugar alkene **74** was synthesized from a protected galactose derivative by means of a Swern oxidation and subsequent Wittig reaction. Then, cross-coupling Heck reactions between the 3-bromoflavones and the 3-bromo-2-styryl-4*H*-chromen-4-ones with the modified sugar alkene **74** were carried out. Regarding the coupling of the 3-bromoflavones **58** and **59** with the sugar alkene **74**, the expected *C*-glycosyl flavones were not achieved. These results suggested that the presence of the aryl group in the C-2 position may cause steric hindrance effects that impede the coupling at the C-3 position. Alternatively, the coupling of the (*E*)-3-bromo-2-styryl-4*H*-chromen-4-ones with the sugar alkene was performed, and a family of *C*-glycosyl 2-styryl-4*H*-chromen-4-ones was synthesized. Although the C-C cross coupling was successful, the presence of isomers was observed by NMR. Several attempts were made to separate the isomers; however, it was not possible.

The hydrogenation of the benzyl groups was challenging, resulting in a complex mixture under all the conditions tested. Further studies are needed to overcome the problems faced at the final part of this work and to get the pure target compounds for further studies of their antiviral activity against SARS-CoV-2.

4.2. Future perspectives

The work developed in this dissertation permitted the synthesis of a family of *C*-glycosyl 2-styryl-4*H*-chromen-4-ones, although the presence of isomers was found. As future work the separation of these isomers will be attempted in order to carry out their unequivocal structural characterization and to perform the cleavage of the protecting group present in both the phenyl ring and the sugar moiety. Also, the conditions of the hydrogenation will be optimized to obtain pure *C*-glycosyl 2-styryl-4*H*-chromen-4-ones hydrogenated at the exocyclic double bonds. Furthermore, the cross-coupling Heck reaction between the 3-bromo-2-methyl-4*H*-chromen-4-one (**50**) and the sugar alkene will be carried out in the near future. Since this compound does not have the styryl group at the

C-2 position we expect to reduce the number of isomers in the final target compound which will facilitate its purification.

Once synthesized, the *C*-glycosyl flavonoids will be tested against the main SARS-CoV-2 targets. Some molecular docking studies will be conducted in collaboration with a group from University of Coimbra to evaluate the potential of *C*-glycosyl flavonoids as inhibitors of SARS-CoV-2 and to understand the interactions of these compounds with the $3CL^{pro}$ and α-glucosidases. The information gathered from these studies will be important to design novel compounds with the appropriate substitution patterns for antiviral activity against this coronavirus.

Chapter 5: Experimental section

5.1. Reagents and equipment

During the realization of this work there where some aspects taken into consideration:

- The reagents and solvents were used without further purification unless otherwise stated;
- Tetrahydrofuran was dried by reflux in the presence of metallic sodium and benzophenone followed by distillation;
- The monitorization of the progress of the chemical reactions was done by TLC in aluminum foil covered with silica gel 60 F_{254}. After TLC development, the plate was visualized under ultraviolet light at λ= 254 and/or 366 nm. To reveal the sugar spots, cerium molybdate stain (Hanessian's stain) was used upon heating;
- The preparative TLC plates were carried out in glass plates (20x20 cm) with silica gel 60 DGF_{254} da Merck, with approximately 0.5 mm of thickness and activated in an oven at 120 °C for 12 hours;
- The column chromatography was performed with silica gel 60 da Merck (70-230 mesh);
- The reactions carried out under sonification were performed in a Bandelin Sonorex Digitec ultrasonic bath;
- The melting points were determined with a Buchi Melting Point B-540 apparatus fitted with a microscope and are uncorrected;
- The NMR spectra were obtained with a 300 or 500 MHz Bruker Avance III NMR spectrometers [300.13 MHz (^{1}H) and 75.47 MHz (^{13}C) or 500.16 MHz (^{1}H) and 125.77 MHz (^{13}C)]. The NMR spectra were obtained at room temperature in a deuterated solvent that is specified for each compound. For the ^{1}H NMR spectra characterization were described the chemical shift (δ, ppm) in relation to TMS, the multiplicity, and the corresponding coupling constant(s) (J, Hz) for each signal. Unequivocal ^{13}C assignments were made based on 2D gHSQC (^{1}H/^{13}C) and gHMBC (delays for one-bond and long-range JC/H couplings were optimised for 145 and 7 Hz, respectively) experiments. In

specific cases, correlated spectroscopy (COSY) or/and Nuclear Overhauser Effect Spectroscopy (NOESY) were also adopted as NMR techniques;

- Positive-ion ESI mass spectra and high-resolution mass spectra [ESI(+)-HRMS] were performed using a Q Exactive Orbitrap mass spectrometer (Thermo Fischer Scientific, Bremen, Germany) controlled by THERMO Xcalibur 4.1. The capillary voltage of the electrospray ionization (ESI) was set to 3000 V. The capillary temperature was 250 ºC. The sheath gas flow rate (nitrogen) was set to 5 (arbitrary unit as provided by the software settings).

5.2. Synthesis of starting compounds

5.2.1. Synthesis of 4-chlorophenyl acetate (43)

Acetyl chloride (2.02 mL, 28.3 mmol) was added to a solution of the appropriate 4-chlorophenol (3.05 g, 23.7 mmol) in dry pyridine (35 mL). The mixture was stirred at room temperature, under nitrogen, for 5 hours. After that period, the mixture was poured into water and ice and acidified with hydrochloric acid at pH = 2. The organic layer was extracted with chloroform, dried over anhydrous sodium sulfate, and purified by column chromatography using dichloromethane as eluent. 4-Chlorophenyl acetate was obtained in very good yield.

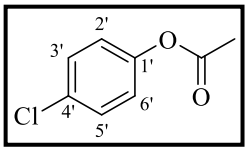

4-Chlorophenyl acetate (**43**), yield: 83% (3.34 g), yellowish oil.

^{1}H NMR (300.13 MHz, $CDCl_3$): δ = 2.27 (s, 3H, C<u>H</u>$_3$), 7.02 (d, 2H, *J* = 8.4 Hz, H-3’ and H-5’), 7.32 (d, 2H, *J* = 8.4, H-2’ and H-6’) ppm.

^{13}C NMR (75.47 MHz, $CDCl_3$): δ = 21.0 (<u>C</u>H$_3$), 123.0 (C-2’ and C-6’), 129.5 (C-3’ and C-5’), 131.2 (C-4’), 149.1 (C-1’), 169.2 (<u>C</u>=O) ppm.

5.2.2. Synthesis of 1-(5-chloro-2-hydroxyphenyl)ethan-1-one (44)

Aluminum chloride (39.2 mmol) was added to 4-chlorophenyl acetate (**43**) (3.34 g, 19.6 mmol). The mixture was stirred under nitrogen at 150°C for 2 hours. After that period, the mixture was diluted with water. The organic layer was extracted with chloroform, and it was purified by column chromatography using dichloromethane as eluent to give 1-(5-chloro-2-hydroxyphenyl)ethan-1-one in very good yield.

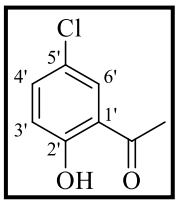

1-(5-Chloro-2-hydroxyphenyl)ethan-1-one (**44**), yield: 89% (2.99 g), light brown solid, m.p. 52.7 – 53.8 °C.

^{1}H NMR (300.13 MHz, $CDCl_3$): δ = 2.63 (s, 3H, C<u>H</u>$_3$), 6.94 (d, 1H, *J* = 8.9 Hz, H-3'), 7.42 (dd, 1H, *J* = 8.9, 2.6 Hz, H-4'), 7.69 (d, 1H, *J* = 2.6 Hz, H-6') ppm.

^{13}C NMR (75.47 MHz, $CDCl_3$): δ = 26.7 (<u>C</u>H$_3$), 120.1 (C-3'), 120.2 (C-1'), 123.6 (C-5'), 129.9 (C-6'), 136.3 (C-4'), 160.9 (C-2'), 203.6 (<u>C</u>=O) ppm.

5.2.3. Synthesis of 3,4-bis(benzyloxy)benzoic acid (47a)

To a solution of 3,4-dihydroxybenzoic acid (**45a**) (2.0 g, 13.0 mmol) in dry DMF (15 mL) were added K_2CO_3 (5.93 g, 42.9 mmol) and benzyl bromide (5.10 mL, 42.9 mmol) and the mixture was left stirring at room temperature under nitrogen, for 18 hours. After that period, the reaction mixture was filtered and the filtrate was diluted with dichloromethane, washed with water and dried over with anhydrous sodium sulfate. The solvent was evaporated to dryness. Benzyl 3,4-bis(benzyloxy)benzoate (**46a**) was obtained as a yellowish solid (4.92 g, 89%)

An aqueous solution of NaOH (3.4 g, 85.0 mmol) was added to benzyl 3,4-bis(benzyloxy)benzoate (**46a**) (4.92 g, 11.6 mmol) in methanol (38.6 mL), and was stirred under nitrogen at 70 °C for 3 hours. After that period, the mixture was diluted with water and acidified with hydrochloric acid (pH = 4). The obtained solid was washed with water. The 3,4-bis(benzyloxy)benzoic acid was obtained in moderate yield.

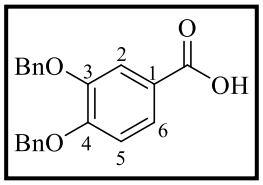

3,4-Bis(benzyloxy)benzoic acid (**47a**), yield: 54% (2.08 g), white solid, m.p. 186.5 – 188.5 °C.

^{1}H NMR (500.16 MHz, DMSO-d_6): δ = 5.18 (s, 2H, 3-OC<u>H</u>$_2$C$_6$H$_5$), 5.22 (s, 2H, 4-OC<u>H</u>$_2$C$_6$H$_5$), 7.16 (d, 1H, *J* = 8.6 Hz, H-5), 7.30 – 7.48 (m, 10H, 3,4-OCH$_2$C$_6$<u>H</u>$_5$), 7.53 – 7.57 (m, 2H, H-2,6) ppm.

^{13}C NMR (125.77 MHz, DMSO-d_6): δ = 70.3 (4-O<u>C</u>H$_2$C$_6$H$_5$), 70.4 (3-O<u>C</u>H$_2$C$_6$H$_5$), 113.5 (C-5), 115.0 (C-2), 123.9 (C-6), 127.9, 128.0, 128.3, 128.4, 128.88 and 128.93 (C-2, 3, 4, 5, 6 of 3,4-OCH$_2$<u>C</u>$_6$H$_5$), 137.2 and 137.5 (C-1 of 3,4-OCH$_2$<u>C</u>$_6$H$_5$), 148.0 (C-3), 152.4 (C-4), 167.5 (<u>C</u>=O) ppm.

MS(ESI$^+$) m/z (%): 335.1 ([M+H]$^+$, 23), 357.2 ([M+Na]$^+$, 100).

5.2.4. Synthesis of (*E*)-3-[3,4-bis(benzyloxy)phenyl]acrylic acid (47b)

To a solution of (*E*)-3-(3,4-dihydroxyphenyl)acrylic acid (**45b**) (4.0 g, 22.0 mmol) in dry DMF (20 mL), were added K_2CO_3 (10.13 g, 73.3 mmol) and benzyl bromide (9 mL, 73.3 mmol) and the mixture was left stirring for 18 hours at room temperature, under nitrogen. The filtrate was diluted with dichloromethane, washed with water, dried over anhydrous sodium sulfate, filtered and the solvent evaporated to dryness. Benzyl (*E*)-3-[3,4-bis(benzyloxy)phenyl]acrylate (**46b**) was obtained as a brownish solid (8.96 g, 90%)

An aqueous solution of NaOH (5.64 g, 141 mmol) was added to benzyl (*E*)-3-(3,4-bis(benzyloxy)phenyl)acrylate (**46b**) (8.96g, 19.9 mmol) in methanol (66 mL), and was stirred under nitrogen at 70°C, for 3 hours. After that period, the mixture was diluted with water and acidified with hydrochloric acid (pH = 4). The obtained solid was filtered and washed with water. (*E*)-3-[3,4-bis(benzyloxy)phenyl]acrylic acid was obtained in very good yield.

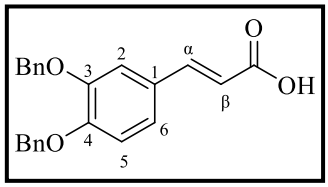

(*E*)-3-[3,4-Bis(benzyloxy)phenyl]acrylic acid (**47b**), yield: 91% (6.55 g), white solid, m.p. 198.2 – 199.7 °C.

^{1}H NMR (300.13 MHz, DMSO-d$_6$): δ = 5.19 (s, 2H, 3-OC$\underline{H}_2$C$_6$H$_5$), 5.20 (s, 2H, 4-OC$\underline{H}_2$C$_6$H$_5$), 6.43 (d, 1H, *J* = 15.9 Hz, H-β), 7.08 (d, 1H, *J* = 8.4 Hz, H-5), 7.20 (dd, 1H, *J* = 8.4, 1.9 Hz, H-6), 7.25-7.74 (m, 12H, H-2, H-α, 3, 4-OCH$_2$C$_6\underline{H}_5$) ppm.

^{13}C NMR (75.47 MHz, DMSO-d$_6$): δ = 70.3 (4-O$\underline{C}$H$_2$C$_6$H$_5$), 70.4 (3-O$\underline{C}$H$_2$C$_6$H$_5$), 113.3 (C-2), 114.3 (C-5), 117.4 (C-β), 123.3 (C-6), 127.8 (C-1), 128.0 and 128.1 (C-2,6 of 3,4-OCH$_2\underline{C}_6$H$_5$), 128.28 and 128.31 (C-4 of 3,4-OCH$_2\underline{C}_6$H$_5$), 128.6 and 128.9 (C-3,5 of 3,4-OCH$_2\underline{C}_6$H$_5$), 137.4 and 137.6 (C-1 of 3,4-OCH$_2\underline{C}_6$H$_5$), 144.4 (C-α), 148.7 (C-3), 150.6 (C-4), 168.3 ($\underline{C}$=O) ppm.

MS(ESI$^+$) m/z (%): 361.1 ([M+H]$^+$, 71), 383.2 ([M+Na]$^+$, 100).

5.3. Synthesis of 3-bromo-2-methyl-4*H*-chromen-4-one, 2-aryl-3-bromo-4*H*-chromen-4-ones and (*E*)-3-bromo 2-styryl-4*H*-chromen-4-ones

5.3.1. Synthesis of 3-bromo-2-methyl-4*H*-chromen-4-one (50)

To a solution of 2'-hydroxyacetophenone (**48**) (1 mL, 8.3 mmol) in dry ethyl acetate (40 mL), metallic sodium (764.2 mg, 33.2 mmol) was added, and the mixture was stirred overnight at room temperature. Upon completion of the reaction, the reaction

mixture was poured into ice water and acidified with hydrochloric acid. The aqueous portion was separated and extracted with dichloromethane. The organic layer was dried over with anhydrous sodium sulfate and evaporated in vacuo.

To the compound obtained in the previous step dissolved in ethanol (33 mL) was gradually added a solution of bromo (2.72 mL) in ethanol (8 mL) over a period of 20 minutes and the mixture was stirred at room temperature for 2 hours. After this period, concentrated hydrochloric acid was added and the mixture was refluxed at 80 °C for another 2 hours. After cooling and diluting with water, the mixture was kept under vigorous stirring for 30 minutes. The organic layer was extracted with dichloromethane, and it was purified by column chromatography using dichloromethane as eluent to give 3-bromo-2-methyl-4*H*-chromen-4-one in low yield.

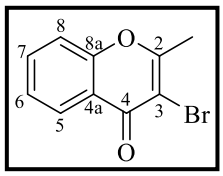

3-Bromo-2-methyl-4*H*-chromen-4-one (**50**), yield: 31% (1.23 g), brown solid, m.p. 108.9 – 111.3 °C.[130]

^{1}H NMR (300.13 MHz, $CDCl_3$): δ = 2.67 (s, 3H, $C\underline{H}_3$), 7.46 – 7.39 (m, 2H, H-6 and H-8), 7.68 (ddd, 1H, *J* = 8.6, 7.1, 1.7 Hz, H-7), 8.23 (dd, 1H, *J* = 8.0, 1.7 Hz, H-5) ppm.

^{13}C NMR (75.47 MHz, $CDCl_3$): δ = 21.7 ($\underline{C}H_3$), 109.7 (C-3), 117.6 (C-8), 121.9 (C-4a), 125.5 (C-6), 126.4 (C-5), 133.8 (C-7), 155.3 (C-8a), 164.0 (C-2), 172.3 (C-4) ppm.

MS(ESI$^+$) m/z (%): 239.0 ($[M+H]^+$, ^{79}Br, 89), 241.0 ($[M+H]^+$, ^{81}Br, 83), 261.0 ($[M+Na]^+$, ^{79}Br, 100), 263.0 ($[M+Na]^+$, ^{81}Br, 92).

HRMS (ESI$^+$) m/z calcd for $C_{10}H_8BrO_2$ $[M+H]^+$ 238.9702; found: 238.9693.

5.3.2. Synthesis of 2-[3,4-bis(benzyloxy)phenyl]-3-bromo-6-chloro-4*H*-chromen-4-one (58)

5.3.2.1. Synthesis of 2-acetyl-4-chlorophenyl 3,4-bis(benzyloxy)benzoate (54)

To 1-(5-chloro-2-hydroxyphenyl)ethan-1-one (**44**) (801.6 mg, 4.69 mmol) were added 25 mL of dichloromethane. Then 1.2 equivalents of 3,4-bis(benzyloxy)benzoic acid (**47a**) (1.88 g, 5.63 mmol) and DCC (1.16 g, 5.63 mmol) and 0.12 equivalents of 4-PPy (83.4 mg, 0.563 mmol) were added to that solution. The reaction was stirred under nitrogen at room temperature for 6 days. The solid formed in the reaction was filtered and washed

with dichloromethane. The filtrate was purified column chromatography using dichloromethane as eluent to give 2-acetyl-4-chlorophenyl 3,4-bis(benzyloxy)benzoate.

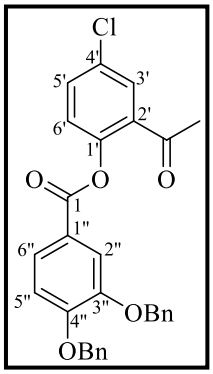

2-Acetyl-4-chlorophenyl 3,4-bis(benzyloxy)benzoate (**54**), yield: quantitative (2.30 g), white solid, m.p. 95.3 – 97.6 °C.

^{1}H NMR (300.13 MHz, $CDCl_3$): δ = 2.46 (s, 3H, C$\underline{H}_3$), 5.22 (s, 2H, 3''-OC$\underline{H}_2C_6H_5$), 5.26 (s, 2H, 4''-OC$\underline{H}_2C_6H_5$), 7.01 (d, 1H, *J* = 8.5 Hz, H-5''), 7.15 (d, 1H, *J* = 8.7 Hz, H-6'), 7.28-7.48 (m, 10H, 3'',4''-$OCH_2C_6\underline{H}_5$), 7.51 (dd, 1H, *J* = 8.7, 2.6 Hz, H-5'), 7.74 (d, 1H, *J* = 2.1 Hz, H-2''), 7.79 (dd, 1H, *J* = 8.5, 2.1 Hz, H-6''), 7.79 (d, 1H, *J* = 2.6 Hz, H-3') ppm.

^{13}C NMR (75.47 MHz, $CDCl_3$): δ = 30.0 ($\underline{C}H_3$), 70.8 (4''-O$\underline{C}H_2C_6H_5$), 71.2 (3''-O$\underline{C}H_2C_6H_5$), 113.3 (C-5''), 115.8 (C-2''), 121.3 (C-1''), 125.1 (C-6''), 125.4 (C-6'), 127.1, 127.4, 128.1, 128.1, 128.6, 128.7 (C-2, 3, 4, 5, 6 of 3'',4''-$OCH_2\underline{C}_6H_5$), 129.9 (C-3'), 131.7 (C-4'), 132.7 (C-2'), 133.1 (C-5'), 136.3 (C-1 of 4''-$OCH_2\underline{C}_6H_5$), 136.6 (C-1 of 3''-$OCH_2\underline{C}_6H_5$), 147.9 (C-1'), 148.5 (C-3''), 153.9 (C-4''), 164.5 (C-1), 196.3 ($\underline{C}$=O) ppm.

MS(ESI$^+$) m/z (%): 487.6 ([M+H]$^+$, ^{35}Cl, 22), 489.6 ([M+H]$^+$, ^{37}Cl, 9), 509.2 ([M+Na]$^+$, ^{35}Cl, 100), 511.3 ([M+Na]$^+$, ^{37}Cl, 39), 525.2 ([M+K]$^+$, ^{35}Cl, 30), 527.2 ([M+K]$^+$, ^{37}Cl, 15).

HRMS (ESI$^+$) m/z calcd for $C_{29}H_{23}ClO_5Na$ [M+Na]$^+$ 509.1126; found: 509.1110.

5.3.2.2. Synthesis of 1-[3,4-bis(benzyloxy)phenyl)-3-(5-chloro-2-hydroxyphenyl]propane-1,3-dione (56/56')

To a solution of 2-acetyl-4-chlorophenyl 3,4-bis(benzyloxy)benzoate (**54**) (2.30g, 4.73 mmol) in DMSO (14 mL) was added 5 equiv. of KOH (1.33 g, 23.7 mmol). The reaction was stirred under nitrogen at room temperature for 2 hours. Then, the reaction was poured over water and ice and acidified at pH = 4 with hydrochloric acid solution. The obtained solid was filtered, dissolved in dichloromethane, and washed with water. The organic layer was dried over anhydrous sodium sulfate and the solvent was evaporated to dryness. The (*Z*)-3-[3,4-bis(benzyloxy)phenyl]-1-(5-chloro-2-hydroxyphenyl)-3-hydroxyprop-2-en-1-one (enolic form, as observed by NMR) was obtained in very good yield.

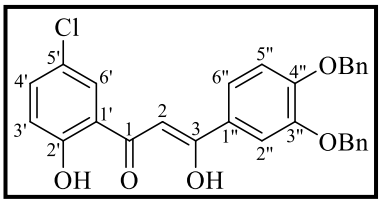

(*Z*)-3-[3,4-Bis(benzyloxy)phenyl]-1-(5-chloro-2-hydroxyphenyl)-3-hydroxyprop-2-en-1-one (**56'**), yield: 90% (2.07 g), yellow solid, m.p. 128.9 – 133.0 °C.

^{1}H NMR (300.13 MHz, $CDCl_3$): δ = 5.26 (s, 2H, 3''-OC<u>H</u>$_2$C$_6$H$_5$), 5.27 (s, 2H, 4''-OC<u>H</u>$_2$C$_6$H$_5$), 6.53 (s, 1H, H-2), 6.95 (d, 1H, *J* = 8.8 Hz, H-3'), 6.99 (d, 1H, *J* = 8.5 Hz, H-5''), 7.28 – 7.52 (m, 12H, H-4', H-2'' and 3'',4''-OCH$_2$C$_6$<u>H</u>$_5$), 7.55 (dd, 1H, *J* = 8.5, 2.2 Hz, H-6''), 7.63 (d, 1H, *J* = 2.5 Hz, H-6'), 12.05 (s, 1H, 2'-O<u>H</u>), 15.68 (s, 1H, 3-O<u>H</u>) ppm.

^{13}C NMR (75.47 MHz, $CDCl_3$): δ = 71.0 and 71.7 (4'',3''-O<u>C</u>H$_2$C$_6$H$_5$), 91.3 (C-2), 113.5 (C-2''), 113.7 (C-5''), 119.9 (C-1'), 120.5 (C-3'), 121.7 (C-6''), 123.9 (C-5'), 126.1 (C-1''), 127.31 (C-2, 3, 4, 5, 6 of 3'',4''-OCH$_2$<u>C</u>$_6$H$_5$), 127.55 (C-6'), 127.60, 128.28, 128.31, 128.8 and 128.9 (C-2, 3, 4, 5, 6 of 3'',4''-OCH$_2$<u>C</u>$_6$H$_5$), 135.3 (C-4'), 136.5 and 136.9 (C-1 of 3'',4''-OCH$_2$<u>C</u>$_6$H$_5$), 148.8 (C-3''), 153.2 (C-4''), 160.9 (C-2'), 178.7 (C-3), 193.5 (C-1) ppm.

MS(ESI$^+$) m/z (%): 487.4 ([M+H]$^+$, ^{35}Cl, 82), 489.3 ([M+H]$^+$, ^{37}Cl, 22), 509.4 ([M+Na]$^+$,^{35}Cl, 16).

HRMS (ESI$^+$) m/z calcd for $C_{29}H_{24}ClO_5$ [M+H]$^+$ 487.1307; found: 487.1292.

5.3.2.3. Synthesis of 2-[3,4-bis(benzyloxy)phenyl]-3-bromo-6-chloro-4*H*-chromen-4-one (58)

<u>Method 1</u>

To a solution of 1-[3,4-bis(benzyloxy)phenyl]-3-(5-chloro-2-hydroxyphenyl)propane-1,3-dione (**56**/**56'**) (0.50 g, 1.03 mmol) in dry THF (10 mL) was added PTT (0.59 g, 1.57 mmol). The reaction was stirred under nitrogen at room temperature for 28 hours, protected from light. Then, the reaction was poured into ice and water and was kept under vigorous stirring for 30 minutes. The organic layer was extracted with chloroform and dried over anhydrous sodium sulfate and the solvent was evaporated to dryness. The residue was recrystallized from ethanol, filtered, and purified by preparative TLC using dichloromethane as eluent. Two compounds were isolated, the major product was 2-[3,4-bis(benzyloxy)phenyl]-3-bromo-6-chloro-4*H*-chromen-4-one (8%, 47.3 mg) and the minor product was 2-[3,4-bis(benzyloxy)phenyl]-6-chloro-4*H*-chromen-4-one (2%, 6.7 mg).

Method 2

To a solution of 1-[3,4-bis(benzyloxy)phenyl]-3-(5-chloro-2-hydroxyphenyl)propane-1,3-dione (**56**/**56'**) (250 mg, 0,513 mmol) in DMF (1 mL), was added cooper(II) bromide (459 mg, 2,05 mmol). The reaction was refluxed at 130 °C under nitrogen for 30 minutes. Then, the reaction was neutralized with $NaHCO_3$. The organic layer was extracted with ethyl acetate and dried over anhydrous sodium sulfate and the solvent was evaporated to dryness. The resultant solid was dissolved in dichloromethane and purified by preparative TLC using dichloromethane as eluent. Two compounds were isolated, the major product was 2-[3,4-bis(benzyloxy)phenyl]-3-bromo-6-chloro-4*H*-chromen-4-one and the minor product was 2-[3,4-bis(benzyloxy)phenyl]-6-chloro-4*H*-chromen-4-one.

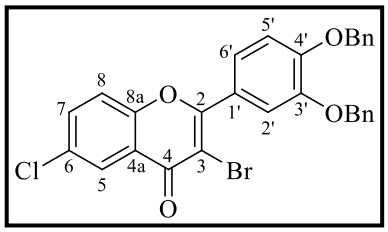

2-[3,4-Bis(benzyloxy)phenyl]-3-bromo-6-chloro-4*H*-chromen-4-one (**58**), yield: 37% (105.2 mg), beige solid, m.p. 146.7 – 148.7 °C.

^{1}H NMR (300.13 MHz, $(CD_3)_2CO$): δ = 5.29 (s, 2H, 3'-OC$\underline{H}_2C_6H_5$), 5.34 (s, 2H, 4'-OC$\underline{H}_2C_6H_5$), 7.30 (d, 1H, *J* = 8.5 Hz, H-5'), 7.33 – 7.47 (m, 6H, H-3,4,5 of 3',4'-$OCH_2C_6\underline{H}_5$), 7.52 – 7.62 (m, 4H, H-2,6 of 3',4'-$OCH_2C_6\underline{H}_5$), 7.59 (dd, 1H, *J* = 8.5, 2.1 Hz, H-6'), 7.70 (d, 1H, *J* = 2.1 Hz, H-2'), 7.72 (d, 1H, *J* = 9.1 Hz, H-8), 7.86 (dd, 1H, *J* = 9.1, 2.6 Hz, H-7), 8.10 (d, 1H, *J* = 2.6 Hz, H-5) ppm.

^{13}C NMR (75.47 MHz, $(CD_3)_2CO$): δ = 70.4 (4'-O$\underline{C}H_2C_6H_5$), 70.9 (3'-O$\underline{C}H_2C_6H_5$), 107.9 (C-3), 113.4 (C-5'), 116.1 (C-2'), 120.6 (C-8), 122.6 (C-4a), 123.6 (C-6'), 124.7 (C-5), 125.1 (C-1'), 127.5 and 127.6 (C-2, 6 of 3',4'-$OCH_2\underline{C}_6H_5$), 127.8, 127.9, 128.4, 128.5 (C-3, 4, 5 of 3',4'-$OCH_2\underline{C}_6H_5$), 130.8 (C-6), 134.3 (C-7), 137.1 and 137.3 (C-1 of 3',4'-$OCH_2\underline{C}_6H_5$), 148.1 (C-3'), 151.6 (C-4'), 154.1 (C-8a), 162.0 (C-2), 171.2 (C-4) ppm.

MS(ESI$^+$) m/z (%): 547.2 ($[M+H]^+$, $^{35}Cl^{79}Br$, 83), 549.2 ($[M+H]^+$, 100), 551.2 ($[M+H]^+$, $^{37}Cl^{81}Br$, 39), 569.3 ($[M+Na]^+$, $^{35}Cl^{79}Br$, 40), 571.3 ($[M+Na]^+$, 45), 573.3 ($[M+Na]^+$, $^{37}Cl^{81}Br$, 23).

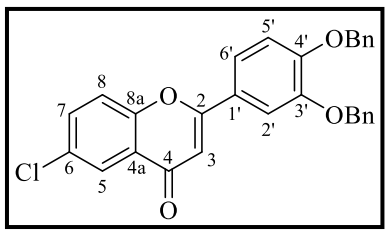

2-[3,4-Bis(benzyloxy)phenyl]-6-chloro-4*H*-chromen-4-one (**60**), yield: 7% (17.1 mg), light-yellow solid, m.p. 148.6 – 150.5 °C.

^{1}H NMR (300.13 MHz, $CDCl_3$): δ = 5.25 (s, 2H, 3'-OC$\underline{H}_2C_6H_5$), 5.26 (s, 2H, 4'-OC$\underline{H}_2C_6H_5$), 6.67 (s, 1H, H-3), 7.03 (d, 1H, *J* = 8.5 Hz, H-5'), 7.30 – 7.52 (m, 12H, H-8, H-2' and 3'',4''-$OCH_2C_6\underline{H}_5$), 7.48 (dd, 1H, *J* = 8.5, 2.0 Hz, H-5'), 7.62 (dd, 1H, *J* = 8.9, 2.6 Hz, H-7), 8.17 (d, 1H, *J* = 2.6 Hz, H-5) ppm.

^{13}C NMR (75.47 MHz, $CDCl_3$): δ = 70.9 and 71.6 (3',4'-O$\underline{C}H_2C_6H_5$), 106.3 (C-3), 112.8 (C-2'), 114.1 (C-5'), 119.7 (C-8), 120.6 (C-6'), 124.2 (C-1'), 124.9 (C-4a), 125.2 (C-5), 127.2, 127.4, 128.1 and 128.7 (C-2, 3, 4, 5, 6 of 3',4'-$OCH_2\underline{C}_6H_5$), 131.1 (C-6), 133.8 (C-7), 136.4 and 136.6 (C-1 of 3',4'-$OCH_2\underline{C}_6H_5$), 148.9 (C-3'), 152.2 (C-4'), 154.4 (C-8a), 163.5 (C-2), 177.1 (C-4) ppm.

MS(ESI$^+$) m/z (%): 469.3 ($[M+H]^+$, ^{35}Cl, 100), 471.3 ($[M+H]^+$, ^{37}Cl, 38), 491.3 ($[M+Na]^+$, ^{35}Cl, 9).

HRMS (ESI$^+$) m/z calcd for $C_{29}H_{22}ClO_4$ $[M+H]^+$ 469.1201; found: 469.1186.

5.3.3. Synthesis of 2-(3,4-bis(benzyloxy)phenyl)-3-bromo-4*H*-chromen-4-one (59)

5.3.3.1. Synthesis of 2-acetylphenyl 3,4-bis(benzyloxy)benzoate (55)

Method 1

To a solution of 2'-hydroxyacetophenone (**48**) (1.0 mL, 8.30 mmol) in dichloromethane (25 mL), were added 3,4-bis(benzyloxy)benzoic acid (**47a**) (3.33 g, 9.97 mmol), DCC (2.06 g, 9.97 mmol) and 4-PPy (147.7 mg, 0.99 mmol). The reaction was stirred under nitrogen at room temperature for 6 days. The solid formed in the reaction was filtered and washed with dichloromethane. The filtrate was purified by column chromatography using dichloromethane as eluent. 2-Acetylphenyl 3,4-bis(benzyloxy)benzoate was obtained in low yield (28%, 1.05 g).

Method 2

To 3,4-bis(benzyloxy)benzoic acid (**47a**) (2.00 g, 5.98 mmol) and 4-PPy (106.4 mg, 0.72 mmol) were added 10 mL of dichloromethane. Then 2'-hydroxyacetophenone (**48**) (1.40 mL, 12.0 mmol) was added and the mixture was stirred on an ice bath for 5 minutes. Later, DCC (1.23 g, 5.98 mmol) was added, and the reaction was stirred under nitrogen on an ice bath for 30 minutes. After that period, the reaction was left at room temperature for 3 hours. The solid formed in the reaction was filtered and washed with dichloromethane. The filtrate was purified by column chromatography using

dichloromethane as eluent to give the 2-acetylphenyl 3,4-bis(benzyloxy)benzoate in low yield.

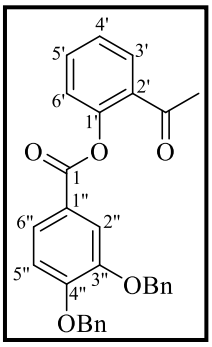

2-Acetylphenyl 3,4-bis(benzyloxy)benzoate (**55**) Yield: 30% (0.80 g), white solid.

^{1}H NMR (300.13 MHz, $CDCl_3$): δ = 2.49 (s, 3H, C$\underline{H}_3$), 5.23 (s, 2H, 3''-OC$\underline{H}_2C_6H_5$), 5.27 (s, 2H, 4''-OC$\underline{H}_2C_6H_5$), 7.01 (d, 1H, *J* = 8.5 Hz, H-5''), 7.20 (dd, 1H, *J* = 8.1, 1.2 Hz, H-6'), 7.28 – 7.50 (m, 11H, H-4' and 3'',4''-$OCH_2C_6\underline{H}_5$), 7.57 (ddd, 1H, *J* = 8.1, 7.4, 1.8 Hz, H-5'), 7.77 (d, 1H, *J* = 2.0 Hz, H-2''), 7.82 (dd, 1H, *J* = 8.5, 2.0 Hz, H-6''), 7.85 (dd, 1H, *J* = 7.9, 1.8 Hz, H-3') ppm.

^{13}C NMR (75.47 MHz, $CDCl_3$): δ = 30.0 ($\underline{C}H_3$), 70.8 (4''-O$\underline{C}H_2C_6H_5$), 71.2 (C-3''-O$\underline{C}H_2C_6H_5$), 113.3 (C-5''), 115.8 (C-2''), 121.8 (C-1''), 123.9 (C-6'), 125.0 (C-6''), 126.1 (C-4'), 127.1, 127.4, 128.0, 128.1, 128.6 and 128.7 (C-2, 3, 4, 5, 6 of 3'',4''-$OCH_2\underline{C}_6H_5$), 130.2 (C-3'), 131.5 (C-2'), 133.3 (C-5'), 136.4 (C-1 of 4''-$OCH_2\underline{C}_6H_5$), 136.7 (C-1 of 3''-$OCH_2\underline{C}_6H_5$), 148.5 (C-3''), 149.5 (C-1'), 153.7 (C-4''), 164.7 (C-1), 197.7 ($\underline{C}$=O) ppm.

MS(ESI$^+$) m/z (%): 475.3 ($[M+Na]^+$, 100), 491.2 ($[M+K]^+$, 17).

HRMS (ESI$^+$) m/z calcd for $C_{29}H_{24}O_5Na$ $[M+Na]^+$ 475.1516, found: 475.1500.

5.3.3.2. Synthesis of 1-[3,4-bis(benzyloxy)phenyl]-3-(2-hydroxyphenyl)propane-1,3-dione (57/57')

To a solution of 2-acetylphenyl 3,4-bis(benzyloxy)benzoate (**55**) (1.05g, 2.32 mmol) in DMSO (7 mL) were added 5 equiv. of KOH (0.651 g, 11.6 mmol). The reaction was stirred under nitrogen at room temperature for 4 hours. Then, the reaction was poured over water and ice and acidified at pH = 4 with hydrochloric acid solution. The obtained solid was filtered, dissolved in dichloromethane, and washed with water. The organic layer was dried over with anhydrous sodium sulfate and the solvent was evaporated to dryness. (*Z*)-3-(3,4-bis(benzyloxy)phenyl)-3-hydroxy-1-(2-hydroxyphenyl)prop-2-en-1-one (enolic form, as observed by NMR) was obtained in very good yield.

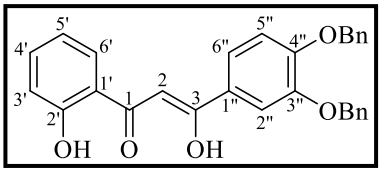

(*Z*)-3-[3,4-Bis(benzyloxy)phenyl]-3-hydroxy-1-(2-hydroxyphenyl)prop-2-en-1-one (**57'**) Yield: 99% (1.04 g), yellow solid, m.p. 106.1 – 109.7 °C.

^{1}H NMR (300.13 MHz, $CDCl_3$): δ = 5.25 (s, 2H, 3''-OC$\underline{H}_2C_6H_5$), 5.26 (s, 2H, 4''-OC$\underline{H}_2C_6H_5$), 6.65 (s, 1H, H-2), 6.88 – 6.95 (m, 1H, H-5'), 6.96 – 7.02 (m, 2H, H-3' and H-5''), 7.28 – 7.55 (m, 13H, H-4', H-2'', H-6'' and 3'',4''-$OCH_2C_6\underline{H}_5$), 7.70 (dd, 1H, *J* = 8.1, 1.7 Hz, H-6'), 12.10 (s, 1H, 2'-O$\underline{H}$), 15.73 (s, 1H, 3-O$\underline{H}$) ppm.

^{13}C NMR (75.47 MHz, $CDCl_3$): δ = 70.9 and 71.6 (3'', 4''-O$\underline{C}H_2C_6H_5$), 91.3 (C-2), 113.30 (C-2''), 113.7 (C-5''), 118.6 (C-1'), 118.77 (C-3'), 119.0 (C-5'), 121.3 (C-6''), 126.4 (C-1''), 127.2, 127.4, 128.06 and 128.09 (C-2, 3, 4, 5, 6 of 3'',4''-$OCH_2\underline{C}_6H_5$), 128.3 (C-6'), 128.6 and 128.7 (C-2, 3, 4, 5, 6 of 3'',4''-$OCH_2\underline{C}_6H_5$), 135.6 (C-4'), 136.4 and 136.8 (C-1 of 3'',4''-$OCH_2\underline{C}_6H_5$), 148.7 (C-3''), 152.8 (C-4''), 162.3 (C-2'), 177.6 (C-3), 194.7 (C-1) ppm.

MS(ESI$^+$) m/z (%): 453.3 ($[M+H]^+$, 84), 475.3 ($[M+Na]^+$, 45), 491.3 ($[M+K]^+$, 11).

HRMS (ESI$^+$) m/z calcd for $C_{29}H_{25}O_5$ $[M+H]^+$ 453.1697; found: 453.1681.

5.3.3.3. Synthesis of 2-[3,4-bis(benzyloxy)phenyl]-3-bromo-4*H*-chromen-4-one (59)

Method 1

To a solution of 1-[3,4-bis(benzyloxy)phenyl]-3-(2-hydroxyphenyl)propane-1,3-dione (**57**/**57'**) (803.3 mg, 1.78 mmol) in DMSO (11 mL), was added *p*-TSA (152.8 mg, 0.89 mmol). The reaction was heated at 90 °C under nitrogen and left stirring 24 hours. Then, the reaction was poured into ice and water and the obtained solid was filtered, dissolved in dichloromethane, and washed with water. The organic layer was dried over anhydrous sodium sulfate and the solvent was evaporated to dryness. 2-[3,4-bis(benzyloxy)phenyl]-4*H*-chromen-4-one (**53**) was obtained in very good yield (99%, 767.8 mg).

To a solution of 2-[3,4-bis(benzyloxy)phenyl]-4*H*-chromen-4-one (**53**) (767.8 mg, 1.77 mmol) in dichloromethane:methanol (8:2), was added NBS (629.0 mg, 3.53 mmol). The reaction was stirred under nitrogen at room temperature for 24 hours. Then, the reaction was evaporated to dryness and recrystallized from ethanol to give the expected 2-[3,4-bis(benzyloxy)phenyl]-3-bromo-4*H*-chromen-4-one in in low purity and limited yield (≈30%, 272.6 mg).

Method 2

To a solution of 1-[3,4-bis(benzyloxy)phenyl]-3-(2-hydroxyphenyl)propane-1,3-dione (**57**/**57'**) (506.9 mg, 1.12 mmol) in dry THF (11 mL), was added PTT (643 mg, 1.71 mmol). The reaction was stirred under nitrogen at room temperature for 28 hours, protected from light. Then, the reaction was poured into ice and water and was kept under vigorous stirring for 30 minutes. The organic layer was extracted with chloroform and dried over anhydrous sodium sulfate and the solvent was evaporated to dryness. The residue was recrystallized from ethanol, filtered, and purified by preparative TLC using dichloromethane as eluent. Two compounds were isolated, the 2-[3,4-bis(benzyloxy)phenyl]-3-bromo-4*H*-chromen-4-one and the 2-[3,4-bis(benzyloxy)phenyl]-4*H*-chromen-4-one.

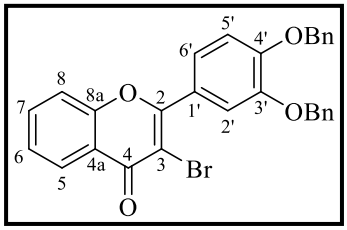

2-[3,4-Bis(benzyloxy)phenyl]-3-bromo-4*H*-chromen-4-one (**59**), yield: 35% (200.9 mg), beige solid, m.p. 135.6 – 136.8 °C.

^{1}H NMR (300.13 MHz, $(CD_3)_2CO$): δ = 5.30 (s, 2H, 3'-OC$\underline{H}_2C_6H_5$), 5.34 (s, 2H, 4'-OC$\underline{H}_2C_6H_5$), 7.30 (d, 1H, *J* = 8.5 Hz, H-5'), 7.32 – 7.47 (m, 6H, H-3,4,5 of 3',4'-$OCH_2C_6\underline{H}_5$), 7.52 – 7.61 (m, 6H, H-6, H-6' and H-2,6 of 3',4'-$OCH_2C_6\underline{H}_5$), 7.65 (dd, 1H, *J* = 8.7, 0.5 Hz, H-8), 7.70 (d, 1H, *J* = 2.2 Hz, H-2'), 7.87 (ddd, 1H, *J* = 8.7, 7.1, 1.7 Hz, H-7), 8.18 (dd, 1H, *J* = 8.0, 1.7 Hz, H-5) ppm.

^{13}C NMR (75.47 MHz, $(CD_3)_2CO$): δ = 70.4 (4'-O$\underline{C}H_2C_6H_5$), 70.9 (3'-O$\underline{C}H_2C_6H_5$), 108.1 (C-3), 113.4 (C-5'), 116.1 (C-2'), 118.2 (C-8), 121.6 (C-4a), 123.5 (C-6'), 125.5 (C-6), 125.69 and 125.71 (C-5 and C-1'), 127.5 and 127.6 (C-2,6 of 3',4'-$OCH_2\underline{C}_6H_5$), 127.8, 127.9, 128.4 and 128.5 (C-3,4,5 of 3',4'-$OCH_2\underline{C}_6H_5$), 134.32 (C-7), 137.2 and 137.3 (C-1 of 3',4'-$OCH_2\underline{C}_6H_5$), 148.1 (C-3'), 151.4 (C-4'), 155.6 (C-8a), 161.7 (C-2), 172.1 (C-4) ppm.

MS(ESI$^+$) m/z (%): 513.2 ($[M+H]^+$, ^{79}Br, 100), 515.2 ($[M+H]^+$, ^{81}Br, 93), 535.1 ($[M+Na]^+$, ^{79}Br, 27), 537.1 ($[M+Na]^+$, ^{81}Br, 25).

HRMS (ESI$^+$) m/z calcd for $C_{29}H_{22}BrO_4$ $[M+H]^+$ 513,0696; found: 513.0679.

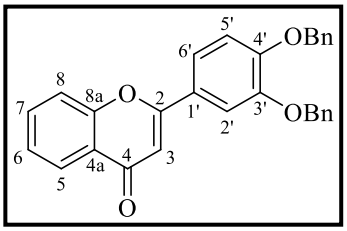

2-[3,4-Bis(benzyloxy)phenyl]-4*H*-chromen-4-one (**53**), yield: 31% (148.9 mg), light yellow solid, m.p. 161.5 – 163.9 °C.

MS(ESI$^+$) m/z (%): 435.3 ($[M+H]^+$, 100), 457.3 ($[M+Na]^+$, 18), 473.3 ($[M+K]^+$, 7).

HRMS (ESI$^+$) m/z calcd for $C_{29}H_{23}O_4$ $[M+H]^+$ 435.1591; found: 435.1575.

5.3.4. Synthesis of (*E*)-2-[3,4-bis(benzyloxy)styryl]-3-bromo-6-chloro-4*H*-chromen-4-one (66)

5.3.4.1. Synthesis of 2-acetyl-4-chlorophenyl (*E*)-3-[3,4-bis(benzyloxy)phenyl] acrylate (62)

To (*E*)-3-[3,4-bis(benzyloxy)phenyl]acrylic acid (**47b**) (2.10 g, 5.83 mmol) and 4-PPy (103.6 mg, 0.7 mmol) were added 10 mL of dichloromethane. Then 1-(5-chloro-2-hydroxyphenyl)ethan-1-one (**44**) (1.99 g, 11.7 mmol) was added and the mixture was stirred on an ice bath for 5 minutes. Later, DCC (1.20 g, 5.83 mmol) was added, and the reaction was stirred under nitrogen on an ice bath for 30 minutes. After that period, the reaction was left at room temperature for 3 hours. The solid formed in the reaction was filtered and washed with dichloromethane. The filtrate was purified by column chromatography using dichloromethane as eluent. 2-Acetyl-4-chlorophenyl (*E*)-3-[3,4-bis(benzyloxy)phenyl]acrylate was obtained in moderate yield.

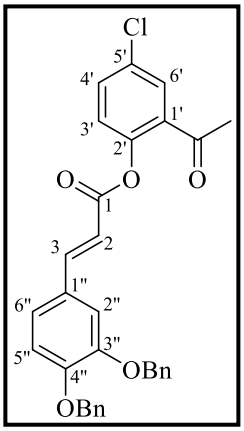

2-Acetyl-4-chlorophenyl (*E*)-3-[3,4-bis(benzyloxy)phenyl]acrylate (**62**), yield: 58% (1.74 g), white solid, m.p. 82.5 – 85.4 °C.

^{1}H NMR (300.13 MHz, $CDCl_3$): δ = 2.52 (s, 3H, C$\underline{H}_3$), 5.16 (s, 4H, 3'', 4''-OC$\underline{H}_2C_6H_5$), 6.48 (d, 1H, *J* = 16.1 Hz, H-2), 6.92 (d, 1H, *J* = 8.2 Hz, H-5''), 7.07 – 7.13 (m, 1H, H-6''), 7.10 (d, 1H, *J* = 8.8 Hz, H-6'), 7.20 (d, 1H, *J* = 2.0 Hz, H-2''), 7.28 – 7.51 (m, 11H, H-5' and 3'',4''-OCH$_2$C$_6$H$\underline{5}$), 7.76 (d, 1H, *J* = 2.8 Hz, H-3'), 7.79 (d, 1H, *J* = 16.1 Hz, H-3) ppm.

^{13}C NMR (75.47 MHz, $CDCl_3$): δ = 29.9 (C$\underline{H}_3$), 70.8 and 71.2 (3'', 4''-O$\underline{C}H_2C_6H_5$), 113.8 (C-2''), 114.0 (C-5''), 114.1 (C-2), 123.8 (C-6''), 125.5 (C-6'), 127.2 (C-1''), 127.4, 127.5, 128.0, 128.1, 128.6 and 128.7 (C-2, 3, 4, 5, 6 of 3'',4''-OCH$_2\underline{C}_6$H$_5$), 129.9 (C-3'), 131.4 (C-4'), 132.6 and 133.05 (C-5' and C-2'), 136.7 and 137.0 (C-1 of 3'',4''-

$OCH_2\underline{C}_6H_5$), 147.7 (C-3), 147.8 (C-1'), 149.0 (C-3''), 151.7 (C-4''), 165.2 (C-1), 196.4 ($\underline{C}$=O) ppm.

MS(ESI$^+$) m/z (%): 535.2 ($[M+Na]^+$, ^{35}Cl, 100), 537.2 ($[M+Na]^+$, ^{37}Cl, 40), 551.2 ($[M+K]^+$, ^{35}Cl, 30).

HRMS (ESI$^+$) m/z calcd for $C_{31}H_{25}O_5ClNa$ $[M+Na]^+$ 535.1283; found: 535.1265.

5.3.4.2. Synthesis of (*E*)-5-[3,4-bis(benzyloxy)phenyl]-1-(5-chloro-2-hydroxyphenyl)pent-4-ene-1,3-dione (64/64')

To a solution of 2-acetyl-4-chlorophenyl (*E*)-3-[3,4-bis(benzyloxy)phenyl]acrylate (**62**) (1.20 g, 2.34 mmol) in DMSO (7 mL) were added 5 equiv. of KOH (0.656 g, 11.7 mmol). The reaction was stirred under nitrogen at room temperature for 4 hours. Then, the reaction was poured over water and ice and acidified at pH = 4 with hydrochloric acid solution. The obtained solid was filtered, dissolved in dichloromethane, and washed with water. The organic layer was dried over anhydrous sodium sulfate and the solvent was evaporated to dryness. (*E*)-5-[3,4-Bis(benzyloxy)phenyl]-1-(5-chloro-2-hydroxyphenyl)pent-4-ene-1,3-dione (in equilibrium with the enolic form, as observed by NMR), was obtained in very good yield.

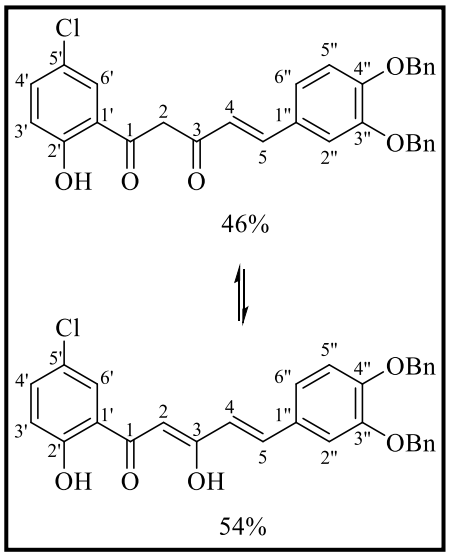

(*E*)-5-[3,4-Bis(benzyloxy)phenyl]-1-(5-chloro-2-hydroxyphenyl)pent-4-ene-1,3-dione (**64**/**64'**), yield: 95% (1.14 g), yellow solid, m.p. 169.8 – 174.1 °C.

MS(ESI$^+$) m/z (%): 513.3 ($[M+H]^+$, ^{35}Cl, 54), 515.3 ($[M+H]^+$, ^{37}Cl, 25), 535.2 ($[M+Na]^+$, ^{35}Cl, 24), 537.4 ($[M+Na]^+$, ^{37}Cl, 20).

HRMS (ESI$^+$) m/z calcd for $C_{31}H_{26}ClO_5$ $[M+H]^+$ 513.1463; found: 513.1466.

5.3.4.3. Synthesis of (*E*)-2-[3,4-bis(benzyloxy)styryl]-3-bromo-6-chloro-4*H*-chromen-4-one (66)

To a solution of (*E*)-5-[3,4-bis(benzyloxy)phenyl]-1-(5-chloro-2-hydroxyphenyl)pent-4-ene-1,3-dione (**64**/**64'**) (749 mg, 1.46 mmol) in DMF (3 mL), was added cooper(II) bromide (1.30 g, 5.84 mmol). The reaction was refluxed at 130 °C under

nitrogen for 30 minutes. Then, the reaction was neutralized with $NaHCO_3$. The organic layer was extracted with ethyl acetate and dried over anhydrous sodium sulfate and the solvent was evaporated to dryness. The resultant solid was dissolved in dichloromethane and purified by preparative TLC using dichloromethane as eluent to give the (*E*)-2-[3,4-bis(benzyloxy)styryl]-3-bromo-6-chloro-4*H*-chromen-4-one in low yield.

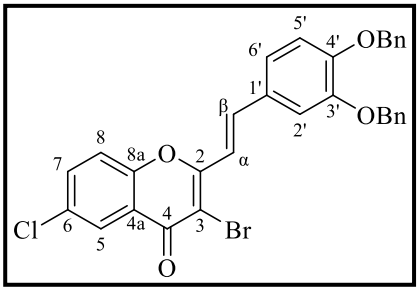

(*E*)-2-[3,4-Bis(benzyloxy)styryl]-3-bromo-6-chloro-4*H*-chromen-4-one (**66**), yield: 37% (307.5 mg), yellow solid, m.p. 175.5 – 179.9 °C.

^{1}H NMR (300.13 MHz, $CDCl_3$): δ = 5.22 and 5.23 (2s, 4H, 3', 4'-$OC\underline{H}_2C_6H_5$), 6.95 (d, 1H, *J* = 8.4 Hz, H-5'), 7.16 (dd, 1H, *J* = 8.4, 2.1 Hz, H-6'), 7.20 (d, 1H, *J* = 2.1 Hz, H-2'), 7.21 (d, 1H, *J* = 15.9 Hz, H-α), 7.29 – 7.52 (m, 11H, H-8 and 3',4'-$OCH_2C_6\underline{H}_5$), 7.56 (d, 1H, *J* = 15.9 Hz, H-β), 7.61 (dd, 1H, *J* = 8.9, 2.6 Hz, H-7), 8.16 (d, 1H, *J* = 2.6 Hz, H-5) ppm.[1]

MS(ESI$^+$) m/z (%): 573.3 ($[M+H]^+$, $^{35}Cl^{79}Br$, 52), 575.4 ($[M+H]^+$, 100), 577.4 ($[M+H]^+$, $^{37}Cl^{81}Br$, 36), 595.2 ($[M+Na]^+$, $^{35}Cl^{79}Br$, 50), 597.2 ($[M+Na]^+$, 59), 599.2 ($[M+Na]^+$, $^{37}Cl^{81}Br$, 27).

5.3.5. Synthesis of (*E*)-2-[3,4-bis(benzyloxy)styryl]-3-bromo-4*H*-chromen-4-one (61)

5.3.5.1. Synthesis of 2-acetylphenyl (*E*)-3-[3,4-bis(benzyloxy)phenyl]acrylate (63)

To (*E*)-3-[3,4-bis(benzyloxy)phenyl]acrylic acid (**47b**) (3.00 g, 8.32 mmol) and 4-PPy (123.4 mg, 0.83 mmol) were added 10 mL of dichloromethane. Then 2'-hydroxyacetophenone (**48**) (2.00 mL, 16.6 mmol) was added and the reaction mixture was left stirring on an ice bath for 5 minutes. Later, was added DCC (1.72 g, 8.32 mmol) and the reaction was stirred under nitrogen on an ice bath for 30 minutes. After that period, the reaction was left at room temperature for 3 hours. The solid formed in the reaction was filtered and washed with dichloromethane. The filtrate was purified by column chromatography using dichloromethane as eluent. 2-Acetylphenyl (*E*)-3-[3,4-bis(benzyloxy)phenyl]acrylate was obtained in moderate yield.

[1] The compound contains some impurities observed in the ^{1}H NMR spectrum.

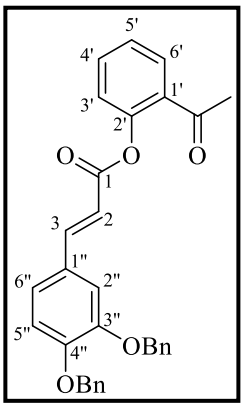

2-Acetylphenyl (*E*)-3-[3,4-bis(benzyloxy)phenyl]acrylate (**63**), yield: 58% (2.39 g), white solid.

^{1}H NMR (300.13 MHz, $CDCl_3$): δ = 2.59 (s, 3H, C$\underline{H}_3$), 5.22 (s, 2H, 3''-OC$\underline{H}_2C_6H_5$), 5.23 (s, 2H, 4''-OC$\underline{H}_2C_6H_5$), 6.52 (d, 1H, *J*= 16.0 Hz, H-2), 6.97 (d, 1H, *J*= 8.4 Hz, H-5''), 7.16 (dd, 1H, *J*= 8.4, 2.0 Hz, H-6''), 7.19 – 7.25 (m, 2H, H-6' and H-2''), 7.31 – 7.54 (m, 11H, H-4' and 3'',4''-OCH$_2$C$_6$H$\underline{5}$), 7.58 (ddd, 1H, *J* = 8.0, 7.4, 1.7 Hz, H-5'), 7.83 (d, 1H, *J*= 16.0 Hz, H-3), 7.85 (dd, 1H, *J*= 7.7, 1.7 Hz, H-3') ppm.

^{13}C NMR (75.47 MHz, $CDCl_3$): δ = 29.9 (C$\underline{H}_3$), 70.9 and 71.3 (3'', 4''-O$\underline{C}H_2C_6H_5$), 113.9 (C-2''), 114.1 (C-5''), 114.6 (C-2), 123.6 (C-6''), 123.9 (C-6'), 126.0 (C-4'), 127.2 and 127.4 (C-2, 3, 4, 5, 6 of 3'',4''-OCH$_2\underline{C}_6$H$_5$), 127.4 (C-1''), 128.1 and 128.7 (C-2, 3, 4, 5, 6 of 3'',4''-OCH$_2\underline{C}_6$H$_5$), 130.1 (C-3'), 131.5 (C-2'), 133.4 (C-5'), 136.7 and 136.9 (C-1 of 3'',4''-OCH$_2\underline{C}_6$H$_5$), 147.3 (C-3), 149.0 (C-3''), 149.3 (C-1'), 151.6 (C-4''), 165.5 (C-1), 197.9 (C=O) ppm.

MS(ESI$^+$) m/z (%): 501.3 ([M+Na]$^+$, 100).

HRMS (ESI$^+$) m/z calcd for $C_{31}H_{26}O_5Na$ [M+Na]$^+$ 501.1672; found: 501.1678.

5.3.5.2. Synthesis of (*E*)-5-[3,4-bis(benzyloxy)phenyl]-1-(2-hydroxyphenyl)pent-4-ene-1,3-dione (65/65')

To a solution of 2-acetylphenyl (*E*)-3-[3,4-bis(benzyloxy)phenyl]acrylate (**63**) (1.20 g, 2.51 mmol) in DMSO (7 mL) were added 5 equiv. of KOH (0.704 g, 12.5 mmol). The reaction was stirred under nitrogen at room temperature for 4 hours. Then, the reaction was poured over water and ice and acidified at pH = 4 with hydrochloric acid solution. The obtained solid was filtered, dissolved in dichloromethane, and washed with water. The organic layer was dried over anhydrous sodium sulfate and the solvent was evaporated to dryness. The expected diketone **65** was obtained in the enolic form, as (2*Z*,4*E*)-5-[3,4-bis(benzyloxy)phenyl]-3-hydroxy-1-(2-hydroxyphenyl)penta-2,4-dien-1-one (**65'**) (as observed by NMR) in very good yield.

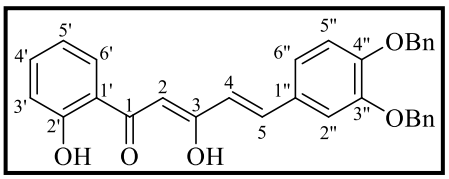

(2*Z*,4*E*)-5-[3,4-Bis(benzyloxy)phenyl]-3-hydroxy-1-(2-hydroxyphenyl)penta-2,4-dien-1-one (**65'**), yield: 99% (1.18 g), yellow solid, m.p. 135.7 – 138.7 °C.

^{1}H NMR (300.13 MHz, $CDCl_3$): δ = 5.20 (s, 2H, 3''-OC<u>H</u>$_2$C$_6$H$_5$), 5.21 (s, 2H, 4''-OC<u>H</u>$_2$C$_6$H$_5$), 6.27 (s, 1H), 6.40 (d, 1H, *J* = 15.7 Hz, H-4), 6.89 (ddd, 1H, *J* = 8.2, 7.2, 1.3 Hz, H-5'), 6.94 (d, 1H, *J* = 8.4 Hz, H-5''), 6.98 (dd, 1H, *J* = 8.4, 1.3 Hz, H-3'), 7.11 (dd, 1H, *J* = 8.4, 2.1 Hz, H-6''), 7.15 (d, 1H, *J* = 2.1 Hz, H-2''), 7.28 – 7.50 (m, 11H, H-4' and 3'',4''-OCH$_2$C$_6$<u>H</u>$_5$), 7.55 (d, 1H, *J* = 15.7 Hz, H-5), 7.69 (dd, 1H, *J* = 8.2, 1.7 Hz, H-6'), 12.26 (s, 1H, 2'-O<u>H</u>), 14.63 (s, 1H, 3-O<u>H</u>) ppm.

^{13}C NMR (75.47 MHz, $CDCl_3$): δ = 71.0 and 71.4 (3'', 4''-O<u>C</u>H$_2$C$_6$H$_5$), 96.5 (C-2), 113.8 (C-2''), 114.3 (C-5''), 118.7 (C-3'), 119.0 (C-5'), 119.1 (C-1'), 120.1 (C-4), 122.9 (C-6''), 127.2, 127.3 and 1280.0 (C-2, 3, 4, 5, 6 of 3'',4''-OCH$_2$<u>C</u>$_6$H$_5$), 128.4 (C-6'), 128.5 (C-1''), 128.6 (C-2, 3, 4, 5, 6 of 3'',4''-OCH$_2$<u>C</u>$_6$H$_5$), 135.7 (C-4'), 136.7 and 136.9 (C-1 of 3'',4''-OCH$_2$<u>C</u>$_6$H$_5$), 139.8 (C-5), 149.0 (C-3''), 151.0 (C-4''), 162.5 (C-2'), 174.9 (C-3), 195.6 (C-1) ppm.

MS(ESI$^+$) m/z (%): 479.2 ([M+H]$^+$, 100), 501.3 ([M+Na]$^+$, 69).

HRMS (ESI$^+$) m/z calcd for $C_{31}H_{27}O_5$ [M+H]$^+$ 479.1853; found: 479.1833.

5.3.4.3. Synthesis of (*E*)-2-[3,4-bis(benzyloxy)styryl]-3-bromo-4*H*-chromen-4-one (61)

To a solution of (*E*)-5-[3,4-bis(benzyloxy)phenyl]-1-(2-hydroxyphenyl) pent-4-ene-1,3-dione (**65**/**65'**) (717 mg, 1.50 mmol) in DMF (3 mL), was added cooper(II) bromide (1.339 g, 6,00 mmol). The reaction was refluxed at 130 °C under nitrogen for 30 minutes. Then, the reaction was neutralized with $NaHCO_3$. The organic layer was extracted with ethyl acetate and dried over anhydrous sodium sulfate and the solvent was evaporated to dryness. The obtained solid was dissolved in dichloromethane and purified by preparative TLC using dichloromethane as eluent. Two compounds were isolated, the major product was (*E*)-2-[3,4-bis(benzyloxy)styryl]-3-bromo-4*H*-chromen-4-one and the minor product was (*E*)-2-[3,4-bis(benzyloxy)styryl]-4*H*-chromen-4-one.

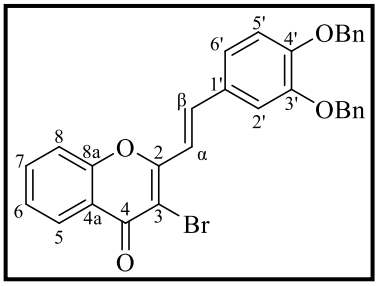

(*E*)-2-[3,4-Bis(benzyloxy)styryl]-3-bromo-4*H*-chromen-4-one (**61**), yield: 48% (390 mg), yellow solid, m.p. 160.8 – 162.7 °C.

^{1}H NMR (300.13 MHz, $(CD_3)_2CO$): δ = 5.28 (s, 2H, 4'-OC<u>H</u>$_2$C$_6$H$_5$), 5.30 (s, 2H, 3'-OC<u>H</u>$_2$C$_6$H$_5$), 7.19 (d, 1H, *J* = 8.4 Hz, H-5'), 7.28 – 7.47 (m, 8H, H-6', H-α and H-3,4,5 of 3',4'-OCH$_2$C$_6$<u>H</u>$_5$), 7.48 – 7.61

(m, 6H, H-6, H-2’ and H-2,6 of 3’,4’-$OCH_2C_6\underline{H}_5$), 7.72 (dd, 1H, *J* = 8.5, 1.0 Hz, H-8), 7.82 – 7.90 (m, 1H, H-7), 7.86 (d, 1H, *J* = 16.0 Hz, H-β), 8.14 (dd, 1H, *J* = 7.8, 1.8 Hz, H-5) ppm.

^{13}C NMR (75.47 MHz, $(CD_3)_2CO$): δ = 70.4 (4’-$O\underline{C}H_2C_6H_5$), 70.7 (3’-$O\underline{C}H_2C_6H_5$), 108.3 (C-3), 113.3 (C-2’), 114.2 (C-5’), 116.7 (C-α), 117.8 (C-8), 122.0 (C-4a), 123.2 (C-6’), 125.4 (C-6), 125.6 (C-5), 127.5 and 127.6 (C-2,6 of 3’,4’-$OCH_2\underline{C}_6H_5$), 127.80, 127.83, 128.41 and 128.43 (C-3,4,5 of 3’,4’-$OCH_2\underline{C}_6H_5$), 128.36 (C-1’), 134.3 (C-7), 137.2 and 137.5 (C-1 of 3’,4’-$OCH_2\underline{C}_6H_5$), 140.0 (C- β), 149.2 (C-3’), 151.4 (C-4’), 155.0 (C-8a), 158.8 (C-2), 171.6 (C-4) ppm.

MS(ESI$^+$) m/z (%): 539.2 ($[M+H]^+$, ^{79}Br, 98), 541.2 ($[M+H]^+$, ^{81}Br, 100), 561.3 ($[M+Na]^+$,^{79}Br, 58), 563.3 ($[M+Na]^+$,^{81}Br, 72).

HRMS (ESI$^+$) m/z calcd for $C_{31}H_{24}BrO_4$ $[M+H]^+$ 539.0852; found: 539.0832.

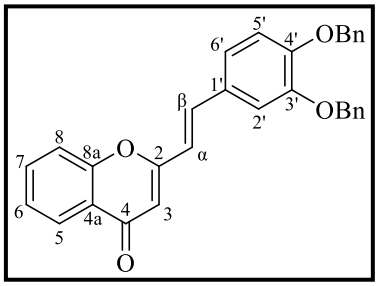

(*E*)-2-[3,4-Bis(benzyloxy)styryl]-4*H*-chromen-4-one (**67**), yield: 8% (51.8 mg), yellow solid, m.p. 171.8 – 178.2 °C.

MS(ESI$^+$) m/z (%): 539.2 ($[M+H]^+$, ^{79}Br, 98), 541.2 ($[M+H]^+$, ^{81}Br, 100), 561.3 ($[M+Na]^+$,^{79}Br, 58), 563.3 ($[M+Na]^+$,^{81}Br, 72).

HRMS (ESI$^+$) m/z calcd for $C_{31}H_{24}BrO_4$ $[M+H]^+$ 539.0852; found: 539.0832.

5.3.6. Synthesis of (*E*)-3-bromo-2-(3,4-dimethoxystyryl)-4*H*-chromen-4-one (70)

To a solution of (*E*)-5-(3,4-dimethoxyphenyl)-1-(2-hydroxyphenyl)pent-4-ene-1,3-dione (**68**) (200.0 mg, 0.61 mmol) in dry THF (6 mL) was added PTT (351.3 mg, 0,94 mmol). The reaction was stirred under nitrogen at room temperature for 42 hours, protected from light. Then, the reaction was poured into ice and water and was kept under vigorous stirring for 30 minutes. The organic layer was extracted with chloroform and dried over anhydrous sodium sulfate and the solvent was evaporated to dryness. The residue was recrystallized from ethanol, filtered, and purified by preparative TLC using dichloromethane as eluent. The expected (*E*)-3-bromo-2-(3,4-dimethoxystyryl)-4*H*-chromen-4-one was obtained in low yield.

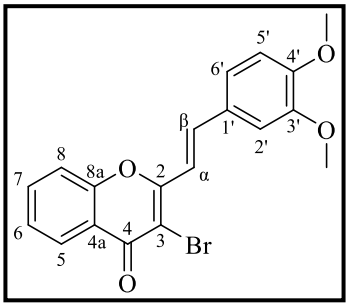

(*E*)-3-Bromo-2-(3,4-dimethoxystyryl)-4*H*-chromen-4-one (**70**), yield: 32 % (79.9 mg), yellow solid.

^{1}H NMR (300.13 MHz, $CDCl_3$): δ = 3.95 (s, 3H, 4'-OC$\underline{H}_3$), 3.99 (s, 3H, 3'-OC$\underline{H}_3$), 6.93 (d, 1H, *J* = 8.4 Hz, H-5'), 7.16 (d, 1H, *J* = 2.1 Hz, H-2'), 7.25 (dd, 1H, *J* = 8.4, 2.1 Hz, H-6'), 7.36 (d, 1H, *J* = 16.0 Hz, H-α), 7.43 (ddd, 1H, *J* = 8.1, 7.1, 1.1 Hz, H-6), 7.55 (dd, 1H, *J* = 8.7, 1.1 Hz, H-8), 7.68 (d, 1H, *J* = 16.0 Hz, H-β), 7.71 (ddd, 1H, *J* = 8.7, 7.1, 1.7 Hz, H-7), 8.25 (dd, 1H, *J* = 8.1, 1.7 Hz, H-5) ppm.

^{13}C NMR (75.47 MHz, $CDCl_3$): δ = 56.0 and 56.1 (3', 4'-O$\underline{C}H_3$), 109.1 (C-3), 109.7 (C-2'), 111.2 (C-5'), 117.0 (C-α), 117.5 (C-8), 122.2 (C-4a), 122.7 (C-6'), 125.3 (C-6), 126.5 (C-5), 128.0 (C-1'), 134.0 (C-7), 139.6 (C-β), 149.4 (C-3'), 151.3 (C-4'), 154.9 (C-8a), 158.8 (C-2), 172.7 (C-4) ppm.

5.3.7. Synthesis of (*E*)-3-bromo-2-(3,4-dimethoxystyryl)-5-methoxy-4*H*-chromen-4-one (71)

To a solution of (*E*)-5-(3,4-dimethoxyphenyl)-1-(2-hydroxy-6-methoxyphenyl)pent-4-ene-1,3-dione (**69**) (200.0 mg, 0.61 mmol) in dry THF (6 mL) was added PTT (321.7 mg, 0,86 mmol). The reaction was stirred under nitrogen at room temperature for 42 hours, protected from light. Then, the reaction was poured into ice and water and was kept under vigorous stirring for 30 minutes. The organic layer was extracted with chloroform and dried over anhydrous sodium sulfate and the solvent was evaporated to dryness. The residue was recrystallized from ethanol, filtered, and purified by preparative TLC using dichloromethane as eluent. The expected (*E*)-3-bromo-2-(3,4-dimethoxystyryl)-5-methoxy-4*H*-chromen-4-one was obtained in low yield.

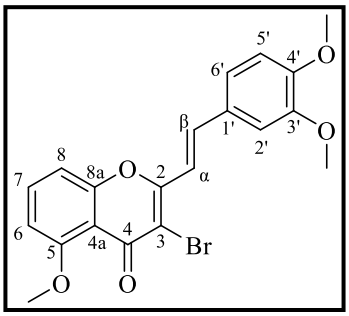

(*E*)-3-Bromo-2-(3,4-dimethoxystyryl)-5-methoxy-4*H*-chromen-4-one (**71**), yield: 26 % (57.2 mg), yellow solid.

^{1}H NMR (300.13 MHz, $CDCl_3$): δ = 3.94 and 3.97 (2s, 6H, 3', 4'-OC$\underline{H}_3$), 3.98 (s, 3H, 5-OC$\underline{H}_3$), 6.82 (dd, 1H, *J* = 8.3, 0.9 Hz, H-6), 6.91 (d, 1H, *J* = 8.3 Hz, H-5'), 7.09 (dd, 1H, *J* = 8.3, 0.9 Hz, H-8), 7.12 (d, 1H, *J* = 1.9 Hz, H-2'), 7.21 (dd, 1H,

J = 8.3, 1.9 Hz, H-6'), 7.26 (d, 1H, *J* = 16.0 Hz, H-α), 7.57 (d, 1H, *J* = 16.0 Hz, H-β), 7.57 (t, 1H, *J* = 8.3 Hz, H-7) ppm.

^{13}C NMR (75.47 MHz, $CDCl_3$): δ = 56.0 and 56.5 (5, 3', 4'-O<u>C</u>H_3), 106.5 (C-6), 109.4 (C-8), 109.7 (C-2'), 110.7 (C-3), 111.2 (C-5'), 112.9 (C-4a), 116.9 (C-α), 122.4 (C-6'), 128.1 (C-1'), 134.0 (C-7), 138.8 (C-β), 149.3 (C-3'), 151.1 (C-4'), 156.8 (C-8a), 156.9 (C-2), 159.8 (C-5), 171.7 (C-4) ppm.

5.4. Synthesis of sugar alkene (74)

5.4.1. Synthesis of 1,2:3,4-di-*O*-isopropylidene-α-D-galacto-hexodialdo-1,5-pyranose (73)

<u>Method 1</u>

To a solution of 1,2:3,4-di-*O*-isopropylidene-α-D-galactopyranose (**72**) (2.12 g, 8.14 mmol) in dichloromethane (10 mL) at 0°C, were slowly added 2 equiv. of Dess-Martin periodinane (6.90 g, 16.28 mmol). The reaction mixture was stirred for 3 hours at room temperature and then it was diluted with diethyl ether (130 mL) and quenched with a solution of 45 g of thiosulfate in 100 mL of $NaHCO_3$ (sat.). After stirring for 30 minutes, the product was extracted with diethyl ether, dried over anhydrous sodium sulfate, filtered and the solvent was evaporated to dryness. The obtained residue was purified by column chromatography using as eluent ethyl acetate:hexane (1:2) to give the 1,2:3,4-di-*O*-isopropylidene-α-D-*galacto*-hexodialdo-1,5-pyranose in good yield.

<u>Method 2</u>

To a stirred solution of oxalyl chloride (0.65 mL, 7.45 mmol) in 15 mL of dichloromethane cooled to -78ºC under argon was added dropwise 1.1 mL (15.5 mmol) of DMSO. After 15 min, a solution of the sugar alcohol (5.5 mmol) in 15 mL of dichloromethane was added and the mixture was stirred at -78 ºC for 30 min. Then, Et_3N was added (2.2 mL, 15.8 mmol) and the mixture was allowed to warm to room temperature and then stirred for further 45 min.. The reaction mixture was quenched with water (15 mL) and then extracted with dichloromethane (2 x 15 mL). The combined organic layers were washed with saturated sodium bicarbonate and brine, dried, filtered and evaporated under reduced pressure to an oil which was used immediately in the next reaction.

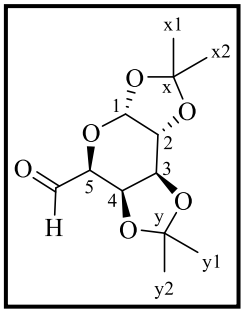

1,2:3,4-Di-*O*-isopropylidene-α-D-*galacto*-hexodialdo-1,5-pyranose (**73**), yield: 65 % (1.36 g), colourless oil.

^{1}H NMR (300.13 MHz, $CDCl_3$): δ =1.29, 1.33, 1.42 and 1.49 (4s, 12H, H-x1, H-x2, H-y1 and H-y2), 4.17 (d, 1H, *J* = 2.1 Hz, H-3), 4.37 (dd, 1H, *J* = 4.9, 2.4 Hz, H-2), 4.58 (dd, 1H, *J* = 7.8, 2.1 Hz, H-4), 4.63 (dd, 1H, *J* = 7.8, 2.4 Hz, H-5), 5.65 (d, 1H, *J* = 4.9 Hz, H-1), 9.59 (CO<u>H</u>) ppm.

^{13}C NMR (75.47 MHz, $CDCl_3$): δ = 24.2, 24.8, 25.8 and 26.0 (C-x1, C-x2, C-y1 and C-y2), 70.3 (C-5), 70.4 (C-2), 71.7 (C-4), 73.2 (C-3), 96.2 (C-1), 109.0 (C-x), 110.0 (C-y), 200.2 (<u>C</u>=O) ppm.

5.4.2. Synthesis of 6,7-dideoxy-1,2:3,4-di-*O*-isopropylidene-α-D-galacto-hept-6-enopyranose (74)

A mixture of 2.4 equiv. of methyltriphenylphosphonium bromide (4.48 g, 12.5 mmol) and 2 equiv. of NaH (251.0 mg, 10.5 mmol) in freshly dried THF (12 mL) was sonicated under nitrogen, for about 1 hour, until the formation of a bright yellow solution. Then, the 1,2:3,4-di-*O*-isopropylidene-α-D-*galacto*-hexodialdo-1,5-pyranose (**73**) (1.36 g, 5.23 mmol) in freshly dried THF (12 mL) was added and the reaction was left stirring for 3 hours. The reaction was quenched with methanol and the solvent was evaporated to dryness. The obtained residue was purified by column chromatography using as eluent ethyl acetate:hexane (1:9) to give the 6,7-dideoxy-1,2:3,4-di-*O*-isopropylidene-α-D-galacto-hept-6-enopyranose.

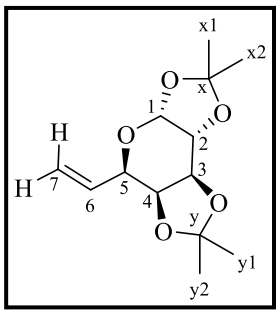

6,7-Dideoxy-1,2:3,4-di-*O*-isopropylidene-α-D-galacto-hept-6-enopyranose (**74**), yield: 81% (1.08 g), light yellowish oil.

^{1}H NMR (300.13 MHz, $CDCl_3$): δ =1.28, 1.40 and 1.47 (3s, 12H, H-x1, H-x2, H-x3 and H-x4), 4.16 (dd, 1H, *J* = 7.8, 1.9 Hz, H-2/ H-3/ H-4/ H-5), 4.20 – 4.30 (m, 2H, 4.16 (dd, 1H, H-2/H-3/H-4/H-5), 4.56 (dd, 1H, *J* = 7.9, 2.4 Hz, H-2/H-3/H-4/H-5), 5.16 – 5.37 (m, 2H, H-7), 5.52 (d, 1H, *J* = 5.2 Hz, H-1), 5.86 (ddd, 1H, *J* = 16.9, 10.6, 5.9 Hz, H-6) ppm.

5.5. Synthesis of *C*-glycosyl 2-styryl-4*H*-chromen-4-ones

To a solution of the appropriate 3-bromo-2-styryl-4*H*-chromen-4-one **61**, **66**, **70**, **71** or **75** (1 equiv.) with the sugar alkene **74** (1.2 equiv.) in dry DMF (10 mL), were added K_2CO_3 (1 equiv), Bu_4NBr (0.1 equiv.) and $Pd(OAc)_2$ (0.05 equiv.). The reaction mixture was heated at 110 °C under nitrogen and left stirring overnight. After this period, water was added (10 mL) and left stirring for 10 minutes. The organic layer was extracted with ethyl acetate and dried over with anhydrous sodium sulfate and the solvent was evaporated to dryness. The resultant residue was purified by column chromatography using ethyl acetate:hexane (1:2) as eluent. In most cases, further purification by preparative TLC was required to obtain the *C*-glycosyl 2-styryl-4*H*-chromen-4-ones **89**–**93** in moderate to good yields.

Target compound	3-Bromo-2-styryl-4*H*-chromen-4-one	Mass (mg)	Mol (mmol)
89	**61**	183.0	0.34
90	**66**	120.0	0.21
91	**70**	78.0	0.20
92	**71**	58.0	0.14
93	**75**	100.0	0.28

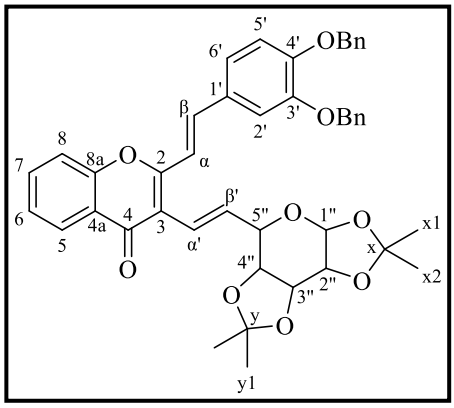

2-[3,4-Bis(benzyloxy)styryl]-3-(6,7-dideoxy-1,2:3,4-di-*O*-isopropylidene-β-D-*galacto*-hept-6-enopyranos-7-yl)-4*H*-chromen-4-one (**89**), yield: 62% (149.7 mg), yellowish oil.

MS(ESI$^+$) m/z (%): 715.3 ([M+H]$^+$, 100), 737.4 ([M+Na]$^+$, 44).

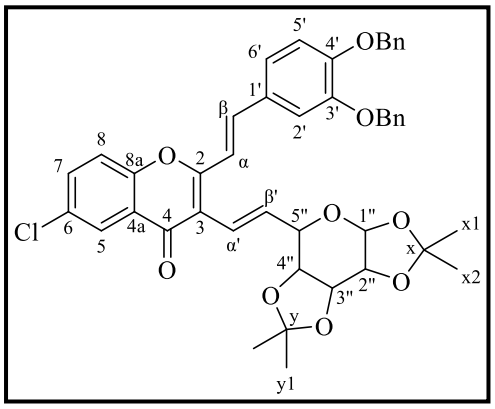

2-[3,4-Bis(benzyloxy)styryl]-6-chloro-3-(6,7-dideoxy-1,2:3,4-di-*O*-isopropylidene-β-D-*galacto*-hept-6-enopyranos-7-yl)-4*H*-chromen-4-one (**90**), yield: 72% (113.1 mg), yellowish oil.

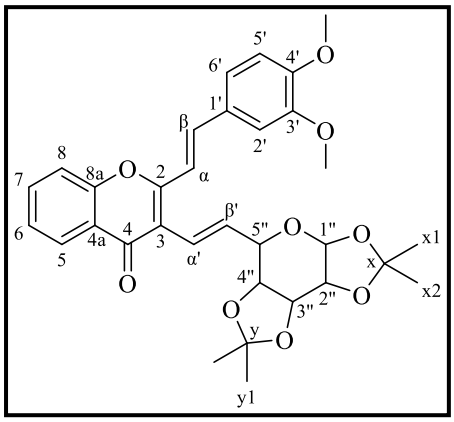

3-(6,7-Dideoxy-1,2:3,4-di-*O*-isopropylidene-β-D-*galacto*-hept-6-enopyranos-7-yl)-2-(3,4-dimethoxystyryl)-4*H*-chromen-4-one (**91**), yield: 74% (83.8 mg), yellowish oil.

MS(ESI$^+$) m/z (%): 563.3 ([M+H]$^+$, 100), 585.4 ([M+Na]$^+$, 71).

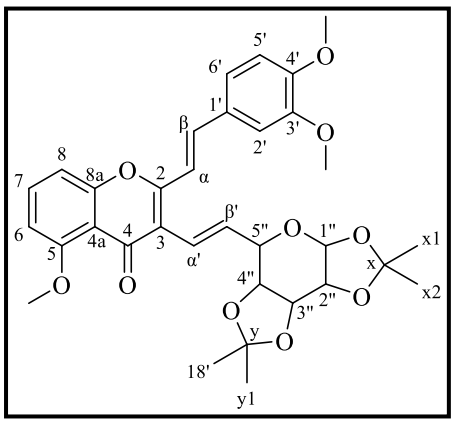

3-(6,7-Dideoxy-1,2:3,4-di-*O*-isopropylidene-β-D-*galacto*-hept-6-enopyranos-7-yl)-2-(3,4-dimethoxystyryl)-5-methoxy-4*H*-chromen-4-one (**92**), yield: 48% (39.6 mg), yellowish oil.

MS(ESI$^+$) m/z (%): 593.3 ([M+H]$^+$, 100), 615.3 ([M+Na]$^+$, 80), 631.4 ([M+K]$^+$, 7).

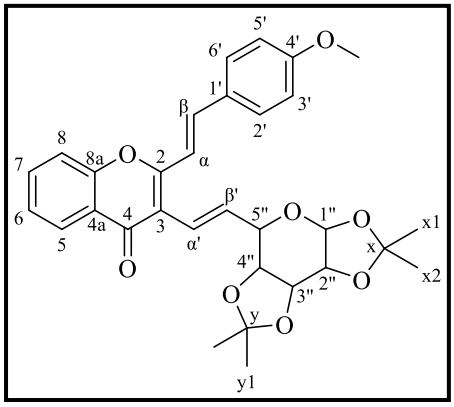

3-(6,7-Dideoxy-1,2:3,4-di-*O*-isopropylidene-β-D-*galacto*-hept-6-enopyranos-7-yl)-2-(4-methoxystyryl)-4*H*-chromen-4-one (**93**), yield: 53% (83.8 mg), yellowish oil.

MS(ESI$^+$) m/z (%): 533.3 ([M+H]$^+$, 100), 555.3 ([M+Na]$^+$, 36).

Chapter 6: References

1. Sun, P.; Lu, X.; Xu, C.; Sun, W.; Pan, B. Understanding of COVID-19 based on current evidence. *J. Med. Virol.* **92**, 548–551 (2020).
2. Wrapp, D.; Wang, N.; Corbett, K.S.; Goldsmith, J.A.; Hsieh, C.-L.; Abiona, O.; Graham, B.S.; McLellan, J.S. Cryo-EM structure of the 2019-nCoV spike in the prefusion conformation. *Science* **367**, 1260–1263 (2020).
3. Zheng, J. SARS-CoV-2: an Emerging coronavirus that causes a global threat. *Int. J. Biol. Sci.* **16**, 1678–1685 (2020).
4. Cui, J.; Li, F.; Shi, Z.-L. Origin and evolution of pathogenic coronaviruses. *Nat. Rev. Microbiol.* **17**, 181–192 (2019).
5. Wang, M.-Y.; Zhao, R.; Gao, L.-J.; Gao, X.-F.; Wang, D.-P.; Cao, J.-M. SARS-CoV-2: Structure, biology, and structure-based therapeutics development. *Front. Cell. Infect. Microbiol.* **10**, 587269 (2020).
6. Perlman, S.; Netland, J. Coronaviruses post-SARS: update on replication and pathogenesis. *Nat. Rev. Microbiol.* **7**, 439–450 (2009).
7. Woo, P.C.Y.; Lau, S.K.P.; Huang, Y.; Yuen, K.-Y. Coronavirus diversity, phylogeny and interspecies jumping. *Exp. Biol. Med.* **234**, 1117–1127 (2009).
8. Duffy, S.; Shackelton, L. A.; Holmes, E. C. Rates of evolutionary change in viruses: patterns and determinants. *Nat. Rev. Genet.* **9**, 267–276 (2008).
9. Harrison, A.G.; Lin, T.; Wang, P. Mechanisms of SARS-CoV-2 transmission and pathogenesis. *Trends Immunol.* **41**, 1100–1115 (2020).
10. Kochi, A. N.; Tagliari, A. P.; Forleo, G. B.; Fassini, G. M.; Tondo, C. Cardiac and arrhythmic complications in patients with COVID-19. *J. Cardiovasc. Electrophysiol.* **31**, 1003–1008 (2020).
11. Berger, J. R. COVID-19 and the nervous system. *J. Neurovirol.* **26**, 143–148 (2020).
12. Hess, D. C.; Eldahshan, W.; Rutkowski, E. COVID-19-Related Stroke. *Transl. Stroke Res.* **11**, 322–325 (2020).
13. Watanabe, Y.; Allen, J. D.; Wrapp, D.; McLellan, J. S.; Crispin, M. Site-specific glycan analysis of the SARS-CoV-2 spike. *Science* **369**, 330–333 (2020).
14. Walls, A. C.; Park, Y.-J.; Tortorici, M.A.; Wall, A.; McGuire, A.T.; Veesler, D. Structure, function, and antigenicity of the SARS-CoV-2 spike glycoprotein. *Cell* **181**, 281-292.e6 (2020).

15. Wang, Q.; Zhang, Y.; Wu, L.; Niu, S.; Song, C.; Zhang, Z.; Lu, G.; Qiao, C.; Hu, Y.; Yuen, K.-Y.; Wang, Q.; Zhou, H.; Yan, J.; Qi, J. Structural and functional basis of SARS-CoV-2 entry by using human ACE2. *Cell* **181**, 894-904.e9 (2020).
16. Williams, S. J.; Goddard-Borger, E. D. α-glucosidase inhibitors as host-directed antiviral agents with potential for the treatment of COVID-19. *Biochem. Soc. Trans.* **48**, 1287–1295 (2020).
17. Shang, J.; Ye, G.; Shi, K.; Wan, Y.; Luo, C.; Aihara, H.; Geng, Q.; Auerbach, A.; Li, F. Structural basis of receptor recognition by SARS-CoV-2. *Nature* **581**, 221–224 (2020).
18. Lan, J.; Ge, J.; Yu, J.; Shan, S.; Zhou, H.; Fan, S.; Zhang, Q.; Shi, X.; Wang, Q.; Zhang, L.; Wang, X. Structure of the SARS-CoV-2 spike receptor-binding domain bound to the ACE2 receptor. *Nature* **581**, 215–220 (2020).
19. Zhao, P.; Praissman, J.L.; Grant, O.C.; Cai, Y.; Xiao, T.; Rosenbalm, K.E.; Aoki, K.; Kellman, B.P.; Bridger, R.; Barouch, D.H.; Brindley, M.A.; Lewis, N.E.; Tiemeyer, M.; Chen, B.; Woods, R.J.; Wells, L. Virus-receptor interactions of glycosylated SARS-CoV-2 spike and human ACE2 receptor. *Cell Host Microbe* **28**, 586-601.e6 (2020).
20. Konwar, M.; Sarma, D. Advances in developing small molecule SARS $3CL^{pro}$ inhibitors as potential remedy for corona virus infection. *Tetrahedron* **77**, 131761 (2021).
21. Mouffouk, C.; Mouffouk, S.; Mouffouk, S.; Hambaba, L.; Haba, H. Flavonols as potential antiviral drugs targeting SARS-CoV-2 proteases ($3CL^{pro}$ and PL^{pro}), spike protein, RNA-dependent RNA polymerase (RdRp) and angiotensin-converting enzyme II receptor (ACE2). *Eur. J. Pharmacol.* **891**, 173759 (2021).
22. Li, Q.; Kang, C. Progress in developing inhibitors of SARS-CoV-2 3C-Like Protease. *Microorganisms* **8**, 1250 (2020).
23. Xu, J.; Zhao, S.; Teng, T.; Abdalla, A.; Zhu, W.; Xie, L.; Wang, Y.; Guo, X. Systematic comparison of two animal-to-human transmitted human coronaviruses: SARS-CoV-2 and SARS-CoV. *Viruses* **12**, 244 (2020).
24. Abdusalam, A.A.A.; Murugaiyah, V. Identification of potential inhibitors of 3CL Protease of SARS-CoV-2 from ZINC database by molecular docking-based virtual screening. *Front. Mol. Biosci.* **7**, 603037 (2020).
25. Kuo, C.-J.; Chao, T.-L.; Kao, H.-C.; Tsai, Y.-M.; Liu, Y.-K.; Wang, L.H.-C.; Hsieh, M.-C.; Chang, S.-Y.; Liang, P.-H. Kinetic characterization and inhibitor screening for

the proteases leading to identification of drugs against SARS-CoV-2. *Antimicrob. Agents Chemother*. **65**, 02577–20 (2021).

26. Freitas, B. T.; Durie, I.A.; Murray, J.; Longo, J.E.; Miller, H.C.; Crich, D.; Hogan, R.J.; Tripp, R.A.; Pegan, S.D. Characterization and noncovalent inhibition of the deubiquitinase and deISGylase activity of SARS-CoV-2 papain-like protease. *ACS Infect. Dis.* **6**, 2099–2109 (2020).
27. Adhikari, N.; Baidya, S. K.; Saha, A.; Jha, T. Structural insight into the viral 3C-Like Protease inhibitors: comparative SAR/QSAR approaches. In *Viral Proteases and Their Inhibitors;* Elsevier BV: Amsterdam, The Netherlands, 2017, 317–409.
28. Dai, W.; Zhang, B.; Jiang, X.-M.; Su, H.; Li, J.; Zhao, Y.; Xie, X.; Jin, Z.; Peng, J.; Liu, F.; Li, C.; Li, Y.; Bai, F.; Wang, H.; Cheng, X.; Cen, X.; Hu, S.; Yang, X.; Wang, J; Liu, X; Xiao, G.; Jiang, H.; Rao, Z.; Zhang, L.-K.; Xu, Y.; Yang, H; Liu, H. Structure-based design of antiviral drug candidates targeting the SARS-CoV-2 main protease. *Science* **368**, 1331–1335 (2020).
29. Ullrich, S.; Nitsche, C. The SARS-CoV-2 main protease as drug target. *Bioorg. Med. Chem. Lett.* **30**, 127377 (2020).
30. Yang, H.; Xie, W.; Xue, X.; Yang, K.; Ma, J.; Liang, W.; Zhao, Q.; Zhou, Z.; Pei, D.; Ziebuhr, J.; Hilgenfeld, R.; Yuen, K.Y.; Wong, L.; Gao, G.; Chen, S.; Chen, Z.; Ma, D.; Bartlam, M.; Rao, Z. Design of wide-spectrum inhibitors targeting coronavirus main proteases. *PLoS Biol.* **3**, e324 (2005).
31. Báez-Santos, Y. M.; St. John, S. E.; Mesecar, A. D. The SARS-coronavirus papain-like protease: Structure, function and inhibition by designed antiviral compounds. *Antiviral Res.* **115**, 21–38 (2015).
32. Yan, S.; Wu, G. Spatial and temporal roles of SARS-CoV PL^{pro} - A snapshot. *FASEB J.* **35**, e21197 (2021).
33. Wu, C.; Liu, Y.; Yang, Y.; Zhang, P.; Zhong, W.; Wang, Y.; Wang, Q.; Xu, Y.; Li, M.; Li, X.; Zheng, M.; Chen, L.; Li, H. Analysis of therapeutic targets for SARS-CoV-2 and discovery of potential drugs by computational methods. *Acta Pharm. Sin. B* **10**, 766–788 (2020).
34. Shin, D.; Mukherjee, R.; Grewe, D.; Bojkova, D.; Baek, K.; Bhattacharya, A.; Schulz, L.; Widera, M.; Mehdipour, A.R.; Tascher, G.; Geurink, P.P.; Wilhem, A.; *et al.* Papain-

like protease regulates SARS-CoV-2 viral spread and innate immunity. *Nature* **575**, 210–216 (2020).

35. Lenschow, D. J.; Lai, C.; Frias-Staheli, N.; Giannakopoulos, N.V.; Lutz, A.; Wolff, T.; Osiak, A.; Levine, B.; Schmidt, R.E.; García-Sastre, A.; *et al.* IFN-stimulated gene 15 functions as a critical antiviral molecule against influenza, herpes, and Sindbis viruses. *Proc. Natl. Acad. Sci. USA* **104***,* 1371–1376 (2007).
36. Picarazzi, F.; Vicenti, I.; Saladini, F.; Zazzi, M.; Mori, M. Targeting the RdRp of emerging RNA viruses: The Structure-Based Drug Design Challenge. *Molecules* **25**, 5695 (2020).
37. Kirchdoerfer, R.N.; Ward, A.B. Structure of the SARS-CoV nsp12 polymerase bound to nsp7 and nsp8 co-factors. *Nat. Commun.* **10**, 1-9 (2019).
38. Ahn, D.-G.; Choi, J.-K.; Taylor, D.R.; Oh, J.-W. Biochemical characterization of a recombinant SARS coronavirus nsp12 RNA-dependent RNA polymerase capable of copying viral RNA templates. *Arch. Virol.* **157**, 2095–2104 (2012).
39. Subissi, L.; Posthuma, C.C.; Collet, A.; Zevenhoven-Dobbe, J.C.; Gorbalenya, A.; Decroly, E.; Snijder, E.; Canard, B.; Imbert, I. One severe acute respiratory syndrome coronavirus protein complex integrates processive RNA polymerase and exonuclease activities. *Proc. Natl. Acad. Sci.* **111**, E3900–E3909 (2014).
40. Gao, Y.; Yan, L.; Huang, Y.; Liu, F.; Zhao, Y.; Cao, L.; Wang, T.; Sun, Q.; Ming, Z.; Zhang, L.; *et al.* Structure of the RNA-dependent RNA polymerase from COVID-19 virus. *Science* **368**, 779–782 (2020).
41. Elfiky, A. A. Ribavirin, Remdesivir, Sofosbuvir, Galidesivir, and Tenofovir against SARS-CoV-2 RNA dependent RNA polymerase (RdRp): A molecular docking study. *Life Sci.* **248**, 117592 (2020).
42. Xiao, J.; Capanoglu, E.; Jassbi, A. R.; Miron, A. Advance on the flavonoid *C*-glycosides and health benefits. *Crit. Rev. Food Sci. Nutr.* **56**, S29–S45 (2016).
43. Forkmann, G.; Martens, S. Metabolic engineering and applications of flavonoids. *Curr. Opin. Biotechnol.* **12**, 155–160 (2001).
44. Falcone Ferreyra, M. L.; Rius, S. P.; Casati, P. Flavonoids: biosynthesis, biological functions, and biotechnological applications. *Front. Plant Sci.* **3**, 222 (2012).
45. Courts, F. L.; Williamson, G. The occurrence, fate and biological activities of *C*-glycosyl flavonoids in the human diet. *Crit. Rev. Food Sci. Nutr.* **55**, 1352–1367 (2015).

46. Sak, K. Cytotoxicity of dietary flavonoids on different human cancer types. *Pharmacogn. Rev.* **8**, 122-146 (2014).

47. Xiao, J. Dietary flavonoid aglycones and their glycosides: Which show better biological significance? *Crit. Rev. Food Sci. Nutr.* **57**, 1874–1905 (2015).

48. Pietta, P.-G. Flavonoids as antioxidants. *J. Nat. Prod.* **63**, 1035–1042 (2000).

49. Rice-Evans, C. Flavonoid antioxidants. *Curr. Med. Chem.* **8**, 797–807 (2001).

50. Ribeiro, D.; Freitas, M.; Tomé, S.M.; Silva, A.M.; Porto, G.; Fernandes, E. Modulation of human neutrophils' oxidative burst by flavonoids. *Eur. J. Med. Chem.* **67**, 280–292 (2013).

51. Maleki, S. J.; Crespo, J. F.; Cabanillas, B. Anti-inflammatory effects of flavonoids. *Food Chem.* **299**, 125124 (2019).

52. Nabavi, S. F.; Braidy, N.; Habtemariam, S.; Orhan, I.E.; Daglia, M.; Manayi, A.; Gortzi, O. Neuroprotective effects of chrysin: From chemistry to medicine. *Neurochem. Int.* **90**, 224–231 (2015).

53. Nakajima, A.; Ohizumi, Y. Potential benefits of nobiletin, a citrus flavonoid, against alzheimer's disease and parkinson's disease. *Int. J. Mol. Sci.* **20**, 3380 (2019).

54. Batra, P.; Sharma, A. K. Anti-cancer potential of flavonoids: recent trends and future perspectives. *3 Biotech* **3**, 439–459 (2013).

55. Abotaleb, M.; Samuel, S.M.; Varghese, E.; Varghese, S.; Kubatka, P.; Líšková, A.; Büsselberg, D. Flavonoids in cancer and apoptosis. *Cancers* **11**, 28 (2018).

56. Proença, C.; Freitas, M.; Ribeiro, D.; Tomé, S.M.; Oliveira, E.F.T.; Viegas, M.F.; Araújo, A.N.; Ramos, M.J.; Silva, A.M.S.; Fernandes, P.A.; Fernandes, E. Evaluation of a flavonoids library for inhibition of pancreatic α-amylase towards a structure–activity relationship. *J. Enzyme Inhib. Med. Chem.* **34**, 577–588 (2019).

57. Ahmad, A.; Kaleem, M.; Ahmed, Z.; Shafiq, H. Therapeutic potential of flavonoids and their mechanism of action against microbial and viral infections—A review. *Food Res. Int.* **77**, 221–235 (2015).

58. Zakaryan, H.; Arabyan, E.; Oo, A.; Zandi, K. Flavonoids: promising natural compounds against viral infections. *Arch. Virol.* **162**, 2539–2551 (2017).

59. Zou, M.; Liu, H.; Li, J.; Yao, X.; Chen, Y.; Ke, C.; Liu, S. Structure-activity relationship of flavonoid bifunctional inhibitors against Zika virus infection. *Biochem. Pharmacol.* **177**, 113962 (2020).

60. Rengasamy, K. R. R.; Khan, H.; Gowrishankar, S.; Lagoa, R.J.; Mahomoodally, F.M.; Khan, Z.; Suroowan, S.; Tewari, D.; Zengin, G.; Hassan, S.T.; *et al.* The role of flavonoids in autoimmune diseases: Therapeutic updates. *Pharmacol. Ther.* **194**, 107–131 (2019).

61. Ji, Y.; Li, B.; Qiao, M.; Li, J.; Xu, H.; Zhang, L.; Zhang, X. Advances on the *in vivo* and *in vitro* glycosylations of flavonoids. *Appl. Microbiol. Biotechnol.* **104**, 6587–6600 (2020).

62. Plaza, M.; Pozzo, T.; Liu, J.; Ara, K.Z.G.; Turner, C.; Karlsson, E.N. Substituent effects on *in vitro* antioxidizing properties, stability, and solubility in flavonoids. *J. Agric. Food Chem.* **62**, 3321–3333 (2014).

63. Slámová, K.; Kapešová, J.; Valentová, K. "Sweet Flavonoids": Glycosidase-catalyzed modifications. *Int. J. Mol. Sci.* **19**, 2126 (2018).

64. Jiang, J.R.; Yuan, S.; Ding, J.F.; Zhu, S.C.; Xu, H.D.; Chen, T.; Cong, X.D.; Xu, W.P.; Ye, H.; Dai, Y.J. Conversion of puerarin into its 7-*O*-glycoside derivatives by Microbacterium oxydans (CGMCC 1788) to improve its water solubility and pharmacokinetic properties. *Appl. Microbiol. Biotechnol.* **81**, 647–657 (2008).

65. Beltrán-García, J.*;* Osca-Verdegal, R.; Pallardó, F.V.; Ferreres, J.; Rodríguez, M.; Mulet, S.; Carbonell, F.; García-Giménez, J.L. Oxidative stress and inflammation in COVID-19-associated sepsis: The potential role of anti-oxidant therapy in avoiding disease progression. *Antioxidants* **9**, 936 (2020).

66. Ninfali, P.; Antonini, E.; Frati, A.; Scarpa, E.-S. *C*-Glycosyl flavonoids from *Beta vulgaris Cicla* and Betalains from *Beta vulgaris rubra* : Antioxidant, anticancer and antiinflammatory activities-A review: Pharmacological activities of green and red beets. *Phytother. Res.* **31**, 871–884 (2017).

67. Wang, J.; Lou, J.; Luo, C.; Zhou, L.; Wang, M.; Wang, L. Phenolic compounds from *Halimodendron halodendron* (Pall.) voss and their antimicrobial and antioxidant activities. *Int. J. Mol. Sci.* **13**, 11349–11364 (2012).

68. Choi, S.-J.; Tai, B. H.; Cuong, N. M.; Kim, Y.-H.; Jang, H.-D. Antioxidative and anti-inflammatory effect of quercetin and its glycosides isolated from mampat (*Cratoxylum formosum*). *Food Sci. Biotechnol.* **21**, 587–595 (2012).

69. Parhiz, H.; Roohbakhsh, A.; Soltani, F.; Rezaee, R.; Iranshahi, M. Antioxidant and anti-inflammatory properties of the citrus flavonoids hesperidin and hesperetin: An

updated review of their molecular mechanisms and experimental models. *Phytother. Res.* **29**, 323–331 (2015).

70. Liskova, A.; Samec, M.; Koklesova, L.; Samuel, S.M.; Zhai, K.; Al-Ishaq, R.K.; Abotaleb, M.; Nosal, V.; Kajo, K.; Ashrafizadeh, M.; *et al.* Flavonoids against the SARS-CoV-2 induced inflammatory storm. *Biomed. Pharmacother.* **138**, 111430 (2021).
71. Wunpathe, C.; Potue, P.; Maneesai, P.; Bunbupha, S.; Prachaney, P.; Kukongviriyapan, U.; Kukongviriyapan, V.; Pakdeechote, P. Hesperidin suppresses renin-angiotensin system mediated NOX2 over-expression and sympathoexcitation in 2K-1C hypertensive rats. *Am. J. Chin. Med.* **46**, 751–767 (2018).
72. Agarwal, O. P. The anti-inflammatory action of nepitrin, a flavonoid. *Agents Actions* **12**, 298–302 (1982).
73. Jin, X.; Liu, M.; Zhang, D.; Zhong, X.; Du, K.; Qian, P.; Yao, W.; Gao, H.; Wei, M. Baicalin mitigates cognitive impairment and protects neurons from microglia-mediated neuroinflammation via suppressing NLRP 3 inflammasomes and TLR 4/ NF -κB signaling pathway. *CNS Neurosci. Ther.* **25**, 575–590 (2019).
74. Liu, Y.; Jing, Y.-Y.; Zeng, C.-Y.; Li, C.-G.; Xu, L.-H.; Yan, L.; Bai, W.-J.; Zha, Q.-B.; Ouyang, D.-Y.; He, X.-H. Scutellarin suppresses NLRP3 inflammasome activation in macrophages and protects mice against bacterial sepsis. *Front. Pharmacol.* **8**, 975 (2018).
75. Chang, J.; Block, T. M.; Guo, J.-T. Antiviral therapies targeting host ER alpha-glucosidases: Current status and future directions. *Antiviral Res.* **99**, 251–260 (2013).
76. Kim, J. S.; Kwon, C. S.; Son, K. H. Inhibition of alpha-glucosidase and amylase by luteolin, a flavonoid. *Biosci. Biotechnol. Biochem.* **64**, 2458–2461 (2000).
77. Shibano, M.; Kakutani, K.; Taniguchi, M.; Yasuda, M.; Baba, K. Antioxidant constituents in the dayflower (*Commelina communis L.*) and their α-glucosidase-inhibitory activity. *J. Nat. Med.* **62**, 349–353 (2008).
78. Choo, C. Y.; Sulong, N. Y.; Man, F.; Wong, T. W. Vitexin and isovitexin from the Leaves of *Ficus deltoidea* with *in-vivo* α-glucosidase inhibition. *J. Ethnopharmacol.* **142**, 776–781 (2012).
79. Wang, T.; Li, Q.; Bi, K. Bioactive flavonoids in medicinal plants: Structure, activity and biological fate. *Asian J. Pharm. Sci.* **13**, 12–23 (2018).

80. Wang, H.-K.; Xia, Y.; Yang, Z.-Y; Morris Natschke, S. L.; Lee, K.-H. Recent advances in the discovery and development of flavonoids and their analogues as antitumor and anti-HIV agents. In *Advances in Experimental Medicine and Biology*; Springer Science and Business Media LLC: Berlin/Heidelberg, Germany, 1998; Volume 439, pp. 191–225.
81. Russo, M.; Moccia, S.; Spagnuolo, C.; Tedesco, I.; Russo, G. L. Roles of flavonoids against coronavirus infection. *Chem. Biol. Interact.* **328**, 109211 (2020).
82. Lalani, S.; Poh, C. L. Flavonoids as antiviral agents for enterovirus A71 (EV-A71). *Viruses* **12**, 184 (2020).
83. Qiu, X.; Kroeker, A.; He, S.; Kozak, R.; Audet, J.; Mbikay, M.; Chrétien, M. Prophylactic efficacy of quercetin 3-β-*O*-D-glucoside against Ebola virus infection. *Antimicrob. Agents Chemother.* **60**, 5182–5188 (2016).
84. Choi, H. J.; Song, J. H.; Park, K. S.; Kwon, D. H. Inhibitory effects of quercetin 3-rhamnoside on influenza A virus replication. *Eur. J. Pharm. Sci.* **37**, 329–333 (2009).
85. Lin, Y.-J.; Chang, Y.-C.; Hsiao, N.-W.; Hsieh, J.-L.; Wang, C.-Y.; Kung, S.-H.; Tsai, F.-J.; Lan, Y.-C.; Lin, C.-W. Fisetin and rutin as 3C protease inhibitors of enterovirus A71. *J. Virol. Methods* **182**, 93–98 (2012).
86. Wang, C.; Wang, P.; Chen, X.; Wang, W.; Jin, Y. *Saururus chinensis* (Lour.) Baill blocks enterovirus 71 infection by hijacking MEK1–ERK signaling pathway. *Antiviral Res.* **119**, 47–56 (2015).
87. Li, B. Q.; Fu, T.; Dongyan, Y.; Mikovits, J.A.; Ruscetti, F.W.; Wang, J.M. Flavonoid baicalin inhibits HIV-1 infection at the level of viral entry. *Biochem. Biophys. Res. Commun.* **276**, 534–538 (2000).
88. Chu, M.; Xu, L.; Zhang, M.; Chu, Z.; Wang, Y. Role of baicalin in anti-influenza virus A as a potent inducer of IFN-gamma. *BioMed Res. Int.* **2015**, 1–11 (2015).
89. Li, X.; Liu, Y.; Wu, T.; Jin, Y.; Cheng, J.; Wan, C.; Qian, W.; Xing, F.; Shi, W. The antiviral effect of baicalin on enterovirus 71 *in vitro*. *Viruses* **7**, 4756–4771 (2015).
90. Tsai, F.-J.; Lin, C.-W.; Lai, C.-C.; Lan, Y.-C.; Lai, C.-H.; Hung, C.-H.; Hsueh, K.-C.; Lin, T.-H.; Chang, H.C.; Wan, L.; *et al.* Kaempferol inhibits enterovirus 71 replication and internal ribosome entry site (IRES) activity through FUBP and HNRP proteins. *Food Chem.* **128**, 312–322 (2011).

91. Gunaseelan, S.; Wong, K.Z.; Min, N.; Sun, J.; Ismail, N.K.B.M.; Tan, Y.J.; Lee, R.C.H.; Chu, J.J.H. Prunin suppresses viral IRES activity and is a potential candidate for treating enterovirus A71 infection. *Sci. Transl. Med.* **11**, eaar5759 (2019).

92. Cao, T.-W. Geng, C.-A.; Jiang, F.-Q.; Ma, Y.-B.; He, K.; Zhou, N.-J.; Zhang, X.-M.; Zhou, J.; Chen, J.-J. Chemical constituents of *Swertia yunnanensis* and their anti-hepatitis B virus activity. *Fitoterapia* **89**, 175–182 (2013).

93. Yarmolinsky, L.; Huleihel, M.; Zaccai, M.; Ben-Shabat, S. Potent antiviral flavone glycosides from *Ficus benjamina* leaves. *Fitoterapia* **83**, 362–367 (2012).

94. Ortega, J. T.; Suárez, A.I.; Serrano, M.L.; Baptista, J.; Pujol, F.H.; Rangel, H.R. The role of the glycosyl moiety of myricetin derivatives in anti-HIV-1 activity *in vitro*. *AIDS Res. Ther.* **14**, 57 (2017).

95. Cai, S.-Q.; Wang, R.; Yang, X.; Shang, M.; Ma, C.; Shoyama, Y. Antiviral flavonoid-type *C*-glycosides from the flowers of *Trollius chinensis*. *Chem. Biodivers.* **3**, 343–348 (2006).

96. Nayak, M. K.; Agrawal, A.S.; Bose, S.; Naskar, S.; Bhowmick, R.; Chakrabarti, S.; Sarkar, S.; Chawla-Sarkar, M. Antiviral activity of baicalin against influenza virus H1N1-pdm09 is due to modulation of NS1-mediated cellular innate immune responses. *J. Antimicrob. Chemother.* **69**, 1298–1310 (2014).

97. Wang, M.; Tao, L.; Xu, H. Chinese herbal medicines as a source of molecules with anti-enterovirus 71 activity. *Chin. Med.* **11**, 1-26 (2016).

98. Huang, J.; Tao, G.; Liu, J.; Cai, J.; Huang, Z.; Chen, J.-X. Current prevention of COVID-19: Natural products and herbal medicine. *Front. Pharmacol.* **11**, 588508 (2020).

99. Huang, F.; Li, Y.; Leung, E.L.-H.; Liu, X.; Liu, K.; Wang, Q.; Lan, Y.; Li, X.; Yu, H.; Cui, L.; *et al.* A review of therapeutic agents and Chinese herbal medicines against SARS-COV-2 (COVID-19). *Pharmacol. Res.* **158**, 104929 (2020).

100. Yang, R.; Liu, H.; Bai, C.; Wang, Y.; Zhang, X.; Guo, R.; Wu, S.; Wang, J.; Leung, E.; Chang, H.; *et al.* Chemical composition and pharmacological mechanism of Qingfei Paidu Decoction and Ma Xing Shi Gan Decoction against Coronavirus Disease 2019 (COVID-19): In silico and experimental study. *Pharmacol. Res.* **157**, 104820 (2020).

101. Solnier, J.; Fladerer, J.-P. Flavonoids: A complementary approach to conventional therapy of COVID-19? *Phytochem. Rev.* **20**, 773–795 (2021).

102. Ngwa, W.; Kumar, R.; Thompson, D.; Lyerly, W.; Moore, R.; Reid, T.-E.; Lowe, H.; Toyang, N. Potential of flavonoid-inspired phytomedicines against COVID-19. *Molecules* **25**, 2707 (2020).

103. Diniz, L. R. L.; Bezerra Filho, C. da S. M.; Fielding, B. C.; de Sousa, D. P. Natural antioxidants: A review of studies on human and animal coronavirus. *Oxid. Med. Cell. Longev.* **2020**, 1–14 (2020).

104. Nguyen, T. T. H.; Woo, H.-J.; Kang, H.-K.; Nguyen, V.D.; Kim, Y.-M.; Kim, D.-W.; Ahn, S.-A.; Xia, Y.; Kim, D. Flavonoid-mediated inhibition of SARS coronavirus 3C-like protease expressed in Pichia pastoris. *Biotechnol. Lett.* **34**, 831–838 (2012).

105. Jo, S.; Kim, H.; Kim, S.; Shin, D. H.; Kim, M. Characteristics of flavonoids as potent MERS-CoV 3C-like protease inhibitors. *Chem. Biol. Drug Des.* **94**, 2023–2030 (2019).

106. Jo, S.; Kim, S.; Shin, D. H.; Kim, M.-S. Inhibition of SARS-CoV 3CL protease by flavonoids. *J. Enzyme Inhib. Med. Chem.* **35**, 145–151 (2020).

107. Su, H.; Yao, S.; Zhao, W.F.; Li, M.J.; Liu, J.; Shang, W.J.; Xie, H.; Ke, C.Q.; Hu, H.C.; Gao, M.N.; *et al.* Anti-SARS-CoV-2 activities in vitro of Shuanghuanglian preparations and bioactive ingredients. *Acta Pharmacol. Sin.* **41**, 1167–1177 (2020).

108. Chen, L.-R.; Wang, Y.-C.; Lin, Y.W.; Chou, S.-Y.; Chen, S.-F.; Liu, L.T.; Wu, Y.-T.; Kuo, C.-J.; Chen, T.S.-S.; Juang, S.-H. Synthesis and evaluation of isatin derivatives as effective SARS coronavirus 3CL protease inhibitors. *Bioorg. Med. Chem. Lett.* **15**, 3058–3062 (2005).

109. Zhang, J.; Huitema, C.; Niu, C.; Yin, J.; James, M.N.; Eltis, L.D.; Vederas, J.C. Aryl methylene ketones and fluorinated methylene ketones as reversible inhibitors for severe acute respiratory syndrome (SARS) 3C-like proteinase. *Bioorganic Chem.* **36**, 229–240 (2008).

110. Shitrit, A.; Zaidman, D.; Kalid, O.; Bloch, I.; Doron, D.; Yarnizky, T.; Buch, I.; Segev, I.; Ben-Zeev, E.; Segev, E.; *et al.* Conserved interactions required for inhibition of the main protease of severe acute respiratory syndrome coronavirus 2 (SARS-CoV-2). *Sci. Rep.* **10**, 1-11 (2020).

111. Su, H.; Zhou, F.; Huang, Z.; Ma, X.; Natarajan, K.; Zhang, M.; Huang, Y.; Su, H. Molecular insights into small-molecule drug discovery for SARS-CoV-2. *Angew. Chem. Int. Ed.* **60**, 9789–9802 (2021).

112. Jo, S.; Kim, S.; Kim, D. Y.; Kim, M.-S.; Shin, D. H. Flavonoids with inhibitory activity against SARS-CoV-2 3CLpro. *J. Enzyme Inhib. Med. Chem.* **35**, 1539–1544 (2020).

113. Dubey, K.; Dubey, R. Computation screening of narcissoside a glycosyloxyflavone for potential novel coronavirus 2019 (COVID-19) inhibitor. *Biomed. J.* **43**, 363–367 (2020).

114. Abian, O.; Ortega-Alarcon, D.; Jimenez-Alesanco, A.; Ceballos-Laita, L.; Vega, S.; Reyburn, H.T.; Rizzuti, B.; Velazquez-Campoy, A. Structural stability of SARS-CoV-2 $3CL^{pro}$ and identification of quercetin as an inhibitor by experimental screening. *Int. J. Biol. Macromol.* **164**, 1693–1703 (2020).

115. Rizzuti, B.; Grande, F.; Conforti, F.; Jimenez-Alesanco, A.; Ceballos-Laita, L.; Ortega-Alarcon, D.; Vega, S.; Reyburn, H.T.; Abian, O.; Velazquez-Campoy, A. Rutin is a low micromolar inhibitor of SARS-CoV-2 main protease $3CL^{pro}$: Implications for drug design of quercetin analogs. *Biomedicines* **9**, 375 (2021).

116. Cherrak, S. A.; Merzouk, H.; Mokhtari-Soulimane, N. Potential bioactive glycosylated flavonoids as SARS-CoV-2 main protease inhibitors: A molecular docking and simulation studies. *PLOS ONE* **15**, e0240653 (2020).

117. A da Silva, F. M.; Da Silva, K.P.A.; De Oliveira, L.P.M.; Costa, E.V.; Koolen, H.H.; Pinheiro, M.L.B.; De Souza, A.Q.L.; De Souza, A.D.L. Flavonoid glycosides and their putative human metabolites as potential inhibitors of the SARS-CoV-2 main protease (Mpro) and RNA-dependent RNA polymerase (RdRp). *Mem. Inst. Oswaldo Cruz* **115**, 200207 (2020).

118. Agrawal, P. K.; Agrawal, C.; Blunden, G. Rutin: A potential antiviral for repurposing as a SARS-CoV-2 Main Protease (M^{pro}) inhibitor. *Nat. Prod. Commun.* **16**, 1-12 (2021).

119. Sharma, A.; Goyal, S.; Yadav, A. K.; Kumar, P.; Gupta, L. *In-silico* screening of plant-derived antivirals against main protease, $3CL^{pro}$ and endoribonuclease, NSP15 proteins of SARS-CoV-2. *J. Biomol. Struct. Dyn.* 1–15 (2020)

120. Pandey, P.; Rane, J.S.; Chatterjee, A.; Kumar, A.; Khan, R.; Prakash, A.; Ray, S. Targeting SARS-CoV-2 spike protein of COVID-19 with naturally occurring phytochemicals: An *in silico* study for drug development. *J. Biomol. Struct. Dyn.* 1–11 (2020)

121. Yao, X.; Ye, F.; Zhang, M.; Cui, C.; Huang, B.; Niu, P.; Liu, X.; Zhao, L.; Dong, E.; Song, C.; *et al. In vitro* antiviral activity and projection of optimized dosing design of hydroxychloroquine for the treatment of severe acute respiratory syndrome coronavirus 2 (SARS-CoV-2). *Clin. Infect. Dis.* **71**, 732–739 (2020).

122. Pandey, P.; Khan, F.; Rana, A.K.; Srivastava, Y.; Jha, S.k.; Jha, N.K. A drug repurposing approach towards elucidating the potential of flavonoids as covid-19 spike protein inhibitors. *Biointerface Res. Appl. Chem.* **11**, 8482-8501 (2021).

123. Jain, A. S.; Sushma, P.; Dharmashekar, C.; Beelagi, M.S.; Prasad, S.K.; Shivamallu, C.; Prasad, A.; Syed, A.; Marraiki, N.; Prasad, K.S. *In silico* evaluation of flavonoids as effective antiviral agents on the spike glycoprotein of SARS-CoV-2. *Saudi J. Biol. Sci.* **28**, 1040–1051 (2021).

124. Biagioli, M.; Marchianò, S.; Roselli, R.; Di Giorgio, C.; Bellini, R.; Bordoni, M.; Gidari, A.; Sabbatini, S.; Francisci, D.; Fiorillo, B.; *et al.* Discovery of a AhR flavonoid agonist that counter-regulates ACE2 expression in rodent models of inflammation and attenuates ACE2-SARS-CoV2 interaction in vitro. *Biochem. Pharmacol.* **188**, 114564 (2021)

125. Güler, H. İ.; Ay Sal, F.; Can, Z.; Kara, Y.; Yildiz, O.; Belduz, A.O.; Çanakci, S.; Kolayli, S. Targeting CoV-2 spike RBD and ACE-2 interaction with flavonoids of Anatolian propolis by *in silico* and *in vitro* studies in terms of possible COVID-19 therapeutics. *Turk J Biol.* **45**, 530-548 (2021).

126. Rameshkumar, M. R.; Indu, P.; Arunagirinathan, N.; Venkatadri, B.; El-Serehy, H.A.; Ahmad, A. Computational selection of flavonoid compounds as inhibitors against SARS-CoV-2 main protease, RNA-dependent RNA polymerase and spike proteins: A molecular docking study. *Saudi J. Biol. Sci.* **28**, 448–458 (2021).

127. Hiremath, S.; Kumar, H.D.V.; Nandan, M.; Mantesh, M.; Shankarappa, K.S.; Venkataravanappa, V.; Basha, C.R.J.; Reddy, C.N.L. *In silico* docking analysis revealed the potential of phytochemicals present in *Phyllanthus amarus* and *Andrographis paniculata*, used in Ayurveda medicine in inhibiting SARS-CoV-2. *3 Biotech* **11**, 1-18 (2021).

128. Imai, K.; Nakanishi, I.; Ohkubo, K.; Ohba, Y.; Arai, T.; Mizuno, M.; Fukuzumi, S.; Matsumoto, K.; Fukuhara, K. Synthesis of methylated quercetin analogues for enhancement of radical-scavenging activity. *RSC Adv.* **7**, 17968-17979 (2017).

129. Azimvand, J. Synthesis of some new derivatives of 2-methyl-4*H*-4-chromenone. *J. Chem. Pharm. Res.* **4**, 3929–3933 (2012).

130. Ibrahim, S. S. Uses of *o*-hydroxybenzoylacetone in the synthesis of some substituted 2-methylchromones, chelating agents, and related materials. *Ind. Eng. Chem. Res.* **40**, 37–39 (2001).

131. Almeida, A., Silva, V., Silva, A., Pinto, D. & Cavaleiro, J. Syntheses of novel (*E*)-*N*-methyl-2-styryl-4-quinolones. *Synlett* **2008**, 2593–2596 (2008).

132. Neises, B.; Steglich, W. Simple method for the esterification of carboxylic acids. *Angew. Chem. Int. Ed. Engl.* **17**, 522–524 (1978).

133. Fougerousse, A.; Gonzalez, E.; Brouillard, R. A convenient method for synthesizing 2-aryl-3-hydroxy-4-oxo-4*H*-1-benzopyrans or flavonols. *J. Org. Chem.* **65**, 583–586 (2000).

134. Santos, C.; Silva, A.; Cavaleiro, J. A novel and efficient route for the synthesis of hydroxylated 2,3-diarylxanthones. *Synlett* **2007**, 3113–3116 (2007).

135. Jacques, J.; Marquet, A. Selective α-bromination of an aralkyl ketone with phenyltrimethylammonium tribromide: 2-bromoacetyl-6-methoxynaphthalene and 2,2-dibromoacetyl-6-methoxynaphthalene. *Org. Synth.* **53**, 111 (1973)

136. Miyake, H.; Nishino, S.; Nishimura, A.; Sasaki, M. New synthesis of 3-bromoflavones via bromination of 1-(2-hydroxyphenyl)-3-arylpropane-1,3-dione by $CuBr_2$, and conversion into 3-aminoflavones. *Chem. Lett.* **36**, 522–523 (2007).

137. Byrne, F. P.; Jin, S.; Paggiola, G; Petchey, T.H.M.; Clark, JH.; Farmer, T.J.; Hunt, A.J.; McElroy, R.; Sherwood, J. Tools and techniques for solvent selection: green solvent selection guides. *Sustain. Chem. Process.* **4**, 1-24 (2016).

138. Ferreira, J. P. A.; Silva, V. L. M.; Elguero, J.; Silva, A. M. S. (*E*)-3-Halo-2-styryl-4*H*-chromen-4-ones: synthesis and transformation to novel pyrazoles. *Tetrahedron* **69**, 9701–9709 (2013).

139. Rho, H. S.; Ko, B.-S.; Kim, H. K.; Ju, Y.-S. Synthesis of 3-bromo derivatives of flavones. *Synth. Commun.* **32**, 1303–1310 (2002).

140. Reen, F. J.; Clarke, S.L.; Legendre, C.; McSweeney, C.M.; Eccles, K.S.; Lawrence, S.E.; O'Gara, F.; McGlacken, G.P. Structure–function analysis of the C-3 position in analogues of microbial behavioural modulators HHQ and PQS. *Org. Biomol. Chem.* **10**, 8903 (2012).

141. Dess, D. B.; Martin, J. C. A Useful 12-I-5 Triacetoxyperiodinane (the Dess-Martin Periodinane) for the Selective Oxidation of Primary or Secondary Alcohols and a Variety of Related 12-I-5 Species. *J. Am. Chem. Soc.* **113**, 7277–7287 (1991).

142. Andrés, José M.; Pedrosa, R. Stereodivergent synthesis of all diastereomers of 4-aminoheptane-3,5-diol from (L)-serine. *Tetrahedron* **54**, 5607–5616 (1998).

143. Zhang, P.; Hevey, R.; Ling, C.-C. Total synthesis of β-D-*ido*-heptopyranosides Rrelated to capsular polysaccharides of *Campylobacter jejuni* HS:4. *J. Org. Chem.* **82**, 9662–9674 (2017).

144. Johansson Seechurn, C. C. C.; Kitching, M. O.; Colacot, T. J.; Snieckus, V. Palladium-catalyzed cross-coupling: A historical contextual perspective to the 2010 Nobel Prize. *Angew. Chem. Int. Ed.* **51**, 5062–5085 (2012).

145. Frappa, I.; Sinou, D. Transition metal catalysed functionalisation at the anomeric center of carbohydrates. *J. Carbohydr. Chem.* **16**, 255–276 (1997).

146. *Handbook of organopalladium chemistry for organic synthesis*. Two volumes Set Edited by Ei-ichi Negishi (Purdue University). John Wiley & Sons, Inc.: Hoboken. 2002.

147. Beletskaya, I. P.; Cheprakov, A. V. The Heck reaction as a sharpening stone of palladium catalysis. *Chem. Rev.* **100**, 3009–3066 (2000).

148. Wall, V. M.; Eisenstadt, A.; Ager, D. J.; Laneman, S. A. The Heck reaction and cinnarnic acid synthesis by heterogeneous catalysis. **43**, 138-145 (1999).

149. Cabri, W.; Candiani, I. Recent developments and new Perspectives in the Heck reaction. *Acc. Chem. Res.* **28**, 2–7 (1995).

150. Jeffery, T. On the efficiency of tetraalkylammonium salts in Heck type reactions. *Tetrahedron* **52**, 10113–10130 (1996).

151. Wellington, K. W.; Benner, S. A. A review: Synthesis of aryl *C*-glycosides via the Heck coupling reaction. *Nucleosides Nucleotides Nucleic Acids* **25**, 1309–1333 (2006).

152. Xiong, D.-C.; Zhang, L.-H.; Ye, X.-S. Oxidant-controlled Heck-type *C*-glycosylation of glycals with arylboronic acids: Stereoselective synthesis of aryl 2-aeoxy-*C*-glycosides. *Org. Lett.* **11**, 1709–1712 (2009).

153. Li, H.-H.; Ye, X.-S. Regio- and stereo-selective synthesis of aryl 2-deoxy-*C*-glycopyranosides by palladium-catalyzed Heck coupling reactions of glycals and aryl iodides. *Org. Biomol. Chem.* **7**, 3855-3861 (2009).

154. Singh, A. K.; Kanaujiya, V. K.; Tiwari, V.; Sabiah, S.; Kandasamy, J. Development of routes for the stereoselective preparation of β-aryl-*C*-glycosides via *C*-1 aryl enones. *Org. Lett.* **22**, 7650–7655 (2020).

155. Kondor, Z.; Fuentes, D.; Vogel, C.; Patonay, T.; Kónya, K. Synthesis of flavonoid/chromonoid–β-D-ribofuranose derivatives by palladium-catalyzed cross-coupling reactions. *Synlett* **27**, 888–892 (2016).

156. Kondor, Z., Herczeg, M., Borbás, A., Patonay, T. & Kónya, K. Application of carbohydrates with methylene or vinyl groups in Heck–Mizoroki cross-coupling reactions with *O*-heterocycles. *Synlett* **27**, 2709–2715 (2016).